

UNIVERSITY OF OKLAHOMA

GRADUATE COLLEGE

TOWARDS EFFICIENT AND ENHANCED WIRELESS COEXISTENCE IN
THE UNLICENSED SPECTRUM

A DISSERTATION

SUBMITTED TO THE GRADUATE FACULTY

in partial fulfillment of the requirements for the

Degree of

DOCTOR OF PHILOSOPHY

in

Electrical & Computer Engineering

By

SIRAJ MUHAMMAD

Norman, Oklahoma

2021

TOWARDS EFFICIENT AND ENHANCED WIRELESS COEXISTENCE IN
THE UNLICENSED SPECTRUM

A DISSERTATION APPROVED FOR THE
SCHOOL OF ELECTRICAL & COMPUTER ENGINEERING

BY THE COMMITTEE CONSISTING OF

Dr. Hazem H. Refai, *Chair*

Dr. Daniel E. Hamlin

Dr. James J. Sluss

Dr. Samuel Cheng

Dr. Mohamad Omar Al-Kalaa

© Copyright by SIRAJ MUHAMMAD 2021
All Rights Reserved.

To my dear parents, Thanaa and Muhammad.

To my brother, Obada, and sisters, Einas and Israa.

To the memory of my beloved uncle, Abdulhadi Sharaf Al-Deen.

Acknowledgements

First and foremost, all praise to the One, the Most High, Almighty God, for this achievement would not have been possible without the countless blessings He bestowed upon me.

I am forever indebted to my advisor, *Dr. Hazem Refai* for his unwavering mentorship, support, and the many opportunities he offered me throughout the years. I have been lucky and privileged to work under his supervision, and I am grateful to him for investing in me and contributing to my growth and success on so many levels.

I would like to also extend my sincere appreciation to my doctoral committee members, Dr. James Sluss, Dr. Samuel Cheng, Dr. Omar Al-Kalaa, and Dr. Daniel Hamlin for their time and insightful comments to improve this work. I would like to acknowledge the late Dr. Thordur Ronulfsson for the wonderful person and amazing inspiration he was, may his soul rest in peace. Special thanks to Dr. Omar Al-Kalaa for supporting me with a fellowship at the U.S. FDA to complete this work. Appreciation goes as well to Michelle Farabough for editing this dissertation and for her educating comments over the years.

I must acknowledge those who blessed me with their friendship and became a second family to me, those whose help and relentless support cannot be overestimated. I am grateful to Dr. Asaad Kaadan, Fahd Babelli, Tamer Al-Amiri, Nabil Asfari, Hasan Tafish, Rami Beydoun, Dr. Obada Al-Zoubi, Dr. Alaa Mourad, and Nigel Hesse-Negm.

To my extended family at OU, especially Ms. Krista Peterson, Ms. Rene

Wagenblatt, Ms. Denise Davis, and the staff at the Student Affairs... I am thankful to you all for a wonderful time at OU-Tulsa and being so helpful every time I needed it.

I cannot begin to express my thanks and appreciation to my family who has inundated me with their love, support, prayers, and encouragement from afar... so much it vanished the thousands of miles that set us apart.

Contents

Acknowledgements	iv
List of Figures	viii
List of Tables	x
Abstract	xi
1 Introduction	1
1.1 Motivation	2
1.2 Contribution	4
2 Technology Overview	5
2.1 5G New Radio-Unlicensed	5
2.1.1 Waveform Numerology	7
2.1.2 Bandwidth Parts (BWPs)	7
2.2 Listen-Before-Talk	8
2.2.1 Channel Access Mechanism in ETSI	9
2.2.2 LBT in 3GPP Specifications	13
2.3 Bluetooth Low Energy 5	16
2.3.1 PHY Modes	16
2.3.2 Channel Selection Algorithm #2	18
2.3.3 Maximum Transmit Power	19
3 Related Work	21
3.1 Wi-Fi’s DCF and EDCA	21
3.2 LTE-LAA and Coexistence with Wi-Fi	22
3.3 Alternative LBT Schemes	24
3.4 Remarks	26
3.5 Coexistence with Bluetooth	26
4 5G NR-U Homogeneous Coexistence Analysis	29
4.1 System Model	30
4.1.1 One-Step Transition Probabilities	32
4.1.2 Steady-State Probabilities	33
4.1.3 Probability of Transmission	40
4.1.4 Formulating a Homogeneous Scenario	41
4.1.5 Model Validation	43
4.2 One-Class Dense Deployment	43

4.2.1	Effective Channel Utilization	44
4.2.2	Mean Access Delay	48
4.2.3	Temporal Fairness	49
4.3	Two-Class Deployment Scenario	50
4.3.1	Effective Channel Utilization	51
4.3.2	Collision Analysis	54
4.3.3	Mean Access Delay	58
4.3.4	Temporal Fairness	60
4.4	Case Study: Intensive Care Unit (ICU)	62
5	Modified LBT Mechanism	64
5.1	Proposed Modification	64
5.2	Performance Evaluation	67
6	Empirical Coexistence Analysis of BLE 5 and Cellular LBT	74
6.1	Introduction	75
6.1.1	Contribution	77
6.2	Experimental Setup	77
6.3	Empirical Results	81
6.3.1	Impact of LBT on BLE 5 Performance	82
6.3.2	Impact of BLE 5 on LBT Performance	87
6.4	Discussion	88
7	Conclusion	94
7.1	Future Work	97
Bibliography		98
Acronyms		109

List of Figures

2.1	Spectrum allocation of the three unlicensed bands—2.4, 5, and 6 GHz [1].	6
2.2	Relationship between bandwidth parts and waveform numerology in 5G NR PHY [2].	8
2.3	Timing diagram of Frame Based Equipment according to ETSI standard [3].	10
2.4	Timing relationship among four priority classes defined in ETSI.	11
2.5	A high-level flowchart demonstrates the LBT procedure for Frame Based Equipment, as stipulated in ETSI standard.	12
2.6	A flowchart describing the early LBT procedure published in TR 36.889 [4].	15
2.7	Link layer packet format for BLE uncoded 1M and 2M PHYs.	17
2.8	Link layer packet format for BLE Coded PHY (LR).	18
2.9	Channel hopping pattern of BLE channel selection algorithms #1 (top) and #2 (bottom) over 100 connection events.	19
2.10	Block diagram of channel selection algorithm #2 introduced in BLE version 5.	20
4.1	State transition diagram of the Markov chain model.	31
4.2	Effective channel utilization vs. number of contending nodes in homogeneous class setting, for both, analytical and simulation results.	44
4.3	ECU as a function of the contending nodes number for all four priority classes sharing the channel homogeneously.	45
4.4	Channel collisions as a function of the contending nodes number for all four priority classes sharing the channel homogeneously.	46
4.5	Probability that at least two stations draw the same number in the backoff stage, as a function of the number of contending nodes n	47
4.6	Mean access delay—in seconds—for different priority classes as a function of the number of contending stations.	49
4.7	Aggregate ECU for different combinations of priority classes: (a) Class 1 and Class 2, (b) Class 2 and Class 3, (c) Class 3 and Class 4, (d) Class 1 and Class 4.	53
4.8	Intra-network and internetwork collisions for different combinations of coexisting priority classes.	57
4.9	Mean access delay for different combinations of coexisting priority classes.	59
4.10	Channel time fairness for individual nodes coexisting with a combination of priority classes.	61

4.11	Latency of connections in ICU environment mapped to various frame priority classes. (a) 2, 3, 4; (b) 1, 2, 3; (c) 1, 1, 2; (d) 1, 1, 1	63
5.1	Timing relationship between colliding packets of the same priority class.	65
5.2	Timing relationship of the proposed LBT scheme illustrating the additional random SIFS period.	66
5.3	Individual PMFs of the RSIFS random process with $m_r = 9$ and the backoff random process with size $W_{c,m_c} = 8$	68
5.4	Joint PMF of the backoff and RSIFS processes.	68
5.5	ECU performance of the proposed modification in dense deployments compared to regular LBT.	69
5.6	Mean access delay of regular LBT for the four priority classes in dense deployments.	70
5.7	Mean access delay of the modified LBT for the four priority classes in dense deployments.	71
5.8	CDF of access delays for regular LBT simulations with 1 to 128 nodes sharing the channel.	72
5.9	CDF of access delays for modified LBT simulations with 1 to 128 nodes sharing the channel.	73
6.1	The experimental setup of the coexistence test illustrating the arrangement of BLE nodes and the three LBT pairs with center frequencies 2412 MHz, 2437 MHz, and 2462 MHz.	79
6.2	Normalized BLE throughput under LBT interferers of class 1, 2, 3, and 4.	83
6.3	Mean IFS durations of BLE PHYs in three tiers as a function of the I/U ratio.	85
6.4	An example of the number of packets that can be sent during one connection event for 2M, 1M, and LR PHYs.	86
6.5	Normalized LBT throughput in the evaluation of three tiers.	89
6.6	Box plot of packet durations for BLE physical layers from tier 1 scenario.	90
6.7	BLE channel histogram as a function of I/U ratio.	91

List of Tables

2.1	Supported Transmission Numerologies in NR Specifications	7
2.2	LBT Priority Classes as Defined in the ETSI Standard	11
2.3	Summary of BLE 5 Physical Layers	18
4.1	AAMI TIR69 Risk Categories	62
6.1	BLE 5 Configuration Parameters	80

Abstract

The 3rd Generation Partnership Project (3GPP) is developing the fifth generation (5G) of wireless broadband technology and has identified the unlicensed spectrum as a principal item on the plan of action. Listen-Before-Talk (LBT) has been recognized as the starting development point for the channel access scheme of future 5G New Radio-Unlicensed (NR-U) networks. Recent technical reports suggest that all sub-7 GHz unlicensed spectrum is targeted for 5G NR-U operation, including the 2.4 GHz Industrial, Scientific, and Medical (ISM) band. Literature is inundated with research on Wi-Fi and LBT-based Long-Term Evolution License-Assisted Access (LTE-LAA) wireless coexistence analysis. While a treasure trove of radio spectrum has been approved for license-exempt use in the 6 GHz band, industry and standard organizations must make sure it is well utilized by enhancing their coexistence schemes. A proper assessment of the homogeneous LBT deployment is imperative under the new use cases and regulatory circumstances. The work presented herein aimed to fill the gap and underline the importance of improving channel access mechanisms in next-generation wireless systems.

The research in this dissertation first analyzed the LBT channel access scheme and analytically evaluated its performance in terms of a metrics set, such as effective channel utilization, collision probability, mean access delay, and temporal fairness among coexisting nodes. Outcomes of the developed analytical model revealed inefficiencies in various cases. For example, high priority classes generally hinder overall effective channel utilization, exhibit a high collision rate, and incur long latencies compared to lower priorities; and low priority classes sustain

longer delays in class-heterogeneous scenarios. The developed framework was then utilized to investigate wireless coexistence in a 5G-enabled intensive care unit, employing remote patient monitoring over 5G NR-U.

A modified LBT scheme is then proposed in this work to enhance overall channel efficiency in homogeneous LBT deployments by reducing the collision probability among coexisting stations based on the analytical investigation of the LBT mechanism.

It is expected that low-power, narrowband frequency hoppers will be allowed to operate in the 6 GHz spectrum based on recent European Communications Committee (ECC) mandates, which raises speculation around coexistence with incumbent radio access technologies (RATs). To address the potential operation of cellular LBT in the 2.4 GHz and frequency hopping systems in the 5- and 6-GHz bands, the coexistence of Bluetooth Low Energy (BLE) 5 and LBT was investigated empirically in an anechoic chamber. The mutual impact was explored by means of throughput, packet error rate, and interframe delays. Empirical evaluation results demonstrated how BLE throughput dropped as the intended-to-unintended signal ratio decreased and the way in which LBT classes exhibited a diminishing effect as the class priority descended. Long Range BLE physical layer (PHY) was found to sustain longer gap times (i.e., delay) than the other two PHYs; however, the LR PHY showed less susceptibility to interference. Results also demonstrated that low data rate BLE PHYs hindered LBT throughput performance since they correspond to longer airtime durations.

Chapter 1

Introduction

Information and Communication Technology (ICT) is ushering in a new era of wireless connectivity. Consumer markets are bustling with new applications and use-cases that put current technical standards under pressure to swiftly adapt and adequately address their demands. For the past two decades, regulatory bodies such as the Institute of Electrical and Electronics Engineers (IEEE) and the 3rd Generation Partnership Project (3GPP) have refined their protocols to meet consumers' needs: improving achieved throughput, enhancing channel access schemes, and accommodating an increasing number of users. Though these improvements have kept current with demand, society is being ever inundated by a staggering number of connected instruments, from smartphones to smart TVs, medical devices, connected and autonomous vehicles, and pervasive Internet of Things (IoT) gadgets.

According to an Ericsson report, traffic generated by smartphones in 2022 is expected to increase 10 times the amount reported in 2016 [5]. This translates to more than 60 exabytes of data per month. This massive amount of data flow is attributed mainly to new use-cases of wireless connectivity projected for the next five years (e.g., online gaming, virtual reality (VR), critical services and infrastructure control, sensor networks, and smart transportation). Such applications rely on three main characteristics of next generation wireless communications, namely

ultra-low-latency, extremely high bandwidth, and massive density.

In the unlicensed spectrum domain, IEEE has responded to these requisites with the introduction of a new member to the 802.11 family, namely 802.11ax High-Efficiency or Wi-Fi 6. The 3GPP on the other hand, has had numerous debates arguing the feasibility of bringing their Long-Term Evolution (LTE) into the unlicensed spectrum for supplementing the demand on a primary link. In release 13 of 3GPP specifications, Long-Term Evolution License-Assisted Access (LTE-LAA) ensued as a result of extensive research that allowed downlink LTE to take place in the 5.0 GHz band. However, LTE-LAA was not the first solution to support an anchor LTE link using unlicensed access. Prior to that, releases 10, 11, and 12 offered a different approach called LTE-Unlicensed (LTE-U) for countries that do not mandate an Listen-Before-Talk (LBT) mechanism. LTE-U relied on an ensemble of heuristic methods that did not require modifications to LTE air interface protocol. Rather, coexistence with other radio access technologies (RATs) was achieved through channel monitoring and adaptive transmission techniques [6]. 3GPP is taking an alternative policy in the evolution of 5th Generation (5G) wireless communications by incorporating unlicensed spectrum access from the early stages of development under the name 5G New Radio-Unlicensed (NR-U).

1.1 Motivation

It is widely recognized that radio spectrum is one of the scarcest and most regulated natural resources; nevertheless, static allocation policy by governmental agencies makes it underutilized. Recently, industry leaders from both 3GPP and IEEE have pressed for changes to make portions of the 1200 megahertz in the 6 GHz (5.925-7.125 GHz) frequency band available for unlicensed use [7-12]. The seemingly insatiable appetite of the telecommunications industry for more wireless bandwidth is driven by cogent reasoning that is simply manifested in the urgency

to accommodate forthcoming immense data flows. On April 23, 2020, the Federal Communications Commission (FCC) voted to adopt new rules for the 6 GHz band, unleashing 1200 megahertz of spectrum for license-exempt use. IEEE has formed a study group to discuss a potential amendment—IEEE 802.11be Extremely High Throughput (EHT)—that builds upon 802.11ax and operates in the new 6 GHz band, as well as the 2.4 and 5 GHz bands by virtue of their Enhanced Distributed Channel Access (EDCA) [13, 14]. Current 3GPP technical reports on NR-based access to unlicensed spectrum are considering the 6 GHz band as part of their study objectives. Furthermore, reports have identified LTE-LAA LBT mechanism as a baseline for the 5 GHz band and a starting point for the design for the 6 GHz band [15]. Despite similarities with EDCA, LTE-LAA became a controversial topic when first proposed by Qualcomm. After gaining momentum from other mobile wireless giants, the suggestion led to an acrimonious predicament between 3GPP and IEEE in terms of coexistence in the Industrial, Scientific, and Medical (ISM) frequency band. Numerous studies have been published on the feasibility of LTE coexisting with Wi-Fi. However, given the vastly presumed NR dense deployments, it is imperative to examine systems performance of next-generation wireless employing the LBT scheme. Considering that a new license-free radio band has been regulated, channel access schemes under new regulations should be revisited to ensure efficiency and fairness from both a homogeneous and heterogeneous standpoint.

Furthermore, some 3GPP technical reports have indicated the potential inclusion of the 2.4 GHz spectrum as part of the NR-U scope of operation [15]. In fact, the European Communications Committee (ECC) has issued mandates to include narrowband Very Low Power (VLP) frequency hoppers in the 6 GHz spectrum [16, 17]. Early proposals are expected to transfer the 2.4 GHz rules to 6 GHz, indicating that Bluetooth-like channel access schemes are expected in the new spectrum. These proposals warrant a closer look at potential coexistence among the developing technologies.

1.2 Contribution

This dissertation evaluates LBT performance as the channel access scheme for cellular systems operating in the unlicensed spectrum. The contributions of this work can be summarized as follows.

1. Analytical evaluation of different priority classes of LBT in a homogeneous coexistence setting, in terms of effective channel utilization and mean access delay [18].
2. Propose a modified LBT scheme for improving overall network performance under the studied scenarios of homogeneous LBT coexistence.
3. Empirical evaluation of the coexistence between cellular LBT systems and Bluetooth Low Energy (BLE) 5, providing an indicative study on how NR-U networks would perform in the 2.4 GHz, as well as reporting their effect on the prospective introduction of a frequency hopping system to the 6 GHz band [19].

The balance of this dissertation is organized as follows. Chapter 2 provides an overview of the discussed technologies, expounding the standardized LBT according to the European Telecommunications Standards Institute (ETSI) regulations. It also highlights new features of BLE 5. Chapter 3 surveys the literature on LTE-LAA and Wi-Fi channel access methods, as well as the coexistence of Wi-Fi with Bluetooth. An analytical model for LBT is developed in Chapter 4, and homogeneous coexistence analysis is presented therein. An improved LBT scheme is introduced and discussed in Chapter 5. Chapter 6 reports on the empirical coexistence evaluation of BLE 5 and cellular LBT systems. Chapter 7 concludes this dissertation and discusses future work.

Chapter 2

Technology Overview

2.1 5G New Radio-Unlicensed

5G NR-U is an evolution of the cellular mobile standard 4G LTE-LAA that has been formalized in Release 16 of the 3GPP specifications. The extension of cellular technologies into unlicensed bands is a promising solution to complement operators' licensed spectrum and, at the same time, bring technological advancements in the cellular air interfaces to the unlicensed medium. NR-U builds upon its predecessor's features by expanding deployment modes and increasing the scope of its viable use cases. Unlicensed channel access in LTE-LAA is possible only in conjunction with a licensed anchor that manages the control plane traffic while the user plane stream is offloaded to the unlicensed spectrum. Two modes of user plane augmentation are defined: 1) carrier aggregation (CA) in which unlicensed access is used only for downlink traffic, and 2) dual connectivity (DC), which supports both downlink and uplink user plane traffic. In addition to these two modes—known as non-standalone (NSA)—NR-U introduces a new standalone (SA) mode that supports operating a 5G network solely in the unlicensed band without requiring a licensed carrier. This particular feature of NR-U is expected to further expand the adoption of 5G beyond traditional cellular deployments and open the door to a multitude of applications and use cases. Promising examples



Figure 2.1: Spectrum allocation of the three unlicensed bands—2.4, 5, and 6 GHz [1].

include private 5G networks, Industry 4.0, new market verticals, such as health care and education to name a few. The frequency range in which NR-U is deployed dictates the required channel access mechanism since radio spectrum rules differ from one band to another. The CA and DC modes (i.e., NSA in NR-U) of LTE-LAA were designed to operate in the 5 GHz band, although NR-U's scope of operation is targeting all sub-7 GHz mid-band ranges in addition to mmWave bands in the 57 to 71 GHz range. Operating in the traditional and highly congested 2.4 and 5 GHz spectrum requires the system to ensure fair and harmonious coexistence with incumbent RATs. NSA modes necessitate stringent time synchronization requirements with the licensed anchor due to the time multiplexing nature of its radio interface, whereas SA mode is considered a green field that will provide greater freedom for technical and implementation concerns. Regardless of deployment mode, radio spectrum regulators in some regions require the technology to implement a channel sensing scheme in the unlicensed bands to detect ongoing transmissions and to prevent harmful interference. The mechanism employed by LTE-LAA, known as LBT, is discussed in detail below in Section 2.2 of this chapter. Despite LBT modifications imposed on NR-U, the technology is characterized by benefits from NR physical layer (PHY). Two such benefits are briefly outlined below.

Table 2.1: Supported Transmission Numerologies in NR Specifications

μ	Δf	CP
0	15 kHz	Normal
1	30 kHz	Normal
2	60 kHz	Normal, Extended
3	120 kHz	Normal
4	240 kHz	Normal

2.1.1 Waveform Numerology

The scalable numerology concept defines a flexible subcarrier spacing (SCS) rather than a fixed one—as in the case of LTE, making it possible to dynamically change waveform parameters (e.g., symbol, slot, and cyclic prefix (CP) durations). Numerologies are formed by scaling a fundamental SCS by an integer μ according to the following relation:

$$\Delta f = 2^\mu \times 15\text{kHz}. \quad (2.1)$$

Supported numerologies in NR specifications are summarized in Table 2.1. The need for such a set of waveform parameters stems from the wide range of operating frequency bands and the different characteristics they exhibit on which a fixed, single, and compatible subcarrier spacing is hard to satisfy.

2.1.2 Bandwidth Parts (BWP)

According to TS 38.211 [20], the carrier can be divided into subsets of contiguous physical resource blocks known as Bandwidth Parts (BWP). Each BWP can have its own numerology, which enables further flexibility and adaptability for supporting various quality of service requirements. Figure 2.2 illustrates the way in which waveform numerology and BWPs are related. This feature allows operators to integrate and multiplex different signals and services. For example, while one BWP may be providing a unique 5G service, another may be extending 4G support to legacy devices on the same carrier. Additionally, BWPs facilitate more control over spectral efficiency and power saving by allowing User Equipment (UE) to

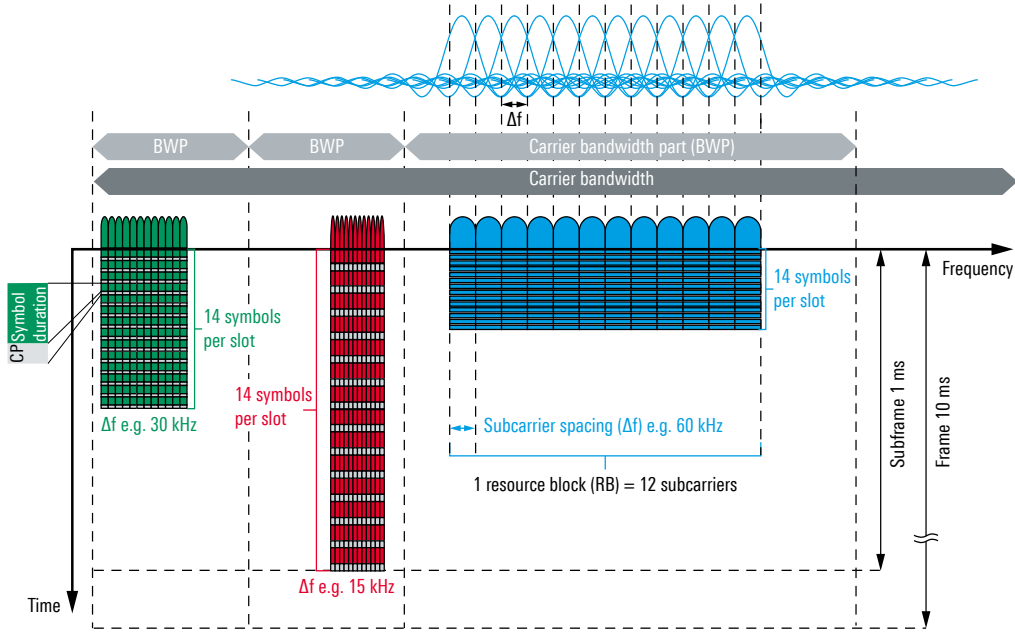


Figure 2.2: Relationship between bandwidth parts and waveform numerology in 5G NR PHY [2].

operate at a lower bandwidth when high data rate is not required. A maximum of 4 BWPs per UE can be configured for downlink and uplink; only one in each stream is active at any given point in time.

2.2 Listen-Before-Talk

Radio spectrum regulators in different regions of the world permit license-free transmissions on certain spectrum frequencies, as long as transmitters abide by a set of rules put forth by said regulators. Such rules guarantee no interference is imposed on other incumbents of the wireless medium. In the United States, for instance, the FCC is the governmental agency concerned with these matters. ETSI takes on that responsibility in the European Union. In the ISM bands, the FCC governs parameters such as maximum allowed transmit power, maximum channel bandwidth, and unintentional emissions of noise, among others. These rules are considered relatively relaxed compared to what ETSI mandates. In addition to FCC requirements, ETSI describes the channel access mechanism in

which devices are expected to exhibit, in addition to energy detection and preamble detection levels. Accordingly, some deem ETSI as the most influential body in the ISM bands, especially since the FCC merely mandates fair coexistence without specifying details and manufacturers tend to develop products that adhere to several markets' regulations.

Wi-Fi employs a method called Carrier Sense Multiple Access with Collision Avoidance (CSMA/CA), which constitutes the core that Distributed Coordination Function (DCF) and EDCA channel access schemes build upon. 3GPP, on the other hand, borrowed a similar technique from ETSI, referred to as *adaptivity* [3]. This section details the ETSI LBT and delineates the difference from 3GPP's early version.

2.2.1 Channel Access Mechanism in ETSI

LBT channel access is formally established in the ETSI EN 301 893 standard [3], termed adaptivity and defined as:

“An automatic mechanism by which a device limits its transmissions and gains access to an Operating Channel.”

The objective of adaptivity is to detect other in-band RATs transmissions and refrain from interfering with them given that the detected power is above a pre-defined threshold. Adaptivity ensures devices do not cause an inhibitory effect on each other. The ETSI standard defines two types of procedures for the purpose of adaptivity, namely Frame-Based Equipment (FBE) and Load-Based Equipment (LBE). In FBE mode, transmissions are framed within fixed time intervals, referred to as *Fixed Frame Period*, which range between one and 10 ms. Nodes operating in FBE mode are still required to perform a Clear Channel Assessment (CCA) before starting a transmission on the channel. CCA duration is defined as a single *Observation Slot*, which must be no less than $9 \mu s$. Multiple transmissions are allowed to take place within a fixed frame period providing the gap between

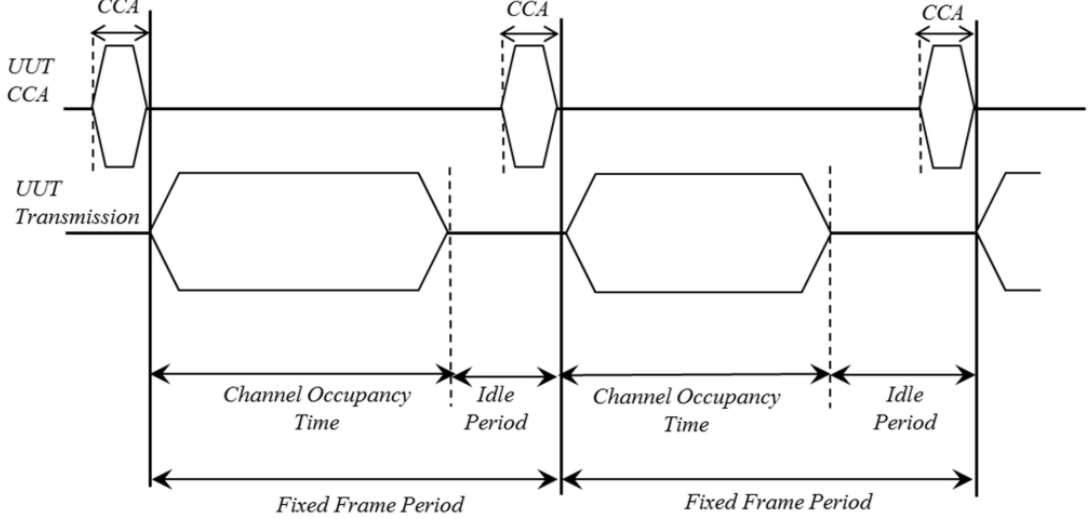


Figure 2.3: Timing diagram of Frame Based Equipment according to ETSI standard [3].

such transmissions does not exceed $16 \mu s$; otherwise, an additional CCA is required. The standard specifies the value of Energy Detection (ED) threshold as a function of the maximum transmit power permitted. Moreover, Channel Occupancy Time (COT) must be less than 95% of the fixed frame period to allow other devices to transmit. Figure 2.3 illustrates the timing of FBE mode operation.

In LBE, devices are demand-driven, and their transmissions are not restricted to time boundaries, like in FBE. In addition, LBE must determine the channel accessibility prior to transmit attempts. As aforementioned, the process through which a device gains access to the channel is referred to as LBT. Both FBE and LBE schemes are allowed to operate in a multi-channel setting, providing nodes with the ability to bond combinations of 20 MHz channels if they satisfy CCA requirements detailed in the standard.

LBE differs from FBE in the definition of priority classes for data frames. Four sets of channel access parameters are assigned to data packets, which determine contention behavior on the channel, as well as duration for which they are allowed to endure. High priority packets are more likely to gain access to the medium, yet for shorter durations. Table 2.2 lists the parameters of these classes. P_0 is the duration of a fixed prioritization interval in which nodes should perform

Table 2.2: LBT Priority Classes as Defined in the ETSI Standard

Class	P0	CW_{min}	CW_{max}	COT [ms]
4	1	4	8	2
3	1	8	16	4
2	3	16	64	6*
1	7	16	1024	6*

*extends to 8 ms if transmission includes 100 μs pauses

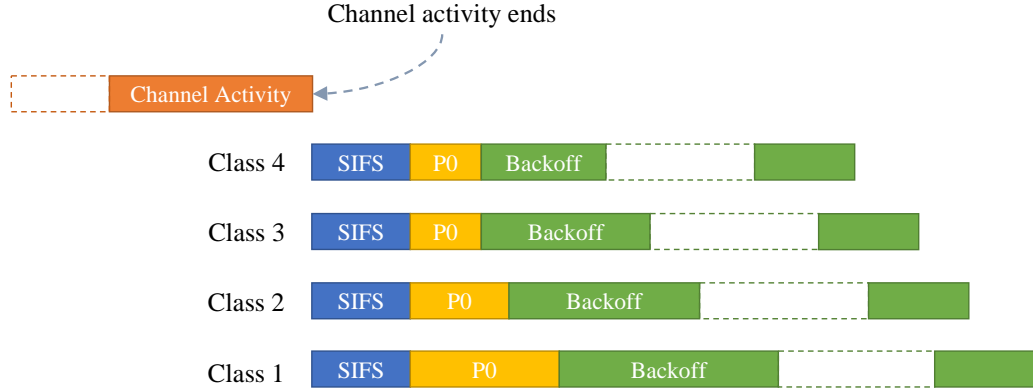


Figure 2.4: Timing relationship among four priority classes defined in ETSI.

before transitioning into the backoff procedure. P0 is basically an extended CCA interval; low priority classes must perform CCA for longer periods. CW_{min} and CW_{max} are the minimum and maximum contention window sizes, respectively. These two parameters dictate the length of the backoff procedure each class must implement. Finally, COT is the maximum channel occupancy time nodes must not exceed when utilizing the channel. P0 values and contention window sizes are determined in terms of the number of observation slots. Figure 2.4 depicts the timing relationship among the four priority classes. It is worth noting that the standard allows classes 1 and 2 to increase their COT to 8 ms, given that pauses of at least 100 μs are inserted during transmission.

The LBT procedure commences with a waiting period equal to 16 μs , referred to as Short Inter-Frame Spacing (SIFS) (See Figure 2.4). Following is the prioritization period, wherein the value is determined by packet class. Given that both periods expire without detected activity on the channel above the ED threshold,

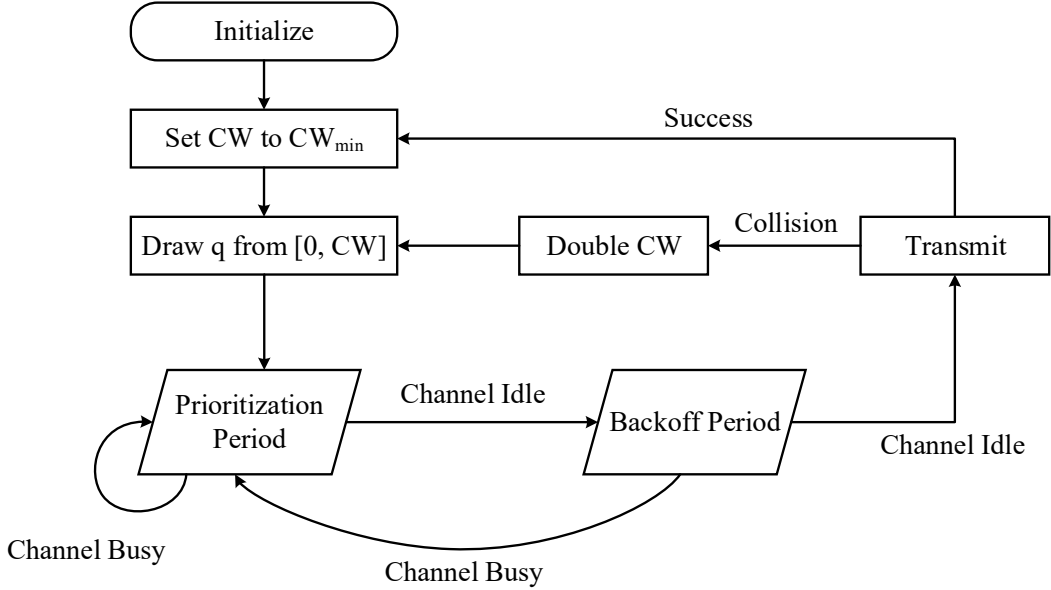


Figure 2.5: A high-level flowchart demonstrates the LBT procedure for Frame Based Equipment, as stipulated in ETSI standard.

the equipment may proceed to initiate the contention process (i.e., each observation slot in SIFS and P0 must pass a CCA). Subsequently, the backoff mechanism starts by initializing channel access parameters, which are also determined by the priority class of data traffic. This includes setting the contention window CW to its minimum value CW_{min} and drawing a random number q between 0 and $CW - 1$. The value of q is the number of time slots for which the device needs to perform CCA. During a single observation slot, the channel is considered occupied if transmissions were detected with a level above the ED threshold, in which case the LBT procedure starts anew with the SIFS period. Otherwise, the value of q is decremented by one. If q reaches 0, the device gains access to the channel and may proceed with transmission. Afterwards, given a failed transmission, the device may attempt a retransmission after adjusting its contention window size. CW is set to $2^i CW$, where i is the backoff stage (i.e., the contention window is doubled). Figure 2.5 demonstrates this procedure in a flowchart. For a more detailed flowchart, see Annex F in [3].

2.2.2 LBT in 3GPP Specifications

The 3GPP early version of LBT was published in Technical Report 36.889 [4] issued in 2015, which was borrowed from ETSI's regulations. Most of the research, including some recent works [21], disseminated on this topic relied on this earlier version of LBT. However, results do not fully comply with ETSI's adaptivity. Later in 2018, 3GPP released its standardized version of LBT in Technical Specifications 36.213 [22], which conforms to adaptivity rules outlined by the European institute. The following section expounds the early version of LBT to accentuate contrasts with the standardized procedure (i.e., ETSI LBT).

The channel access operation in TR 36.889 is classified into the following categories.

1. Category 1: No LBT.

Devices access the channel without performing a Clear Channel Assessment (CCA).

2. Category 2: LBT without random backoff.

Devices sense the channel for a deterministic period before transmission to ascertain that the channel is idle.

3. Category 3: LBT with random backoff and fixed contention window size.

LBT is implemented without binary exponential increase. (i.e., contention window size is not doubled, given collisions or failures).

4. Category 4: LBT with random backoff and binary exponential increase of contention window size.

Category 4 LBT is the recommended baseline scheme for implementation in TR 36.889 and other technical reports, owing to its near conformance with ETSI's regulations. This LBT scheme is split into two phases: 1) initial CCA (iCCA) and 2) extended CCA (ECCA). The procedure commences with iCCA. Given that the channel is sensed idle for $34 \mu s$, the equipment transmits for COT pertaining to

the frame’s priority class. Otherwise, ECCA phase starts by generating a random number from the contention window range. The equipment then waits for the channel to become idle for a deferment period of $34 \mu s$. Afterwards—for each observation slot in which the channel is sensed idle, the equipment decrements its backoff counter by one. Given this does not occur, the process restarts with ECCA. When the counter reaches 0, the device proceeds to transmit its packet. In the event of collisions and failures, contention window size is doubled. Figure 2.6 depicts a flowchart describing the procedure. Notably, the ECCA phase is very similar to ETSI’s adaptivity, and the iCCA at the beginning of the procedure gives the Category 4 LBT device an advantage over other coexisting devices implementing a random backoff period. This is the key difference between the early LBT scheme in TR 36.889 and the standardized scheme in TS 36.213.

Although the introduction of LBT makes LTE-LAA and NR-U on a par with Wi-Fi in the unlicensed spectrum, parameters of the two mechanisms are different, which may give LBT-enabled equipment an edge over Wi-Fi. For instance, 3GPP also defines frame priority classes in their LBT, similar to Table 2.2. However, values are larger for classes 1 and 2 (i.e., 8 ms), whereas COT values for EDCA classes range between 2.528 ms and 6.016 ms [23]. Moreover, EDCA mandates that data packets are assigned priorities relevant to the type of payload being sent (e.g., background, best effort, video, and voice). LBT does not impose a similar requirement on transmitting devices, and priorities are assigned regardless of the payload type.

The remainder of this dissertation addresses standardized 3GPP LBT as stipulated in ETSI’s EN 301 893, hereafter referred to as Listen-Before-Talk (LBT).

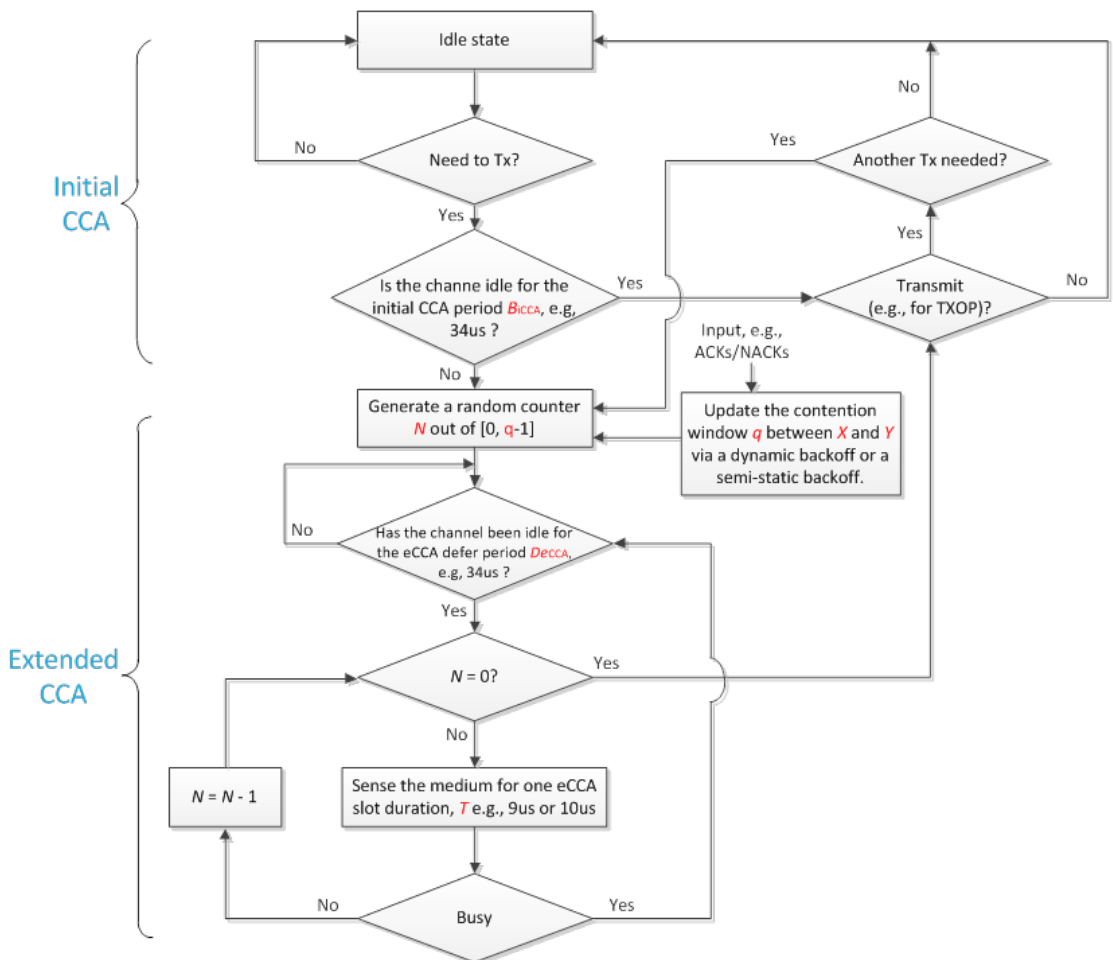


Figure 2.6: A flowchart describing the early LBT procedure published in TR 36.889 [4].

2.3 Bluetooth Low Energy 5

BLE 5 has ushered in major improvements; some of the most relevant are highlighted below.

2.3.1 PHY Modes

Prior to version 5, BLE utilized a single PHY with a symbol rate of 1 mega symbol per second (Msym/s). This remains the default setting in the new specifications and serves as a mandatory option in which all BLE 5 devices are required to support. However, new applications are emerging with requirements for higher data rates and low-power wireless communications (e.g., firmware upgrades delivering new functionalities and security improvements or uploading accrued sensor data to a companion device, such as a smartphone or a PC). A similar trend has been taking place in the health care industry (e.g., remote multi-lead electrocardiogram (ECG) devices [24, 25]). Hence, the Bluetooth SIG has introduced a 2 Msym/s PHY (2M PHY), promising twice the data rate as the original 1M PHY. The link layer packet format for both modes is the same, as depicted in Figure 2.7. Depending on utilized PHY, the preamble can be 1 byte (1M PHY) or 2 bytes (2M PHY) to maintain an $8 \mu\text{s}$ duration. This is followed by 4 bytes for the access address, 2 to 258 bytes of payload in the Packet Data Unit (PDU) field, and 3 bytes for CRC checksum and error detection. Both PHY modes utilize Gaussian Frequency Shift Keying (GFSK) modulation; however, since a higher symbol rate might produce inter-symbol interference (ISI), 370 kHz frequency deviation is used in 2M, while 185 kHz continues to be used in 1M PHY. No coding scheme is employed, and, therefore, error correction is not possible with these two physical layers. Since 2M PHY offers double the speed of the original 1M PHY, airtime used for transmitting a given amount of data is reduced. This, in turn, improves power consumption and spectral efficiency.

When long-range communication links are advantageous or when reliability

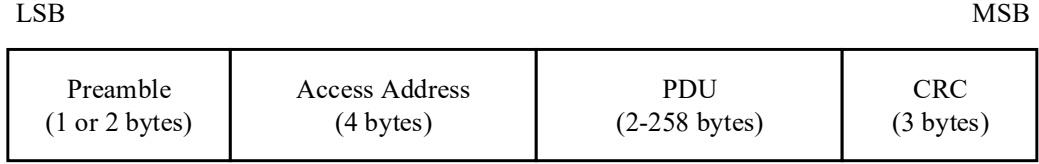


Figure 2.7: Link layer packet format for BLE uncoded 1M and 2M PHYs.

and robustness against interference is desirable, a third physical layer introduced by the Bluetooth SIG in version 5 of their core specification plays a convenient role. Long Range (LR)—technically known as Coded PHY—extends BLE feasible communication range beyond the typical 50-meter mark to achieve more than 1 km in distance, as reported by Nordic Semiconductor [26]. LR PHY makes use of Forward Error Correction (FEC) with symbol coding of 2 (S2) or 8 (S8) symbols per bit. Since this mode uses a physical rate of 1 Msym/s, resulting data rates are reduced to 500 kbps and 125 kbps for S2 and S8, respectively. A different link layer packet format is employed in LR PHY, as illustrated in Figure 2.8. Each packet comprises a preamble, FEC block 1, and FEC block 2. The preamble is 10 bytes long and not coded to allow cross-PHY detection. FEC block 1 consists of a 4-byte access address, coding indicator (CI), which denotes the coding scheme used in the following FEC block 2 (i.e., S2 or S8), and 3-byte termination field (TERM1). FEC block 1 is always coded with 8 symbols per bit regardless of the packet coding configuration (CI field). FEC block 2 contains the PDU, which is 2-257 bytes, 3-byte CRC, and a second 3-byte termination field (TERM2). The second FEC block is coded with either a S2 or S8 scheme. Notably, although coded PHY exhibits higher reliability than 2M and 1M PHYs by virtue of FEC, it also incurs lower throughput and higher power consumption due to larger packet sizes, which lead to longer radio-on times. Table 2.3 summarizes the three physical layers.

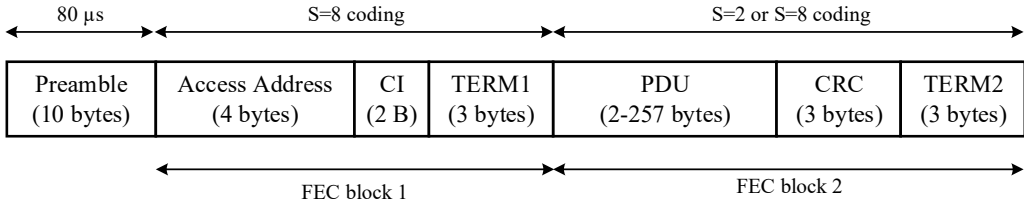


Figure 2.8: Link layer packet format for BLE Coded PHY (LR).

Table 2.3: Summary of BLE 5 Physical Layers

PHY	1M	Coded		2M
		S2	S8	
Symbol Rate	1 Msym/s	1 Msym/s	1 Msym/s	2 Msym/s
Data Rate	1 Mbps	500 kbps	125 kbps	2 Mbps
Error Detection	CRC	CRC	CRC	CRC
Error Correction	No	Yes	Yes	No
Requirement	Mandatory	Optional	Optional	Optional

2.3.2 Channel Selection Algorithm #2

Bluetooth technology employs Adaptive Frequency Hopping (AFH) to maneuver in-band interference. The link layer classifies the radio frequency (RF) channels into used channels and unused channels, creating a map that is applied during data transmission [27]. Before BLE 4, the channel sequence generation process utilized an algorithm that produced incremental, easy-to-track hopping patterns that were suboptimal for avoiding interference, given that hopping was not random and packets of the same connection event would use the same channel [28]. The new Channel Selection Algorithm (CSA) #2 is a more complex method and generates harder-to-track pseudo random sequences. In Figure 2.9, the hopping pattern of the two CSAs are compared across 100 connection events simulated in MATLAB using the Communication Toolbox™ Library [29]. CSA #2 employs a Pseudo Random Number Generator (PRNG) engine that requires two 16-bit inputs, a channel identifier, and a counter that increments with each connection event. The connection identifier is fixed for any given connection and is calculated by a bitwise XOR operation of the upper two bytes with the lower two bytes of the access

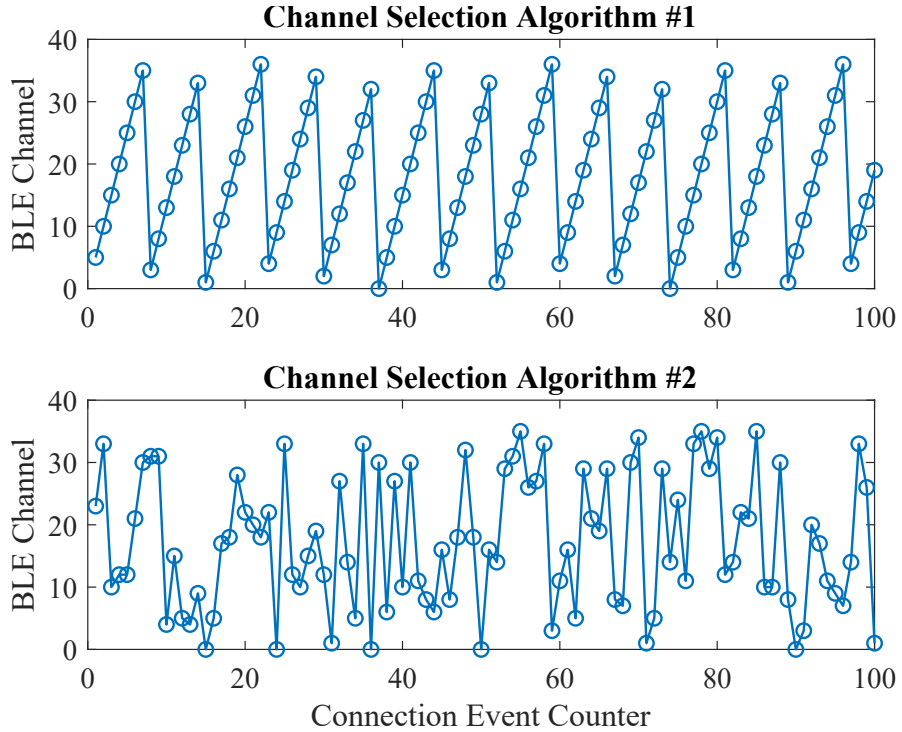


Figure 2.9: Channel hopping pattern of BLE channel selection algorithms #1 (top) and #2 (bottom) over 100 connection events.

address. PRNG output serves as the channel index for the next connection event. Since the link layer might classify some channels as unused, the generated channel index is remapped, given that it falls within the excluded channel list. Figure 2.10 depicts a high-level block diagram of the procedure. Readers interested in more details are referred to Section 4.5.8, Vol. 6, Part B in [27].

2.3.3 Maximum Transmit Power

To enhance link quality of BLE connections, version 5 specifications raised the maximum transmit power to 20 dBm (100 mW)—an increase from the previous limit of 10 dBm (10 mW). Furthermore, version 5.2 introduced a power control mechanism in which transmit power level of a connected remote device could be controlled to prevent receiver saturation and link failures in short-range use cases.

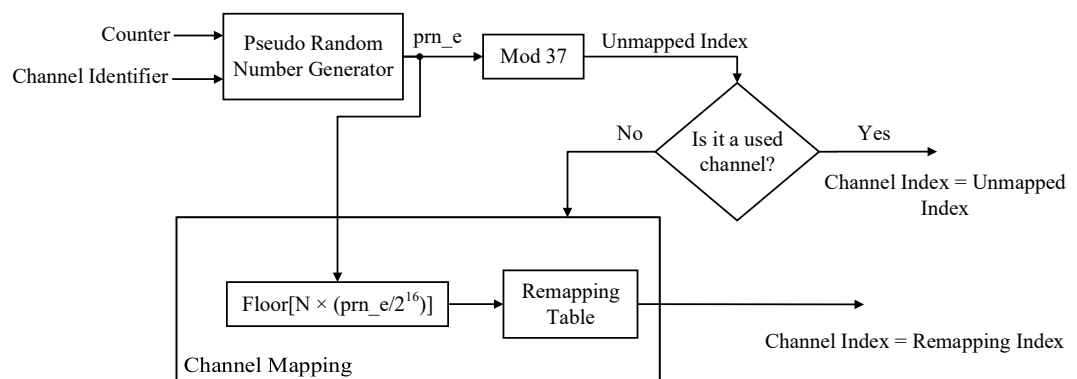


Figure 2.10: Block diagram of channel selection algorithm #2 introduced in BLE version 5.

Chapter 3

Related Work

The rivalry between LBT and EDCA constituents—from academic institutions and industry alike—have conducted significant research over the past few years pertaining to harmonious coexistence and adaptability. Before that, a great deal of research had been published on the modeling and analysis of EDCA’s precursor, DCF, which was defined in amendment 802.11b in 1999. Bianchi modeled DCF using Markov chains [30] and brought the attention to a powerful and novel tool. Thereafter, Markov chains has been the method of choice for analytical assessment of such systems. Works on channel access methods of LTE-LAA and Wi-Fi, in addition to their coexistence with Bluetooth, are discussed in this chapter.

3.1 Wi-Fi’s DCF and EDCA

In [31, 32] a Bianchi model was derived to analyze priority schemes in 802.11 EDCA. Saturation throughput and delay were investigated for two of the four access categories defined in the standard, namely background, best effort, video, and voice. A more complex model was proposed by Lee and Lee [33] in which they incorporated the Arbitrary Inter-Frame Spacing (AIFS) counter in their derivation. Analysis accuracy was compared with other models’. Kong et al. [34] proposed a similar Markov chain wherein counter freezing was modeled in the state space of the system. However, some transitions in the state diagram do not accurately

capture EDCA behavior as stipulated in the standard. Saturation throughput and delay of two access categories were examined, as well. Additionally, a heterogeneous case of the two access categories was also considered. Zheng [35] and Chatzimisios [36] took traffic load (i.e., non-saturated buffers) into account. Zheng discussed the effect of different factors, such as the imperfect wireless channel and the distribution of packet size. Chatzimisios evaluated the performance of 802.11a in terms of throughput, delay, and probability of packet drop, considering transmission errors and retransmission limit. A simplified analysis of binary exponential backoff algorithm utilized in DCF and EDCA was presented in [37], as were two different proposals for contention window adjustment. The paper offered analytical delay analyses for those algorithms with finite and infinite retransmission cases. Additional EDCA topics found in literature include proposals for backoff procedures other than binary exponential increase. In [38] a distributed backoff reservation technique was suggested. The authors aimed to tackle both fairness and collision-free channel access problems. The developed protocol assigns a backoff value for each contending station in a round robin fashion and relies on observing and counting the number of successful and unsuccessful transmissions on the channel to calculate a reserved contention value.

3.2 LTE-LAA and Coexistence with Wi-Fi

Mehrnoosh et al. [39] looked into the coexistence of LTE-LAA with Wi-Fi networks. Analysis was detailed by means of a Bianchi model variant and was validated by experimental simulation. Effect of energy detection threshold on throughput performance was investigated. The authors reported the impact of channel access parameters on the coexisting network (e.g., Wi-Fi or LTE-LAA). In technical specification 36.213 of release 13, 3GPP introduced a new channel access parameter which dictates the number of retransmissions a station could perform on a maximum backoff stage. This new addition to the LTE-LAA stan-

dard was modeled in [40] and coexistence with Wi-Fi was examined, including the impact of retransmission parameter. Authors in [41] modeled LBT and EDCA channel access schemes with traffic priorities as a Markov chain, employing packet arrival rate and probability of saturation. An approximate closed form for the probability of successful transmission was derived, as well. The authors simulated coexistence of LTE and Wi-Fi nodes, each serving four access categories. Co-existence was characterized in terms of achieved throughput, average contention delay, probability of successful transmission, and collision—all as a function of an equal number of LTE-LAA/Wi-Fi transmitters. LTE-LAA was assessed in [42], with respect to traffic priorities. Basic access and request-to-send/clear-to-send (RTS/CTS) mechanisms were examined. The paper addressed a mixed-priority case, but only controlled the number of Class 2 nodes in the scenario. Co-channel coexistence was empirically evaluated for LTE-LAA and Wi-Fi in [43]. Achieved throughput was investigated for both networks during a coexistence period, and channel occupancy of LTE-LAA system was measured for different Modulation and Coding Schemes (MCSs) without Wi-Fi interference. Xiao et al. purported in [44] that the time-synchronized subframes defined in release 13 create a problematic “gap” in a homogeneous LTE-LAA coexistence scenario. According to the authors, when a station captures the channel after a contention period, it waits for the boundary of the next subframe to transmit. This waiting gap could delude other contending stations that the channel remains idle. Consequently, stations collide at the next subframe. However, the standard clearly defines a reservation signal that fills the empty interval for preventing other contenders from occupying the channel [4]. The argument contended that the standard does not indicate the content and that duration of the reservation signal was irrelevant. The subsequent assumption of empty interval creates an obvious collision with other contending nodes.

Several studies have pointed to a case wherein coexisting RATs exhibit non-equal time slots. They note that the LTE-LAA standard specifies such a unit to

be *at least* 9 μ s. Therefore, nodes might adopt a longer time slot in their LBT procedure, which introduces an asynchronous behavior with other systems that use different timing values. In [45] this observation was modeled using a technique called heterogeneous superframe, which exploits the fact that the timing relationship between two time-shifted systems is restored after a busy slot. Authors compared their results with the regular Markov chain model and presented their findings in terms of normalized throughput. Ma et al. [46, 47] considered this observation as a jamming effect that could be disadvantageous to LTE-LAA when coexisting with Wi-Fi whilst utilizing a shorter time slot. The authors suggested a mechanism to overcome the alleged jamming effect by making LTE-LAA nodes reduce their slot duration to that of Wi-Fi's for one counter decrement after a channel busy duration, and then bringing it back to its default value.

Other investigations found in literature have looked at solutions to control coexistence among RATs in a shared wireless medium in the unlicensed band. In [48] an external controller was introduced to monitor the environment and adjust transmission power and bandwidth of LTE-LAA eNodeB (i.e., base station of LTE network) in order to alleviate harm caused to Wi-Fi in the vicinity. A similar approach, based on reported interference measurements and incurred contention delay, was proposed in [49] to control channel assignment of mobile operators running in the unlicensed spectrum.

3.3 Alternative LBT Schemes

In light of the heated discussion on feasibility of LTE operating alongside the long-time incumbent Wi-Fi in the unlicensed spectrum, some researchers have embarked on exploring means of improving the proposed LBT procedure. In [50] Challita et al. resorted to deep reinforcement learning and long short-term memory (LSTM) models to exploit past observations of the network state and predict channel availability and usage over a defined period. Authors leveraged the

experience an agent (i.e., LTE-LAA node) develops over time to allocate resources accordingly and achieve long-term airtime fairness with other LTE-LAA stations, as well as other incumbents. A similar application of reinforcement learning was reported in [51]. The proposed design relies on Q-Learning to teach the agent to find the optimal contention window size in a Wi-Fi environment. The proposed algorithm was simulated and compared with several other LTE access schemes in the unlicensed spectrum; algorithm feasibility was demonstrated. However, the authors assumed Wi-Fi access points would broadcast the number of users they serve, which might raise security concerns. Additionally, prioritized access was not considered in the design and analysis. In [52], contention window was adjusted dynamically such that all terminals in the channel utilized a fair and equal amount of airtime. Notably, the authors leaned on the work published in [53], which estimates statistics of the channel (e.g., idle slots, number of nodes, error probability, among others) and confused the results with the contention window size of each node observed on the channel.

Other endeavors have introduced cooperative communication into the unlicensed access of 5G NR [54]. The cooperative mechanism comprises communicating the backoff states of nodes through a primary licensed link. Hence, the work only considers non-standalone NR-U mode. When one or more stations seize the unlicensed medium, they cooperatively reuse the channel while mitigating interference by virtue of null-steering techniques. In their work, the authors reported that collision probability was reduced by 35% for NR-U devices. A p -persistent LBT was proposed in [55], wherein stations transmit with a probability of p after their backoff counters expire. The heterogeneous superframe approach was used to model the system and an optimization problem was formulated and solved for throughput-fairness trade-off.

3.4 Remarks

Although previous state-of-the-art studies have touched on important research questions and topics pertaining to LBT, the majority have been oriented towards coexistence with Wi-Fi and enhancing performance thereof. With the exception of [34] on EDCA and [42] on LBT, most of the reviewed work overlooked a same-technology analysis with respect to multi-class scenarios. Likewise, researchers failed to provide a comprehensive overview of the interplay of different class priorities relative to overall channel efficiency, per-node delay, and fairness. A study considering these variables would guide the development of better and more efficient channel access mechanisms for NR-U wireless systems and their operation in the new 6 GHz unlicensed band.

3.5 Coexistence with Bluetooth

Bluetooth and Wi-Fi have been longtime incumbents of the 2.4 GHz ISM band. Consequently, many works have addressed coexistence issues between the two. Howitt, et al. [56] presented an empirical analysis of coexistence relative to the IEEE 802.11b network and an early version of Bluetooth. The authors' investigation evaluated the interference power at which a retransmission is required. In [57], researchers evaluated the impact of Bluetooth 2.1 on the accuracy of Wi-Fi positioning algorithms. AFH was found to decrease the adverse effect on positioning performance. Analytical PHY analysis of BLE, 802.15.4 (ZigBee), and 802.11b (Wi-Fi) was presented in [58]. Expressions for packet error rates were derived as a function of distance provided by path-loss models and symbol error rates. PHY models of affected technologies were used to calculate the symbol error rate as a function of signal to interference ratio facilitated by path-loss models. However, analytical expressions did not capture the behavior of Medium Access Control (MAC) layer mechanisms, such as CSMA/CA and AFH. Instead, an experimental study was conducted to assess their behaviors. Performance of intra-vehicular

BLE-based and ZigBee-based wireless sensor networks was investigated in [59] in the presence of classical Bluetooth, as well as Wi-Fi interference. Results indicated Wi-Fi degrades both sensor network performances, although BLE-based networks demonstrated better resilience and robustness than ZigBee-based networks. Classical Bluetooth was evaluated empirically in [60] for music streaming and hands-free calling under interference from three 802.11n networks employing non-overlapping Wi-Fi channels (i.e., 1, 6, and 11). The study demonstrated the criticality of classical Bluetooth channels 71 through 78 for sustaining connectivity in a Wi-Fi-crowded environment. Results also indicated that a hands-free calling profile is more susceptible to interference than music streaming due to lack of retransmissions in the former. An extension to this work in the automotive domain when considering the mobility effect was reported in [61]. Bronzi, et al. [62] investigated BLE with one, two, and three Wi-Fi access points occupying the 2.4 GHz band, as well as in a vehicular communication setting. In [63], Ancans, et al. assessed the throughput of a BLE 5 device under test (DUT) in the presence of a single-channel Wi-Fi network with up to four BLE interferers in the environment. Several parameters of the DUT were investigated (e.g., connection interval, PHY layer, and packet size). Results suggested that the 1M BLE PHY layer is more robust to interference than the newly introduced 2M PHY in BLE 5, despite the fact that 2M PHY offers higher application throughput. Authors also reported the effect of multiple BLE links on a single BLE DUT as a function of its connection interval. Results revealed that a) application throughput deteriorates as the number of BLE devices sharing the spectrum increases and b) DUT becomes more susceptible to interference with longer connection interval—a behavior also observed in this dissertation under LBT interference and discussed in Section 6.3.1. In [64], a performance comparison of the three PHY modes of BLE 5 was presented; trade-offs, with respect to energy consumption, link reliability, and throughput were evaluated. Robustness to Wi-Fi interference was considered with only a single channel running 802.11b protocol. Another empirical study reported

in [65] compared BLE 5 operating in coded PHY (i.e., long range) with its precursor (i.e., BLE 4) in an indoor and outdoor setting in terms of communication range and throughput.

Chapter 4

5G NR-U Homogeneous Coexistence Analysis

In this chapter the channel access model of LBT is developed using Markov chains. The approach used herein follows the one proposed by Bianchi [30] to model 802.11 DCF. After the state space of the system is formed, one-step transition probabilities are determined to describe the LBT procedure. Thereafter, steady-state probabilities are derived as a function of a reference state and solved by imposing the normalization condition. The model is validated with simulation. Subsequently, same-technology homogeneous coexistence analysis is presented for one-class and two-class deployments. Finally, a case study on a 5G NR-U-enabled intensive care unit (ICU) hospital environment is presented to highlight how the selection of channel access parameters can impact the wireless coexistence of 5G-enabled medical devices with diverse risk profiles when operating in the unlicensed spectrum.

4.1 System Model

Each station¹ is assumed to operate in a saturation condition (i.e., a station always has data to transmit), and, consequently, is always trying to access the channel. In addition, the model assumes that each station is sending a single class of traffic (i.e., each station represents one priority class $c \in \mathcal{C} = \{1, 2, 3, 4\}$). Consider a number n_c of contending nodes. Since saturation condition is assumed, each node has a packet to transmit immediately and another to send after every successful transmission. When an attempt fails, the station moves to the next backoff stage until reaching the maximum level corresponding to its priority class m_c . Failed transmissions (or collisions) occur with a probability p_c with the assumption of ideal channel conditions to eliminate the effect of hidden terminals and channel errors on the collision probability.

Let $s(t)$ and $k(t)$ be stochastic processes that represent the backoff stage i and backoff counter j at time t , respectively. It is worth noting that each station's backoff counter is dependent upon the number of retransmissions the station has incurred. In this way, the process is said to be non-Markovian, since it depends on the history of transmissions and not just the current state. However, given the assumption that stations of the same priority class exhibit a constant collision probability (p_c) that is independent of retransmissions, the process $\{s(t), k(t)\}$ can be modeled using a Discrete-Time Markov Chain (DTMC), as depicted in Figure 4.1. Let $W_{c,i}$ be the contention window size of class c at backoff stage i , then by the definition of exponential backoff scheme

$$W_{c,i} = 2^i W_c \quad : \quad i \in [0, m_c], \quad (4.1)$$

where $W_c = CW_{c,min}$ is the minimum contention window size of class c , and m_c is the maximum backoff stage. By this definition, the maximum contention window size at the maximum backoff stage is given by:

¹“station” and “node” will be used interchangeably throughout this dissertation to refer to base stations, user equipment, and gNodeB.

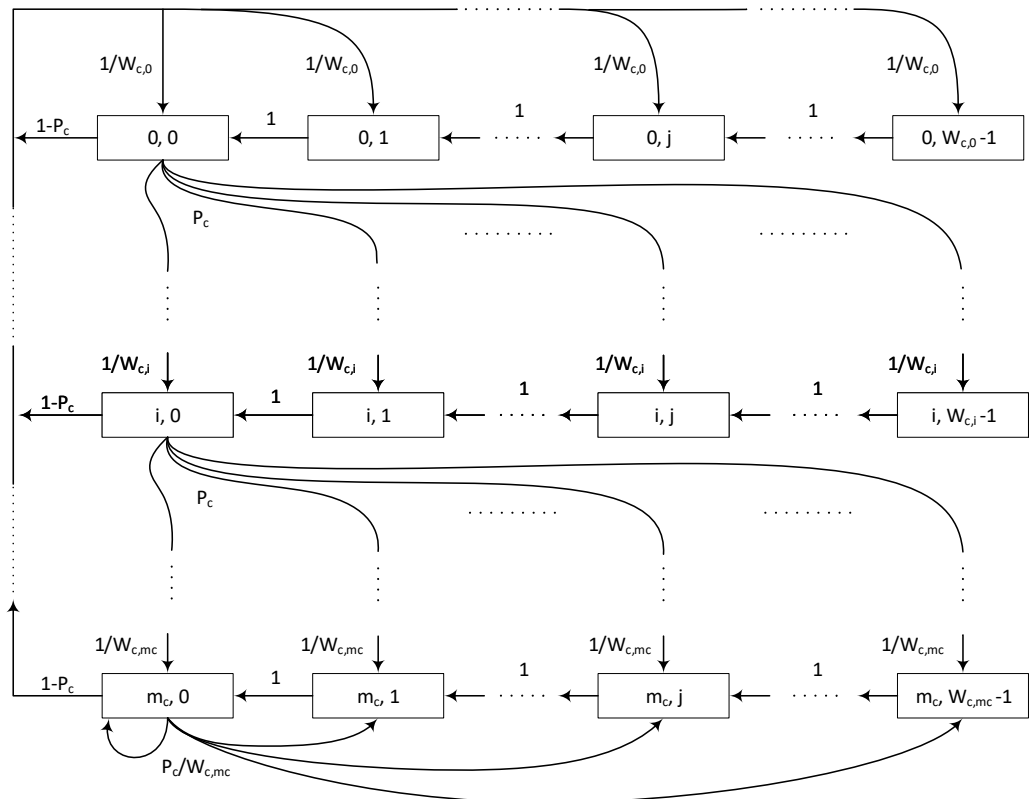


Figure 4.1: State transition diagram of the Markov chain model.

$$W_{c,m_c} = 2^{m_c} W_c.$$

States (i, j) , where $0 \leq i \leq m_c$ and $1 \leq j \leq W_{c,i} - 1$, model the backoff phase of a given station, while states $(i, 0)$ for $0 \leq i \leq m_c$ model the transmission attempts. Next, the one-step transition probabilities are derived.

4.1.1 One-Step Transition Probabilities

At any backoff stage $i \in [0, m_c]$, the backoff counter $j \in [1, W_{c,i} - 1]$ decrements at the beginning of an idle time slot, as per the LBT procedure discussed in Section 2.2. Thus,

$$\Pr\{i, j \mid i, j + 1\} = 1 \quad : \quad i \in [0, m_c], j \in [0, W_{c,i} - 2].$$

Following successful packets, stations begin with backoff stage 0 when attempting to serve a new packet. Such transitions occur with a probability of $1 - p_c$. Since the initial backoff counter value is chosen randomly and uniformly in the range $[0, W_{c,0} - 1]$, transition probabilities from any transmission state (i.e., $(i, 0)$ for $i \in [0, m_c]$) to backoff stage 0 (i.e., states $(0, j)$ for $j \in [0, W_{c,0} - 1]$) can be expressed as:

$$\Pr\{0, j \mid i, 0\} = \frac{1 - p_c}{W_{c,0}} \quad : \quad i \in [0, m_c], j \in [0, W_{c,0} - 1].$$

When transmissions in states $(i, 0)$ result in collisions, the station moves to the next backoff stage of its priority class. Such collisions occur with a probability p_c . Given the uniform distribution nature of selected random backoff counter values, the probability of transitioning to the next backoff stage is given by:

$$\Pr\{i, j \mid i - 1, 0\} = \frac{p_c}{W_{c,i}} \quad : \quad i \in [1, m_c], j \in [0, W_{c,i} - 1].$$

Finally, when collisions occur in the maximum backoff stage m_c , the back-

off process does not increment in subsequent packet retransmissions; instead, it remains in stage m_c until the packet is successfully transmitted. Therefore,

$$Pr\{m_c, j \mid m_c, 0\} = \frac{p_c}{W_{c,m_c}} \quad : \quad j \in [0, W_{c,m_c} - 1].$$

All one-step transitions are summarized in the following group of equations.

$$\left\{ \begin{array}{ll} Pr\{i, j \mid i, j + 1\} = 1 & : \quad i \in [0, m_c], j \in [0, W_{c,i} - 2] \\ Pr\{0, j \mid i, 0\} = \frac{1-p_c}{W_{c,0}} & : \quad i \in [0, m_c], j \in [0, W_{c,0} - 1] \\ Pr\{i, j \mid i - 1, 0\} = \frac{p_c}{W_{c,i}} & : \quad i \in [1, m_c], j \in [0, W_{c,i} - 1] \\ Pr\{m_c, j \mid m_c, 0\} = \frac{p_c}{W_{c,m_c}} & : \quad j \in [0, W_{c,m_c} - 1] \end{array} \right. \quad (4.2)$$

4.1.2 Steady-State Probabilities

A chain is called *irreducible* if all states can be reached pairwise from one another, i.e.,

$$\forall i, j \in S, \exists n \geq 1 : p_{i,j}^{(n)} > 0,$$

where S is the state space and $p_{i,j}^{(n)}$ is the n -step transition probability from state i to state j . In this same context, let d_i refer to the period of state i . As such, d_i is defined as the greatest common divisor of the number of steps n to revisit state i . That is, $d_i = \gcd(n) : p_{ii}^{(n)} > 0$. State i is called *aperiodic* if its $d_i = 1$. An irreducible, aperiodic DTMC with all states being positive recurrent is called an *ergodic* Markov chain [66].

Given the one-step transitions found in the previous section, the chain in Figure 4.1 is irreducible, aperiodic, and ergodic DTMC. Hence, according to properties of ergodic DTMCs [66], there exists a stationary distribution that is independent of the initial probability vector and comprises the unique steady-state probability distribution. Let $\pi(i, j)$ be the steady-state probability of state (i, j) , then

$$\pi(i, j) = \lim_{t \rightarrow \infty} Pr\{s(t) = i, k(t) = j\} \quad : \quad i \in [0, m_c], j \in [0, W_{c,i} - 1].$$

By virtue of chain regularities, one can show that a closed-form solution for steady-state probabilities of the considered Markov chain is feasible.

For $0 < i < m_c$ one can write

$$\begin{aligned}\pi(i, 0) &= \frac{p_c}{W_{c,i}}\pi(i-1, 0) + \pi(i, 1) \\ \pi(i, 1) &= \frac{p_c}{W_{c,i}}\pi(i-1, 0) + \pi(i, 2) \\ \pi(i, 2) &= \frac{p_c}{W_{c,i}}\pi(i-1, 0) + \pi(i, 3) \\ &\vdots \\ \pi(i, W_{c,i} - 2) &= \frac{p_c}{W_{c,i}}\pi(i-1, 0) + \pi(i, W_{c,i} - 1) \\ \pi(i, W_{c,i} - 1) &= \frac{p_c}{W_{c,i}}\pi(i-1, 0).\end{aligned}$$

By recursively substituting expressions backward,

$$\begin{aligned}\pi(i, W_{c,i} - 2) &= \frac{p_c}{W_{c,i}}\pi(i-1, 0) + \frac{p_c}{W_{c,i}}\pi(i-1, 0) = \frac{2p_c}{W_{c,i}}\pi(i-1, 0) \\ \pi(i, W_{c,i} - 3) &= \frac{2p_c}{W_{c,i}}\pi(i-1, 0) + \frac{p_c}{W_{c,i}}\pi(i-1, 0) = \frac{3p_c}{W_{c,i}}\pi(i-1, 0) \\ &\vdots \\ \pi(i, 2) &= \frac{W_{c,i} - 2}{W_{c,i}}p_c\pi(i-1, 0) \\ \pi(i, 1) &= \frac{W_{c,i} - 1}{W_{c,i}}p_c\pi(i-1, 0) \\ \pi(i, 0) &= \frac{W_{c,i}}{W_{c,i}}p_c\pi(i-1, 0) \Rightarrow \pi(i, 0) = p_c\pi(i-1, 0).\end{aligned}$$

This leads to

$$\pi(i, 0) = p_c^i\pi(0, 0) \quad : \quad 0 < i < m_c. \quad (4.3)$$

Similarly, for $i = m_c$:

$$\begin{aligned}
\pi(m_c, 0) &= \frac{p_c}{W_{c,m_c}} \pi(m_c - 1, 0) + \frac{p_c}{W_{c,m_c}} \pi(m_c, 0) + \pi(m_c, 1) \\
&\Rightarrow \left(1 - \frac{p_c}{W_{c,m_c}}\right) \pi(m_c, 0) = \frac{p_c}{W_{c,m_c}} \pi(m_c - 1, 0) + \pi(m_c, 1) \\
\pi(m_c, 1) &= \frac{p_c}{W_{c,m_c}} \pi(m_c - 1, 0) + \frac{p_c}{W_{c,m_c}} \pi(m_c, 0) + \pi(m_c, 2) \\
\pi(m_c, 2) &= \frac{p_c}{W_{c,m_c}} \pi(m_c - 1, 0) + \frac{p_c}{W_{c,m_c}} \pi(m_c, 0) + \pi(m_c, 3) \\
&\vdots \\
\pi(m_c, W_{c,m_c} - 2) &= \frac{p_c}{W_{c,m_c}} \pi(m_c - 1, 0) + \frac{p_c}{W_{c,m_c}} \pi(m_c, 0) + \pi(m_c, W_{c,m_c} - 1) \\
\pi(m_c, W_{c,m_c} - 1) &= \frac{p_c}{W_{c,m_c}} \pi(m_c - 1, 0) + \frac{p_c}{W_{c,m_c}} \pi(m_c, 0).
\end{aligned}$$

By recursive backward substitution:

$$\begin{aligned}
\pi(m_c, W_{c,m_c} - 2) &= \frac{2p_c}{W_{c,m_c}} [\pi(m_c - 1, 0) + \pi(m_c, 0)] \\
\pi(m_c, W_{c,m_c} - 3) &= \frac{3p_c}{W_{c,m_c}} [\pi(m_c - 1, 0) + \pi(m_c, 0)] \\
&\vdots \\
\pi(m_c, 2) &= \frac{W_{c,m_c} - 2}{W_{c,m_c}} p_c [\pi(m_c - 1, 0) + \pi(m_c, 0)] \\
\pi(m_c, 1) &= \frac{W_{c,m_c} - 1}{W_{c,m_c}} p_c [\pi(m_c - 1, 0) + \pi(m_c, 0)] \\
\left(1 - \frac{p_c}{W_{c,m_c}}\right) \pi(m_c, 0) &= \frac{p_c}{W_{c,m_c}} \pi(m_c - 1, 0) \\
&\quad + \frac{W_{c,m_c} - 1}{W_{c,m_c}} p_c [\pi(m_c - 1, 0) + \pi(m_c, 0)] \\
\Rightarrow \left(1 - \frac{p_c}{W_{c,m_c}}\right) \pi(m_c, 0) &= p_c \pi(m_c - 1, 0) + \frac{W_{c,m_c} - 1}{W_{c,m_c}} p_c \pi(m_c, 0) \\
\Rightarrow \left[1 - \left(\frac{1}{W_{c,m_c}} + \frac{W_{c,m_c} - 1}{W_{c,m_c}}\right) p_c\right] \pi(m_c, 0) &= p_c \pi(m_c - 1, 0) \\
\Rightarrow (1 - p_c) \pi(m_c, 0) &= p_c \pi(m_c - 1, 0).
\end{aligned}$$

Using relation (4.3),

$$\begin{aligned}(1 - p_c)\pi(m_c, 0) &= p_c \times p_c^{m_c-1}\pi(0, 0) = p_c^{m_c}\pi(0, 0) \\ \Rightarrow \pi(m_c, 0) &= \frac{p_c^{m_c}}{1 - p_c}\pi(0, 0).\end{aligned}\tag{4.4}$$

The remaining steady-state probabilities $\pi(i, j)$ for $1 \leq j \leq W_{c,i} - 1$ and $0 \leq i \leq m_c$ can be expressed in terms of transmission states probabilities $\pi(i, 0)$, and, in turn, of steady-state probability $\pi(0, 0)$ by means of relation (4.3). One can derive these probabilities by breaking them down into three groups: 1) initial backoff stage $i = 0$; 2) middle backoff stages $0 < i < m_c$; and 3) maximum backoff stage $i = m_c$.

Consider backoff stage $i = 0$:

$$\begin{aligned}\pi(0, W_{c,0} - 1) &= \frac{1 - p_c}{W_{c,0}} \sum_{i=0}^{m_c} \pi(i, 0) \\ \pi(0, W_{c,0} - 2) &= \pi(0, W_{c,0} - 1) + \frac{1 - p_c}{W_{c,0}} \sum_{i=0}^{m_c} \pi(i, 0) \\ &= \frac{2}{W_{c,0}}(1 - p_c) \sum_{i=0}^{m_c} \pi(i, 0) \\ &\vdots \\ \pi(0, 2) &= \frac{W_{c,0} - 2}{W_{c,0}}(1 - p_c) \sum_{i=0}^{m_c} \pi(i, 0) \\ \pi(0, 1) &= \frac{W_{c,0} - 1}{W_{c,0}}(1 - p_c) \sum_{i=0}^{m_c} \pi(i, 0).\end{aligned}$$

By induction, one can generalize

$$\pi(0, j) = \frac{W_{c,0} - j}{W_{c,0}}(1 - p_c) \sum_{i=0}^{m_c} \pi(i, 0) \quad : \quad j \in [1, W_{c,i} - 1].$$

Summation in this expression is a geometric series that can be simplified as follows.

$$\sum_{i=0}^{m_c} \pi(i, 0) = \pi(0, 0) + \sum_{i=1}^{m_c-1} \pi(i, 0) + \pi(m_c, 0).$$

Using relations (4.3) and (4.4),

$$\begin{aligned}
\sum_{i=0}^{m_c} \pi(i, 0) &= \pi(0, 0) + \sum_{i=1}^{m_c-1} p_c^i \pi(0, 0) + \frac{p_c^{m_c}}{1-p_c} \pi(0, 0) \\
&= \pi(0, 0) \left(1 + \frac{p_c^{m_c}}{1-p_c} + \sum_{i=1}^{m_c-1} p_c^i \right) \\
&= \pi(0, 0) \left(1 + \frac{p_c^{m_c}}{1-p_c} + \frac{p_c(1-p_c^{m_c-1})}{1-p_c} \right) \\
&= \frac{1}{1-p_c} \pi(0, 0).
\end{aligned}$$

This, in turn, yields

$$\pi(0, j) = \frac{W_{c,0} - j}{W_{c,0}} \pi(0, 0) \quad : \quad j \in [1, W_{c,0} - 1]. \quad (4.5)$$

When $0 < i < m_c$,

$$\begin{aligned}
\pi(i, W_{c,i} - 1) &= \frac{p_c}{W_{c,i}} \pi(i-1, 0) \\
\pi(i, W_{c,i} - 2) &= \frac{p_c}{W_{c,i}} \pi(i-1, 0) + \pi(i, W_{c,i} - 1) \\
&\vdots \\
\pi(i, 2) &= \frac{p_c}{W_{c,i}} \pi(i-1, 0) + \pi(i, 3) \\
\pi(i, 1) &= \frac{p_c}{W_{c,i}} \pi(i-1, 0) + \pi(i, 2).
\end{aligned}$$

By substituting probabilities of higher backoff counter stages into the lower ones, all steady-state probabilities at a given backoff stage can be described in terms of

a preceding transmission state:

$$\begin{aligned}
\pi(i, W_{c,i} - 1) &= \frac{p_c}{W_{c,i}} \pi(i - 1, 0) \\
\pi(i, W_{c,i} - 2) &= \frac{2p_c}{W_{c,i}} \pi(i - 1, 0) \\
&\vdots \\
\pi(i, 1) &= \frac{W_{c,i} - 1}{W_{c,i}} p_c \pi(i - 1, 0)
\end{aligned}$$

Thus,

$$\pi(i, j) = \frac{W_{c,i} - j}{W_{c,i}} p_c \pi(i - 1, 0).$$

Since $0 < i < m_c$, using (4.3),

$$\pi(i, j) = \frac{W_{c,i} - j}{W_{c,i}} \pi(i, 0) \quad : \quad 0 < i < m_c, j \in [1, W_{c,i} - 1]. \quad (4.6)$$

Finally, for $i = m_c$:

$$\begin{aligned}
\pi(m_c, W_{c,m_c} - 1) &= \frac{p_c}{W_{c,m_c}} \pi(m_c - 1, 0) + \frac{p_c}{W_{c,m_c}} \pi(m_c, 0) \\
&= \frac{p_c}{W_{c,m_c}} [\pi(m_c - 1, 0) + \pi(m_c, 0)] \\
\pi(m_c, W_{c,m_c} - 2) &= \frac{p_c}{W_{c,m_c}} [\pi(m_c - 1, 0) + \pi(m_c, 0)] + \pi(m_c, W_{c,m_c} - 1) \\
&\vdots \\
\pi(m_c, 1) &= \frac{p_c}{W_{c,m_c}} [\pi(m_c - 1, 0) + \pi(m_c, 0)] + \pi(m_c, 2).
\end{aligned}$$

Like the previous case, the expressions can be rewritten as

$$\begin{aligned}\pi(m_c, W_{c,m_c} - 1) &= \frac{p_c}{W_{c,m_c}} [\pi(m_c - 1, 0) + \pi(m_c, 0)] \\ \pi(m_c, W_{c,m_c} - 2) &= \frac{2p_c}{W_{c,m_c}} [\pi(m_c - 1, 0) + \pi(m_c, 0)] \\ &\vdots \\ \pi(m_c, 1) &= \frac{W_{c,m_c} - 1}{W_{c,m_c}} p_c [\pi(m_c - 1, 0) + \pi(m_c, 0)]\end{aligned}$$

and, in general,

$$\pi(m_c, j) = \frac{W_{c,m_c} - j}{W_{c,m_c}} p_c [\pi(m_c - 1, 0) + \pi(m_c, 0)].$$

This can be further simplified by making use of relations (4.3) and (4.4):

$$\begin{aligned}p_c [\pi(m_c - 1, 0) + \pi(m_c, 0)] &= p_c \left(p_c^{m_c-1} \pi(0, 0) + \frac{p_c^{m_c}}{1-p_c} \pi(0, 0) \right) \\ &= \left(p_c^{m_c} + \frac{p_c^{m_c+1}}{1-p_c} \right) \pi(0, 0) \\ &= \left(\frac{p_c^{m_c}}{1-p_c} \right) \pi(0, 0) \\ &= \pi(m_c, 0).\end{aligned}$$

Accordingly,

$$\pi(m_c, j) = \frac{W_{c,m_c} - j}{W_{c,m_c}} \pi(m_c, 0) \quad : \quad j \in [1, W_{c,m_c} - 1]. \quad (4.7)$$

Relations (4.5), (4.6), and (4.7) can be rewritten concisely as

$$\pi(i, j) = \frac{W_{c,i} - j}{W_{c,i}} \pi(i, 0) \quad : \quad i \in [0, m_c], j \in [1, W_{c,i} - 1]. \quad (4.8)$$

Thus, by means of expressions (4.3), (4.4), and (4.8), steady-state probabilities of all states are described as a function of the probability $\pi(0, 0)$ and probability of collision p_c . In the next section, the probability of transmission τ_c is derived.

4.1.3 Probability of Transmission

A station of class c transmits when the backoff counter expires at any stage, given that the channel is determined to be idle. Such a station transmits with a probability τ_c given by:

$$\tau_c = \sum_{i=0}^{m_c} \pi(i, 0) = \frac{\pi(0, 0)}{1 - p_c}.$$

By imposing the normalization condition, it is possible to find $\pi(0, 0)$ as a function of the conditional collision probability p_c .

$$\begin{aligned} 1 &= \sum_{i=0}^{m_c} \sum_{j=0}^{W_{c,i}-1} \pi(i, j) \\ &= \sum_{i=0}^{m_c} \sum_{j=0}^{W_{c,i}-1} \frac{W_{c,i} - j}{W_{c,i}} \pi(i, 0) \\ &= \sum_{i=0}^{m_c} \pi(i, 0) \sum_{j=0}^{W_{c,i}-1} \frac{W_{c,i} - j}{W_{c,i}} \\ &= \sum_{i=0}^{m_c} \pi(i, 0) \frac{W_{c,i} + 1}{2} \\ &= \frac{1}{2} \left[\sum_{i=0}^{m_c} \pi(i, 0) W_{c,i} + \sum_{i=0}^{m_c} \pi(i, 0) \right]. \end{aligned}$$

The second term has been shown to be $\sum_{i=0}^{m_c} \pi(i, 0) = \frac{1}{1-p_c} \pi(0, 0)$, and using (4.1):

$$\begin{aligned}
1 &= \frac{1}{2} \left[\sum_{i=0}^{m_c} \pi(i, 0) 2^i W_c + \frac{1}{1-p_c} \pi(0, 0) \right] \\
&= \frac{1}{2} \left[\sum_{i=0}^{m_c-1} \pi(i, 0) 2^i W_c + 2^{m_c} W_c \pi(m_c, 0) + \frac{1}{1-p_c} \pi(0, 0) \right] \\
&= \frac{1}{2} \left[\sum_{i=0}^{m_c-1} 2^i p_c^i W_c \pi(0, 0) + 2^{m_c} W_c \frac{p_c^{m_c}}{1-p_c} \pi(0, 0) + \frac{1}{1-p_c} \pi(0, 0) \right] \\
&= \frac{\pi(0, 0)}{2} \left[W_c \sum_{i=0}^{m_c-1} (2p_c)^i + 2^{m_c} W_c \frac{p_c^{m_c}}{1-p_c} + \frac{1}{1-p_c} \right] \\
&= \frac{\pi(0, 0)}{2} \left(W_c \frac{(2p_c)^{m_c} - 1}{2p_c - 1} + \frac{W_c (2p_c)^{m_c} + 1}{1-p_c} \right) \\
&= \frac{\pi(0, 0)}{2} \left(\frac{(1-2p_c)(W_c+1) + p_c W_c (1-(2p_c)^{m_c})}{(1-2p_c)(1-p_c)} \right) \\
\Rightarrow \pi(0, 0) &= \frac{(1-2p_c)(1-p_c)}{(1-2p_c)(W_c+1) + p_c W_c (1-(2p_c)^{m_c})}.
\end{aligned}$$

Thus, probability of transmission becomes

$$\tau_c = \frac{(1-2p_c)}{(1-2p_c)(W_c+1) + p_c W_c (1-(2p_c)^{m_c})}. \quad (4.9)$$

Probability that a class c station transmits a packet in a randomly selected time slot is a function of the conditional probability of collision p_c ; the minimum contention window size of that class W_c .

4.1.4 Formulating a Homogeneous Scenario

Analyses presented in this chapter are technology agnostic. That is to say, evaluation of metrics, such as percentage of successful transmission and collision, are calculated based on channel occupancy times (COT) pertaining to each frame priority class, regardless of modulation scheme and bit rate used. Consequently, even when packets collide, it is assumed that stations transmit for the entire period of their COT.

From the perspective of stations, a transmitted packet—in spite of its subse-

quent outcome of being successful or not—collides with a conditional probability p_c (i.e., probability that at least one of the remaining $n_c - 1$ stations transmit concurrently). Put differently, the probability that a given station *transmits* and *succeeds* is $\tau_c(1 - p_c)$. Equivalently, it is the probability that a considered station *transmits* while the other $n_c - 1$ *do not* (i.e., $\tau_c(1 - \tau_c)^{n_c-1}$). Thus,

$$\begin{aligned} \tau_c(1 - p_c) &= \tau_c(1 - \tau_c)^{n_c-1} \Rightarrow \\ p_c &= 1 - (1 - \tau_c)^{n_c-1}. \end{aligned} \tag{4.10}$$

Equations (4.9) and (4.10) form a nonlinear system in two unknowns: τ_c and p_c . The remaining variables are known once the priority class of a station is determined. Numerically solving the system of equations yields the unknowns.

Assuming a homogeneous scenario where all nodes are of the same class, let γ_c be the probability that at least one station of class c transmits:

$$\gamma_c = 1 - (1 - \tau_c)^{n_c}. \tag{4.11}$$

Then, the probability that a successful transmission of class c occurs on the channel is given by conditioning the probability that *exactly one* station transmits by the probability that *at least one* station transmits:

$$\rho_c = \frac{n_c \tau_c (1 - \tau_c)^{n_c-1}}{\gamma_c}. \tag{4.12}$$

Let ψ_c be the effective channel utilization of class c —defined as the ratio of time the channel is used to successfully transmit packets of class c over the average channel time. Hence,

$$\psi_c = \frac{\gamma_c \rho_c T_c}{(1 - \gamma_c)\sigma + \gamma_c \rho_c T_c + \gamma_c(1 - \rho_c)T_c}, \tag{4.13}$$

where σ is the unit time slot duration (observation slot) and $T_c = COT$ is the max-

imum class occupancy time. Average channel time in the denominator accounts for: a) idle time slots that occur with probability $1 - p_c$, b) successful transmission slots, with probability $\gamma_c \rho_c$, and c) collisions, with probability $\gamma_c(1 - \rho_c)$.

4.1.5 Model Validation

To validate the analytical model and appraise its accuracy, an event-driven stochastic simulator was developed in C++ for imitating the LBT procedure, as described in ETSI regulations discussed in Section 2.2.1. The simulator closely follows the detailed description of channel access mechanism for LBE and the flowchart found in Annex F of [3]. Same as the assumptions of the analytical model, the simulator postulates ideal channel conditions, lack of hidden-terminals, and saturated single-class-traffic stations. Once they capture the channel, stations transmit for the time period corresponding to their priority class reported in Table 2.2.

Figure 4.2 depicts the effective channel utilization obtained from the simulator and equation (4.13) of the analytical model. The figure shows channel utilization of homogeneous coexistence for different priority classes, each with a varying number of contending nodes n_c . It also demonstrates the accuracy of the derived DTMC model, where analytical results represented by solid lines significantly overlap with simulation results illustrated by round markers. All simulation results were obtained from independent runs of the simulator equivalent to 200 seconds of airtime. Microsecond-precision statistics on idle, successful, and collision times were collected to calculate corresponding metrics.

4.2 One-Class Dense Deployment

The model developed in Section 4.1 facilitates the investigation of various scenarios and settings of coexistence. Two main cases are inspected in this chapter. The first is one-class coexistence, where the wireless medium is assumed to be utilized by same-class nodes for investigating and separately comparing performance of

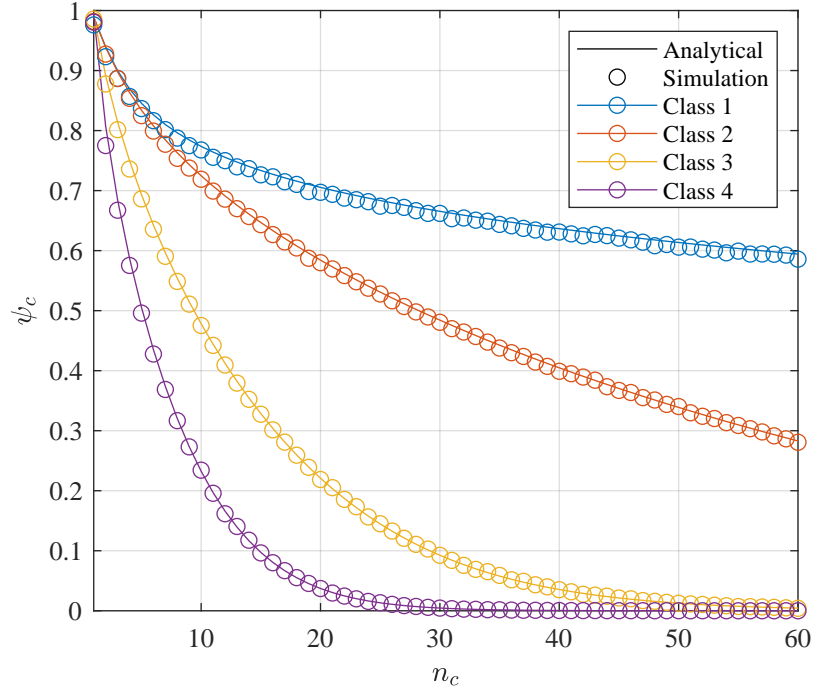


Figure 4.2: Effective channel utilization vs. number of contending nodes in homogeneous class setting, for both, analytical and simulation results.

each priority level. In the second case, channel access priorities are studied in pairs later in Section 4.3 to gauge repercussions of one LBT priority on another. Channel utilization, collision probability, and access delay are examined for those cases.

Assuming a scenario where all coexisting devices are of the same priority class, this section defines and evaluates various metrics for all four priority classifications.

4.2.1 Effective Channel Utilization

Effective Channel Utilization (ECU) is defined as the percentage of aggregate time the channel is occupied to successfully transmit packets by any coexisting station. If a station successfully completes a transmission, then it has occupied the channel for a period of COT pertaining to its class without colliding with another station's transmission. ECU offers a comprehensive overview on the extent to which the channel is efficiently utilized without collisions.

Figure 4.2, above, resembles a typical dense deployment of a future NR-U network. Figure 4.3 takes the example to an extreme case, where ECU is evaluated

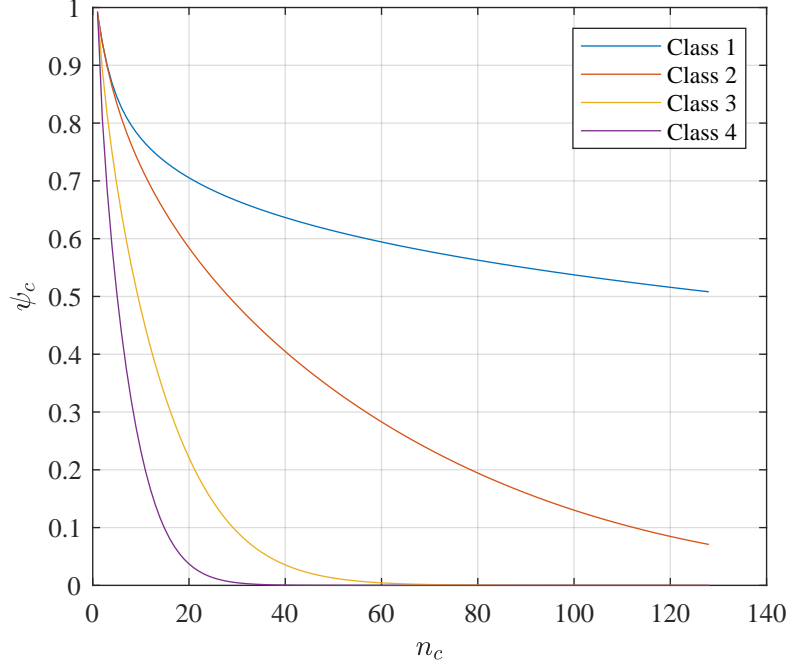


Figure 4.3: ECU as a function of the contending nodes number for all four priority classes sharing the channel homogeneously.

for a number of stations varying from 1 to 128. Results indicate that ECU declines dramatically as the number of contending stations increases. Classes 3 and 4 exhibit an inferior performance compared to the two lower priority types; class 2 drops well below 50% after 30 devices share the channel. In contrast, at 20 nodes, ECU of classes 3 and 4 drops to 22% and 3.7%, respectively. Since saturation conditions are assumed, idle times have a negligible effect on channel utilization. This observation suggests that decline in ECU is largely caused by collisions on the channel.

Let ϕ_c denote the normalized time the channel contains collisions from priority class c traffic. Hence, similar to the definition of ψ_c in (4.13), ϕ_c is defined as

$$\phi_c = \frac{\gamma_c(1 - \rho_c)T_c}{(1 - \gamma_c)\sigma + \gamma_c\rho_cT_c + \gamma_c(1 - \rho_c)T_c}. \quad (4.14)$$

Figure 4.4 plots the percentage of channel collisions for each priority class as a function of the number of contending stations. The plot corroborates that under saturation condition ψ_c and ϕ_c compose most of the channel time, whereas idle time slots are insignificant. Consequently, deteriorating ECU is attributed to

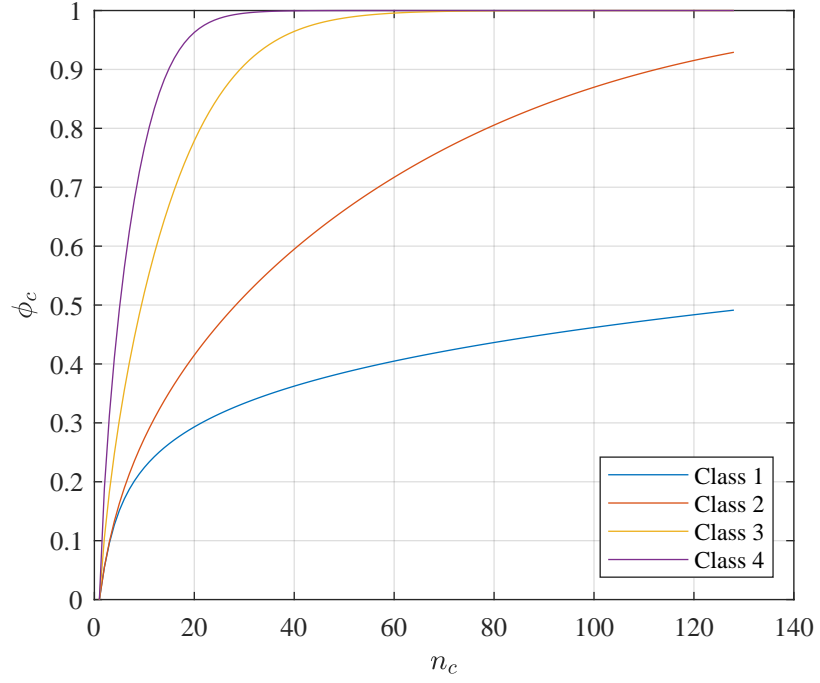


Figure 4.4: Channel collisions as a function of the contending nodes number for all four priority classes sharing the channel homogeneously.

collisions on the channel. Since the scenario at issue is a homogeneous case with ideal channel assumption, channel collisions can be imputed due to the fact that multiple nodes pick the same value during backoff procedure after the channel becomes idle. When their counters expire, stations transmit simultaneously at the exact moment. Given that classes 3 and 4 exhibit smaller contention window sizes, these classes are more susceptible to intra-network collisions (i.e., within networks of the same type) than the other two priority types.

This scenario is similar to the Birthday Problem, which states that in a room of 23 persons there is a 50% chance that at least two people have the same birthday. Similarly, the probability is greater than 50% that at least two of the four class 4 stations in a maximum backoff stage will select the same backoff value. This possibility is easily found in terms of complement probability $\bar{p}(n)$ that all $n = 4$ stations select *different* backoff values. In the maximum backoff stage there are

eight possibilities ($CW_{max} = 8$), including zero, from which a station could choose.

$$\begin{aligned}\bar{p}(n) &= 1 \times \left(1 - \frac{1}{8}\right) \times \left(1 - \frac{2}{8}\right) \times \left(1 - \frac{3}{8}\right) \\ &= 0.41015625 \\ \Rightarrow 1 - \bar{p} &= 0.58984375\end{aligned}$$

This process can be generalized to a number of n stations, where $p(n, w)$ is the probability that at least two stations select the same backoff value in stage m_c corresponding to a contention window size w :

$$p(n, w) = 1 - \prod_{k=1}^{n-1} \left(1 - \frac{k}{w}\right).$$

Figure 4.5 illustrates this probability for various contention window sizes that are compatible with priority classes 4, 3, and 2. Given a fixed number of stations, probability will drop as the window size increases. This phenomenon explains why classes 1 and 2 perform better than classes 3 and 4.

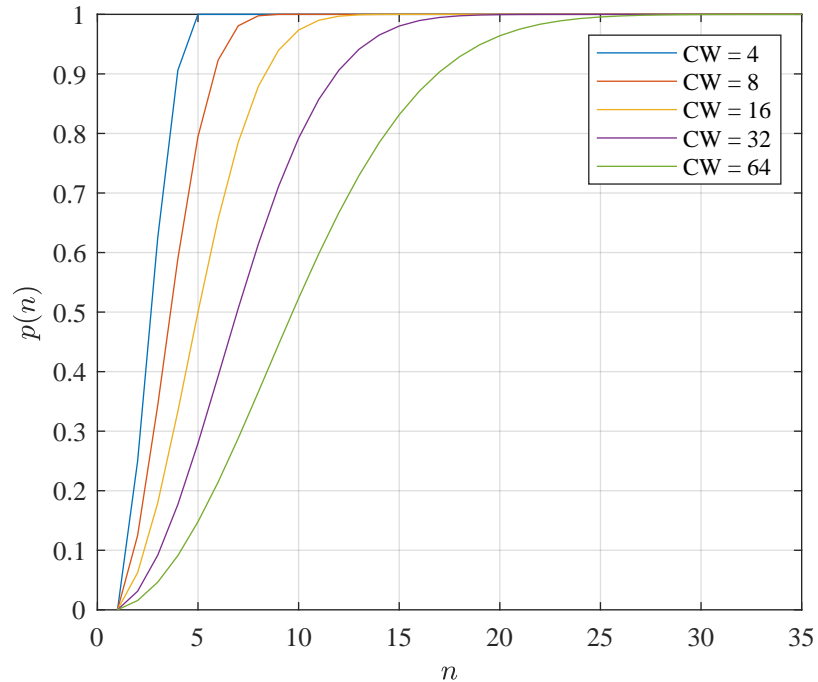


Figure 4.5: Probability that at least two stations draw the same number in the backoff stage, as a function of the number of contending nodes n .

4.2.2 Mean Access Delay

Mean recurrence time of a DTMC state i is defined as the average time to return to state i . Section 4.1.2 demonstrated that the developed Markov model is an ergodic DTMC. A property of ergodic Markov chains informs that steady-state probabilities $\pi(i, j)$ and mean recurrence times $m_{i,j}$ for corresponding states are inversely proportional:

$$\pi(i, j) = \frac{1}{m_{i,j}}, \quad \forall i, j \in S.$$

This relation is exploited to calculate mean access delay of stations (i.e., time between successful packet transmissions). Since the analysis in this dissertation is concerned with time to return to any transmission state (i.e., $\pi(i, 0), \forall i \in [0, m_c]$), then normalized probability ψ_c can be used to calculate mean time between two successfully transmitted packets. Therefore, delay of a priority class c is expressed in number of steps:

$$D_c = \frac{1}{\psi_c}.$$

One can express D_c in seconds by multiplying it by the length of a frame,

$$D_c = \frac{T_c}{\psi_c},$$

where T_c is the channel occupancy time of traffic with priority class c . For all contending nodes in the channel, mean access delay becomes

$$D_c = \frac{n_c T_c}{\psi_c}. \quad (4.15)$$

Figure 4.6 illustrates this expression for all four priority types of one-class dense deployments under the considered scenario. The figure reveals that classes 4 and 3 sustain longer delay for low number of contending stations. Also, their trends increase sharply when compared to classes 1 and 2. Low priority traffic would still incur delay longer than 1 second when contending stations exceed 50 and 90 nodes for priority classes 2 and 1, respectively. Long delays are attributed

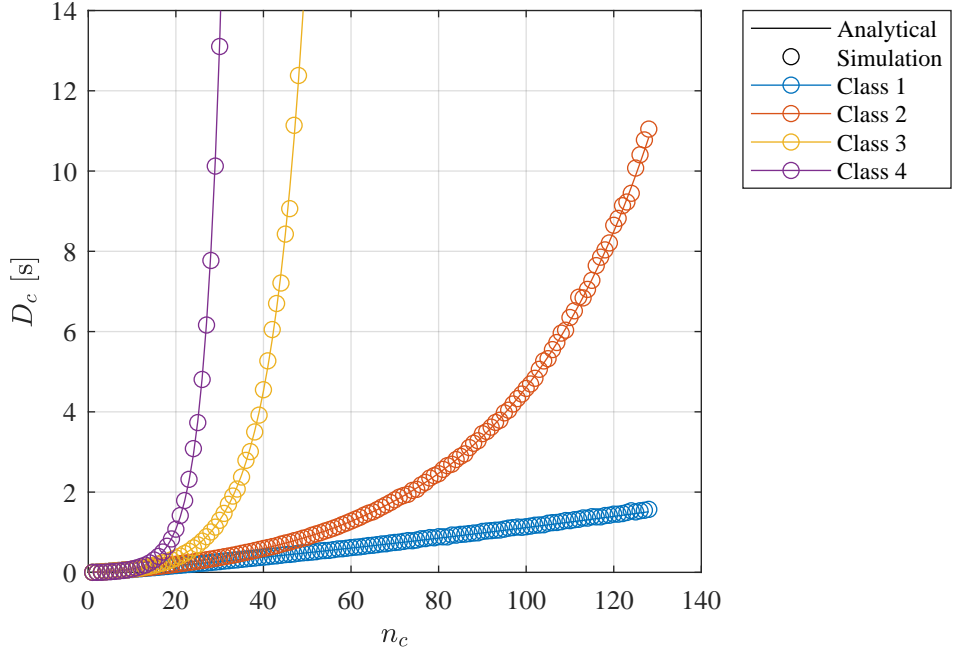


Figure 4.6: Mean access delay—in seconds—for different priority classes as a function of the number of contending stations.

to accompanying increase in collisions pertinent to each traffic type.

4.2.3 Temporal Fairness

Channel time fairness can be intuitively defined as the share of physical time each single node uses to successfully transmit on the channel. In homogeneous one-class scenario, all coexisting nodes serve the same traffic priority type. Aggregate channel time utilized to successfully transmit packets ψ_c derived in Section 4.1.4 accounts for all contending nodes by means of ρ_c , probability that a successful transmission of class c occurs on the channel:

$$\rho_c = \frac{n_c \tau_c (1 - \tau_c)^{n_c-1}}{\gamma_c}.$$

In that vein, all n_c coexisting nodes will equally share channel time, given they have same traffic priority class.

4.3 Two-Class Deployment Scenario

The simultaneous effect of different priority class traffics sharing the medium is analyzed in this section. It is important for same-technology, homogeneous networks to operate harmoniously and efficiently without inhibitory effect on other incumbent users. Hence, it is necessary to understand how NR-U devices employing various quality of service requirements would coexist, excluding interference from other technologies.

Analytical expressions for multi-class scenarios must be obtained for metrics of interest (i.e., ECU, collision probability, and mean access delay). Each class is considered a separate system with independent transmission probability τ_c . Therefore, the conditional probability of collisions p_c must account for other stations serving different frame types. Equation (4.10) can be rewritten to reflect the existence of other stations with different priority classes trying to access the channel:

$$p_c = 1 - (1 - \tau_c)^{n_c - 1} \prod_{k \in \mathcal{C}, k \neq c} (1 - \tau_k)^{n_k}. \quad (4.16)$$

The probability that a) at least one station transmits and b) a transmission is successful remains the same as defined in (4.11) and (4.12), respectively. In contrast, ψ_c given in (4.13) should be redefined to incorporate the effect of other stations in the medium:

$$\psi_c = \frac{\gamma_c \rho_c T_c \prod_{k \in \mathcal{C}, k \neq c} (1 - \gamma_k)}{T_N}. \quad (4.17)$$

T_N represents the normalized time that accounts for every possible event on the channel. It consists of idle slots, successful transmissions, and multi-node concurrent transmissions (i.e., collisions).

Suppose that $\mathcal{S} = \{0, 1, 2\}$ is a set for the three possible states for an arbitrary NR-U network: 1) no transmission (idle), 2) exactly one transmission, and 3) at least two transmissions, respectively. As defined in Section 4.1, $\mathcal{C} = \{1, 2, 3, 4\}$ is the set of priority classes attributed to networks. Let there be a function \mathcal{P} :

$\mathcal{C} \times \mathcal{S} \mapsto [0, 1]$ defined by the following expression, where $s \in \mathcal{S}$ and $c \in \mathcal{C}$:

$$\mathcal{P}(c, s) = \begin{cases} 1 - \gamma_c & : s = 0 \\ \gamma_c \rho_c & : s = 1 \\ \gamma_c(1 - \rho_c) & : s = 2 \end{cases} \quad (4.18)$$

In this context, $\mathcal{P}(c, 0)$ denotes the probability that a class c network is idle; $\mathcal{P}(c, 1)$ is the probability that a class c network has exactly one transmission on the channel; and $\mathcal{P}(c, 2)$ is the probability that a class c network has at least two transmissions on the channel.

Consider four networks—each with a priority class $c \in \mathcal{C}$ and number of nodes n_c sharing the medium, T_N can be expressed as:

$$T_N = \sum_{i,j,l,k} \mathcal{P}(c_a, i) \mathcal{P}(c_b, j) \mathcal{P}(c_c, l) \mathcal{P}(c_d, k) T_{i,j,l,k} \quad : (i, j, l, k) \in \mathcal{S}^4 \quad (4.19)$$

$T_{i,j,l,k}$ represents the time corresponding to each combination.

4.3.1 Effective Channel Utilization

For a two-class scenario wherein two networks with priority classes c_a and c_b serve n_{c_a} and n_{c_b} stations, respectively, ECUs ψ_{c_a} and ψ_{c_b} are given by relation (4.17):

$$\begin{aligned} \psi_{c_a} &= \frac{\gamma_{c_a} \rho_{c_a} (1 - \gamma_{c_b}) T_{c_a}}{T_N} \\ \psi_{c_b} &= \frac{\gamma_{c_b} \rho_{c_b} (1 - \gamma_{c_a}) T_{c_b}}{T_N}, \end{aligned} \quad (4.20)$$

and T_N according to the more general relation (4.19) reduces to:

$$\begin{aligned}
T_N &= \sum_{i,j} \mathcal{P}(c_a, i)\mathcal{P}(c_b, j)T_{i,j} \\
&= \mathcal{P}(c_a, 0)\mathcal{P}(c_b, 0)T_{0,0} + \mathcal{P}(c_a, 1)\mathcal{P}(c_b, 0)T_{1,0} + \mathcal{P}(c_a, 2)\mathcal{P}(c_b, 0)T_{2,0} + \\
&\quad \mathcal{P}(c_a, 0)\mathcal{P}(c_b, 1)T_{0,1} + \mathcal{P}(c_a, 1)\mathcal{P}(c_b, 1)T_{1,1} + \mathcal{P}(c_a, 2)\mathcal{P}(c_b, 1)T_{2,1} + \\
&\quad \mathcal{P}(c_a, 0)\mathcal{P}(c_b, 2)T_{0,2} + \mathcal{P}(c_a, 1)\mathcal{P}(c_b, 2)T_{1,2} + \mathcal{P}(c_a, 2)\mathcal{P}(c_b, 2)T_{2,2}.
\end{aligned}$$

Replacing the probabilities according to (4.18) yields

$$\begin{aligned}
T_N &= (1 - \gamma_{c_a})(1 - \gamma_{c_b})\sigma + (\gamma_{c_a}\rho_{c_a})(1 - \gamma_{c_b})T_{c_a} + \gamma_{c_a}(1 - \rho_{c_a})(1 - \gamma_{c_b})T_{c_a} + \\
&\quad (1 - \gamma_{c_a})(\gamma_{c_b}\rho_{c_b})T_{c_b} + (\gamma_{c_a}\rho_{c_a})(\gamma_{c_b}\rho_{c_b})\min(T_{c_a}, T_{c_b}) + \\
&\quad \gamma_{c_a}(1 - \rho_{c_a})(\gamma_{c_b}\rho_{c_b})T_{c_a} + (1 - \gamma_{c_a})\gamma_{c_b}(1 - \rho_{c_b})T_{c_b} + \\
&\quad (\gamma_{c_a}\rho_{c_a})\gamma_{c_b}(1 - \rho_{c_b})T_{c_b} + \gamma_{c_a}(1 - \rho_{c_a})\gamma_{c_b}(1 - \rho_{c_b})\max(T_{c_a}, T_{c_b}).
\end{aligned} \tag{4.21}$$

Evaluating expressions (4.20) and (4.21) for different combinations of priority classes and variable number of stations gives corresponding channel efficiencies. Total ECU $\psi = \psi_{c_a} + \psi_{c_b}$ for adjacent priorities (i.e., coexisting networks priorities c_a and c_b differ in one level) is depicted in Figure 4.7. The inner edges of the plots report the ECUs discussed previously in Figure 4.3, since they correspond to single-class situations. As more nodes of higher priorities are added to the channel, total ECU drops significantly due to the negative effect of collisions they insinuate, as discussed in Section 4.2. This can be noticed in Figures 4.7a and 4.7b which demonstrate total ECU for classes 1-2, and 2-3, respectively. For the case of classes 3 and 4 networks depicted in Figure 4.7c, ECU acutely drops due to adverse effect of collisions in both types. Because of the similarities in the parameters of their backoff procedure, both classes contribute almost equally to the degradation of total channel ECU.

One can observe that this degradation is comparatively imputed to higher

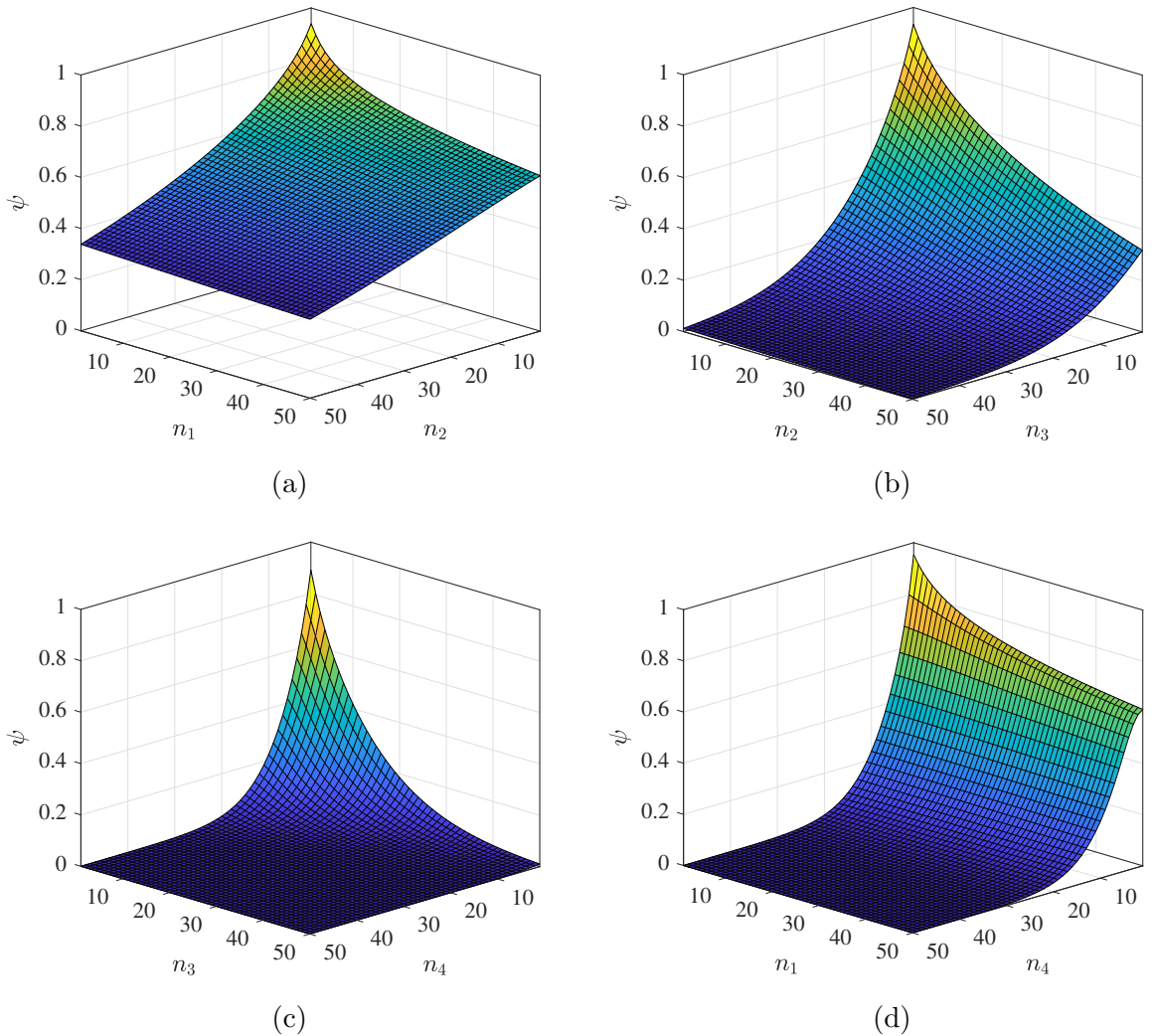


Figure 4.7: Aggregate ECU for different combinations of priority classes: (a) Class 1 and Class 2, (b) Class 2 and Class 3, (c) Class 3 and Class 4, (d) Class 1 and Class 4.

priority class in the channel. To better illustrate this observation, consider another possible scenario of classes 1 and 4, as shown in Figure 4.7d. This case further elucidates that remark due to disparity in coexisting priority levels. As the number of nodes increases, class 1 nodes do not influence the channel as much as class 4. For example, the ECU of five class 1 and a single class 4 stations is approximately 85%. Adding five more class 4 stations results in total ECU reduction to 50.44%. In contrast, 50.54% ECU for a single class 4 device encounters declination to 46.33% ECU with a ten times denser network of 50 class 1 nodes. This influence of class 1 network subsides as more class 4 devices join the channel and class 4 becomes the predominant variable affecting total channel efficiency.

It is prudent to conclude that when sharing the medium with stations of lesser priority, higher priority class stations exhibit an inhibitory effect on overall channel efficiency performance. The impact on the channel exacerbates as priorities of coexisting stations increase.

4.3.2 Collision Analysis

Analyzing collisions in multi-class scenarios can help to better understand the effect of mutual interplay among different channel access priorities in the vicinity, as well as overall channel performance. Such analysis offers explanations and deeper insights on total makeup of channel utilization to comprehend and pinpoint the reason behind ECU degradation. The developed analytical model in Section 4.1 makes it possible to investigate and break down collisions that occur during heterogeneous class deployments. The following discussion will address collisions in two-class scenarios as a three-component metric—*intra-network* (one for each priority class) and *inter-network* collisions.

The portion of normalized time that relates to collisions in T_N from equation

(4.21) is

$$T_C = \overbrace{\gamma_{c_a}(1 - \rho_{c_a})(1 - \gamma_{c_b})T_{c_a}}^{(a)} + \overbrace{(1 - \gamma_{c_a})\gamma_{c_b}(1 - \rho_{c_b})T_{c_b}}^{(b)} + \overbrace{\begin{aligned} &(\gamma_{c_a}\rho_{c_a})(\gamma_{c_b}\rho_{c_b}) \min(T_{c_a}, T_{c_b}) + \gamma_{c_a}(1 - \rho_{c_a})(\gamma_{c_b}\rho_{c_b})T_{c_a} + \\ &(\gamma_{c_a}\rho_{c_a})\gamma_{c_b}(1 - \rho_{c_b})T_{c_b} + \gamma_{c_a}(1 - \rho_{c_a})\gamma_{c_b}(1 - \rho_{c_b}) \max(T_{c_a}, T_{c_b}). \end{aligned}}^{(c)} \quad (4.22)$$

Terms (a) and (b) correspond to collisions within networks of class c_a and c_b , respectively. Group (c) terms model collisions due to simultaneous transmissions from both networks. These terms account for exactly one node from each network and at least two nodes or more. Time duration for each case depends on the number of transmissions in each network that occur on the channel.

Expressions that model the normalized time collision components makeup are similar to ECU defined in (4.20). For a two-class scenario, c_a and c_b with a number of nodes n_{c_a} and n_{c_b} , respectively, probabilities are given as follows.

$$\begin{aligned} \phi_{c_a} &= \frac{\gamma_{c_a}(1 - \rho_{c_a})(1 - \gamma_{c_b})T_{c_a}}{T_N} \\ \phi_{c_b} &= \frac{\gamma_{c_b}(1 - \rho_{c_b})(1 - \gamma_{c_a})T_{c_b}}{T_N} \\ \phi_{c_a c_b} &= \frac{T_C - \gamma_{c_a}(1 - \rho_{c_a})(1 - \gamma_{c_b})T_{c_a} - \gamma_{c_b}(1 - \rho_{c_b})(1 - \gamma_{c_a})T_{c_b}}{T_N} \end{aligned} \quad (4.23)$$

Results of evaluating relations (4.23) for combinations of c_a and c_b relevant to those examined in the previous Subsection 4.3.1 are shown in Figure 4.8. Pursuant to findings from previous discussion on ECU, class 1 and class 2 broadly show lower collisions than other higher levels of priority (See Figure 4.8a). The figure explains the relatively superior performance of this scenario over others in terms of ECU, which is attributed to the wide range of backoff values these two classes incorporate in their procedure. A noteworthy observation is that inter-network collisions contribute as much as 28% of the time when the channel has between five and 25 class 2 stations. Subsequently, the bulk of collisions are ascribed to the higher priority in the medium, that is class 2.

Figures 4.8b and 4.8c show a different pattern with classes 2-3 and 3-4, respectively. Intra-network collisions hinder the channel when one class has more users than the other. However, this component is still responsible for up to 60% in class 2 and up to more than 90% in class 3, as Figure 4.8b suggests. As more users join the channel, internetwork collisions start to gradually increase until they have ascendancy over intra-network components. Interestingly, the rate at which internetwork collisions escalates depends on the class and number of stations added to the channel. Figures 4.8a and 4.8b demonstrate this behavior. Since class 3 and class 4 have similar contention parameters, they equally share the responsibility of collisions. Their intra-network components are roughly the same, with class 4 slightly exceeding class 3, while a majority of collisions is attributed to internetwork component (See Figure 4.8c).

Like the discussion earlier on disparate priority levels (e.g., classes 4 and 1), collisions in such a scenario have been analyzed and depicted in Figure 4.8d. Results substantiate findings in the previous section that it is the higher level—class 4—that dominates the channel. Furthermore, this figure suggests that class 4 intra-network collisions inhibit performance in the shared medium. The impact of class 4 starts when as few as two devices join the channel and exponentially grows as more nodes are added. Class 1 intra-network collisions, on the other hand, have negligible impact compared to the other two components. However, class 1 stations contribute to internetwork collisions with less than five class 4 devices; afterward, higher priority level intra-network collisions start to dominate.

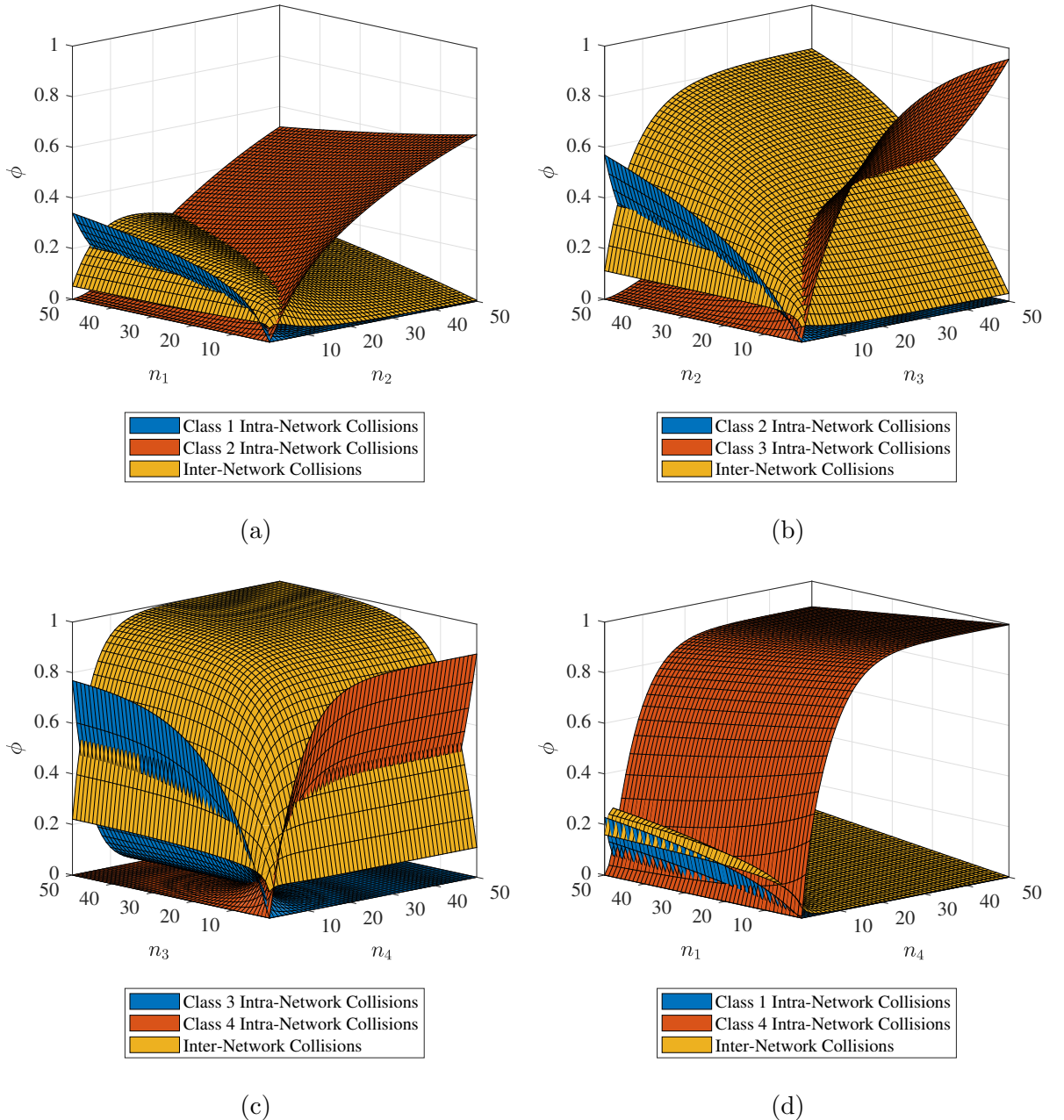


Figure 4.8: Intra-network and internetwork collisions for different combinations of coexisting priority classes.

These findings corroborate the drawn conclusion in ECU discussion that high priority class stations hamper overall performance on the channel due to collisions among their devices. The results do not totally absolve other coexisting nodes. In fact, analysis revealed that a large portion of collisions is attributed to the internetwork component, especially with adjacent priority classes.

4.3.3 Mean Access Delay

The average delay each station experiences in accessing the channel and sending a successful packet is evaluated in accordance with equation (4.15). This relation depends on achieved ECU; therefore, to isolate delay incurred by class c_a network from class c_b network, the classes' ECUs must be decomposed from the aggregate ECU of the channel. Leveraging relation (4.20) yields the required metric,

$$D_c = \frac{n_c T_c}{\psi_c}.$$

Figure 4.9 demonstrates mean access delay for scenarios discussed in the previous two subsections. These plots reveal an intriguing observation about the effect of different priority levels on each other—one that does not translate directly from the one-class situation discussed in Section 4.2. Figure 4.6 showed high priority classes in one-class deployments undergo longer delay times compared to low priorities. In the two-class case, Figure 4.9 suggests that high priority classes incur a more negative effect on lower class networks than they do among their nodes.

Consider the example of classes 1-2. When coexisting homogeneously without other priorities, class 1 outperforms class 2 at all network densities. As more nodes of the former join the channel, the odds shift in favor of class 2. Effect of class 1 is trivial on both network performances when compared to the higher priority level at low network densities. Performance scales up with denser class 2 mediums, as can be extrapolated from Figure 4.9a. The same observation can be expressed for classes 2-3 and 3-4. However, the magnitude is much larger than the relatively alleviated case of classes 1-2, as Figures 4.9b and 4.9c illustrate.

Continuing the analysis of class 1 and class 4 presented in this section as an example of the effect of extreme priorities on each other, their mean spectral access delay has been evaluated and is depicted in Figure 4.9d. Similarly, the lower-level priority network is afflicted with the delay caused by higher-level coexisting neighbors, which appears to be more influencing on both networks' delays. As

more class 4 nodes access the channel, both networks incur delay; however, class 1 nodes are more sensitive to the effect induced by the former network. Mean delay for class 1 exponentially increases to 500 seconds at 25 nodes of class 4. The same delay is experienced in the latter when its network extends to 45 nodes.

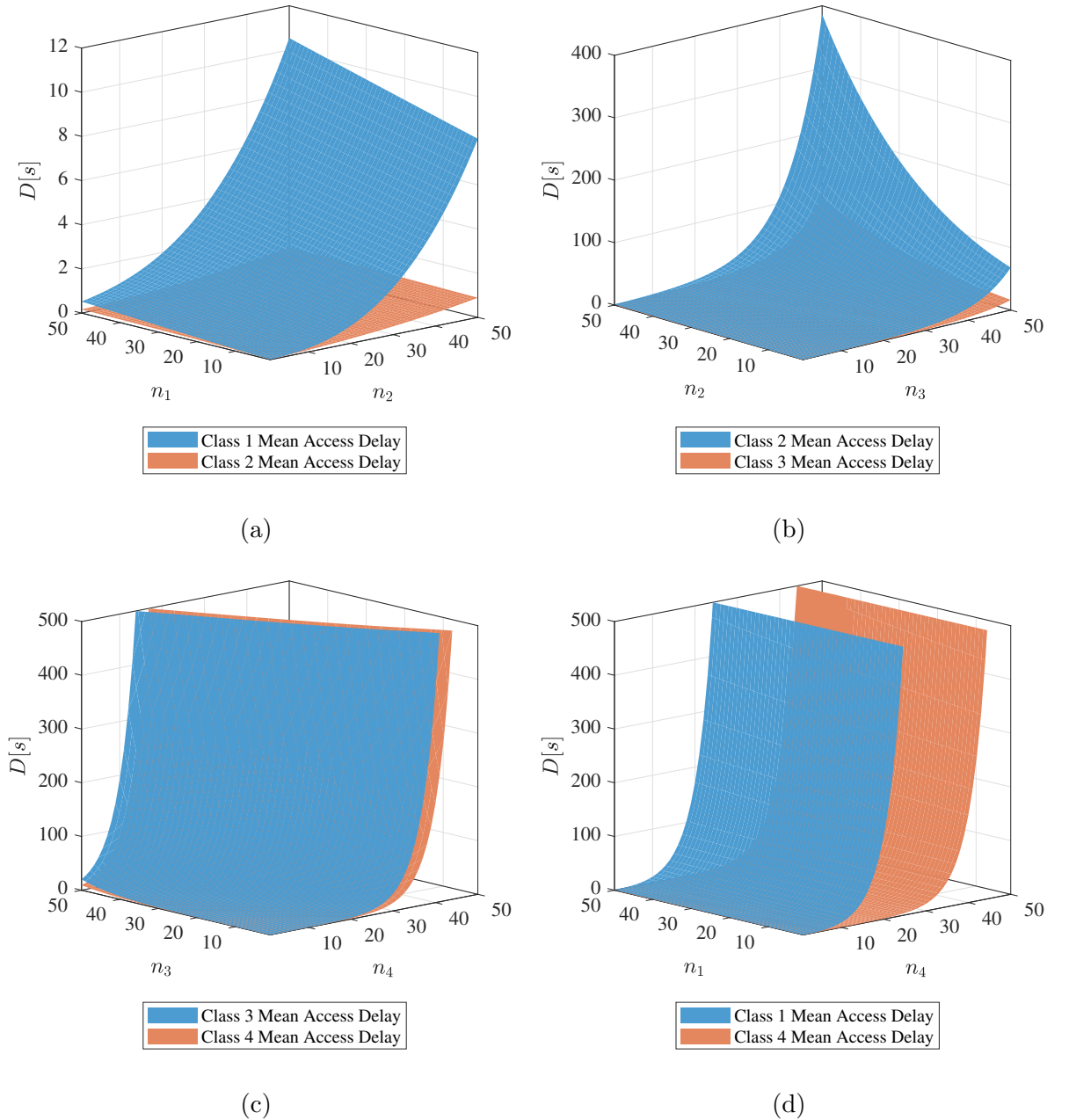


Figure 4.9: Mean access delay for different combinations of coexisting priority classes.

This behavior is attributed to the fact that high levels of priorities cause more collisions on the channel, as previously discussed. In addition to the significant likelihood of accessing the medium that stems from their small contention windows, high-priority classes allow very little time for lower priorities to transmit. Therefore, low priority class stations sustain longer delays than higher classes when coexisting heterogeneously.

4.3.4 Temporal Fairness

The effective channel utilization discussed in Subsection 4.3.1 offers a holistic view of channel performance. The effect of different traffic classes on the channel is illustrated and delineates how two networks—each assigned a priority level—perform when coexisting in the same channel. However, there is no indication of fairness of each class usage. This subsection is concerned with addressing this gap. Average airtime that individual nodes of different priority classes utilize is assessed. Dividing ECU of the class under consideration—defined in equation (4.20)—by number of nodes utilizing the channel reveals temporal fairness.

Figure 4.10 depicts results for class combinations considered in this section. Given the sizable number of data points associated with each scenario (e.g., 50×50 data points), only select cases are investigated. Number of nodes on the channel for both classes (n_a, n_b) is a combination of 1, 5, 15, and 30 nodes. The bar graph in Figure 4.10 shows the percentage of time each node of both classes attains to successfully transmit packets.

Results deduce that stations share the channel fairly at low densities and traffic priorities. However, it also appears that as priority levels increase, high classes occupy more airtime at the expense of coexisting lower priorities. The example of one node per class network illustrates this observation across different classes. Furthermore, this unfair behavior manifests in scenarios with multitude of nodes, wherein the channel includes more than one station of class c_a or c_b . For instance, when five class 2 nodes share the medium with a single class 3 device, the latter

seizes 21% of the channel, leaving the other five class 2 devices with 11% share each. As networks become more dense, the situation aggravates for lower priorities on the channel.

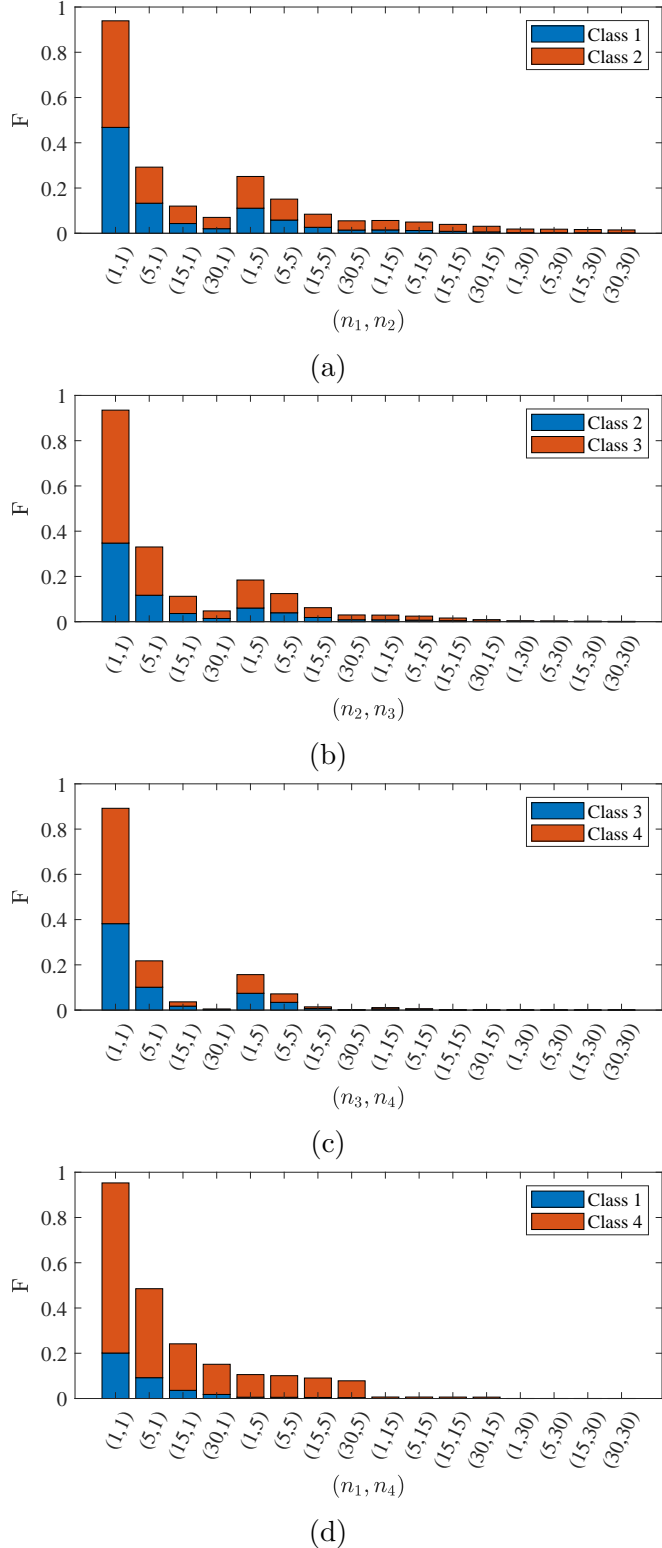


Figure 4.10: Channel time fairness for individual nodes coexisting with a combination of priority classes.

Table 4.1: AAMI TIR69 Risk Categories

Category	Risk and result of failure, disruption, or delay of wireless communication
Category A	High Risk Level—could result in death or serious injury
Category B	Medium Risk Level—could result in injury or impairment requiring professional medical intervention
Category C	Low Risk Level—could result in temporary injury or impairment, not requiring professional medical intervention
Category D	No Significant Risk Level—could result, at the most, in inconvenience or temporary discomfort

4.4 Case Study: Intensive Care Unit (ICU)

The number of ICU beds with full remote vital readings is expected to be around 100 by 2035 [67], and given limited hospital area, the high density of connections required to monitor patients could pose challenges to wireless networks [68]. The AAMI TIR69—Risk Management of Radio-Frequency Wireless Coexistence for Medical Devices and Systems [69]—specifies four risk categories for medical device wireless functions (See Table 4.1). The analysis presented hereafter could inform the design, development, and deployment of 5G-enabled healthcare applications. Assume an ICU environment with 75 active connections belonging to AAMI TIR69 risk categories A, B, and C distributed across 25 beds. Expressions (4.16) and (4.17) can be expanded to reflect a three-class scenario. Assuming latency incurred by connections is equal to only the mean access delay, time delay behavior in this scenario can be estimated using (4.15).

3GPP permits manufacturers to assign packet priorities regardless of the payload type. Mapping risk categories to various frame priority classes and plotting mean access delay results in Figure 4.11. Assume that class priorities 2, 3, and 4 are mapped to connections of risk categories C, B, and A. Accordingly, elevated connection latency associated with connections of risk categories B and C can be determined as shown in Figure 4.11a. Even for a type A connection, average delay is approximately 380 s. Designing functions with risk categories A, B, C to

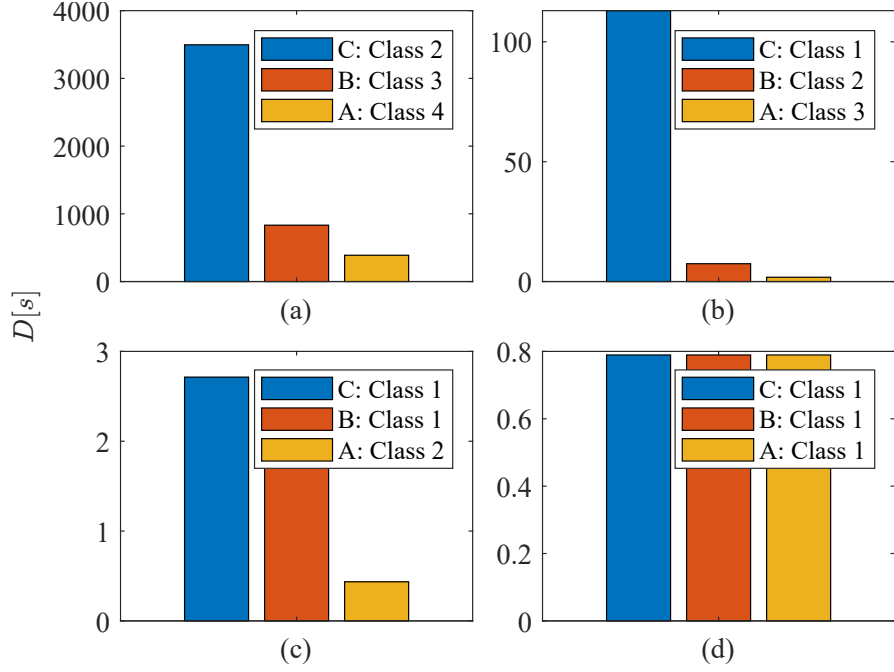


Figure 4.11: Latency of connections in ICU environment mapped to various frame priority classes. (a) 2, 3, 4; (b) 1, 2, 3; (c) 1, 1, 2; (d) 1, 1, 1

transmit using priority classes 3, 2, 1, respectively, improves latency by orders of magnitude, as illustrated in Figure 4.11b. Another design choice could be clustering connection types into two groups. For example, categories C and B could be assigned one class priority while category A is given a higher priority, as depicted in Figure 4.11c. Using priority classes 2 and 3 improves performance over using a three-class assignment. The effect is more so with lower priorities 1 and 2, reducing latency to less than three seconds for categories C and B and less than one second for category A. Additionally, given that high priority classes are guaranteed absent, one-class mapping can offer lower latency, as shown in Figure 4.11d. This example highlights the importance of carefully designing a medical device's wireless function to achieve intended functionality in the use environment.

Chapter 5

Modified LBT Mechanism

The regular LBT investigated in the previous chapter relies on a random process allowing nodes to select a value from a predefined set. Consider the single-class scenario discussed in Section 4.2. Coexisting stations of the same class differ in the value of the random counter selected in the backoff stage. Under assumptions detailed in Chapter 4, the only explanation for two stations colliding is the value of their backoff counter. Because contention window size depends on the priority class of data packet sent, classes exhibit different behaviors. Figure 5.1 illustrates the timing relationship between colliding stations. The problem exacerbates when the contention window size is small (e.g., class 4 in which the maximum CW_{max} is 7, per Table 2.2). At best, eight devices can share the channel without colliding—since the backoff counter value is drawn from the range $[0, CW_{max}]$. This fact (e.g., the Birthday Paradox analogy) was alluded to in Section 4.2.1.

In this chapter, a modified LBT mechanism is proposed to increase the effective channel efficiency and reduce collision probability among single-class stations.

5.1 Proposed Modification

The basic premise behind this proposition is decreasing the probability that at least two stations select the same backoff value while contending for the channel. Although the contention window sizes of priority classes can be increased, addi-

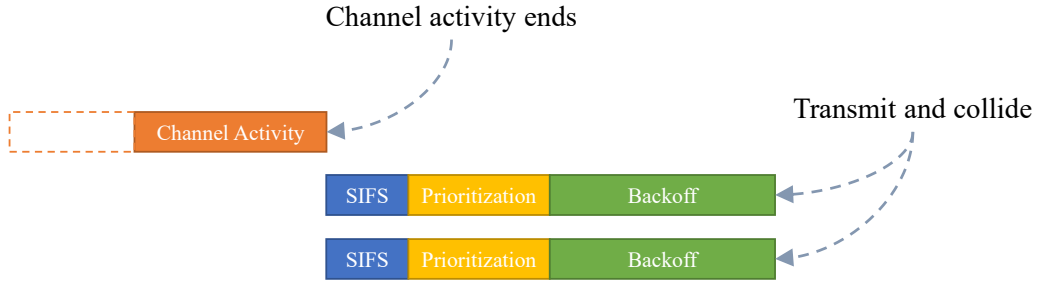


Figure 5.1: Timing relationship between colliding packets of the same priority class.

tional delay for the worst-case scenario arises, considering that backoff slots are 9 μs each. Alternatively in this proposition, a random period is introduced in addition to SIFS, prioritization, and backoff periods of the LBT process. The difference lies in the values of this period, which are in absolute time (i.e., microsecond) instead of 9 μs slots, termed Random Short Interframe Spacing (RSIFS). Figure 5.2 demonstrates the proposed mechanism's timing. Two things must occur for two stations of the same class to collide: 1) the random process for both nodes must select the same backoff counter *and* 2) the RSIFS random process must select the same value for both nodes. The two random processes decrease the collision probability significantly. RSIFS values are not expressed in time slots because total sum of time slots drawn in the two random processes of multiple stations might be equal. For example, one station could draw a value of 1 and 2 for the two processes while the other station could draw a value of 0 and 3. In this instance, the total number of contention slots for both stations is 3, which would eventually result in a collision on the channel. Hence, by setting the unit of RSIFS values to microseconds, different selections yield different outcomes while also keeping total latency overhead low.

The rationale behind this mechanism can be explained mathematically as follows. Let (Ω, \mathcal{F}, P) be the probability space that constructs the mathematical formulation of random processes, where

1. Ω is the sample space that contains all possible outcomes,

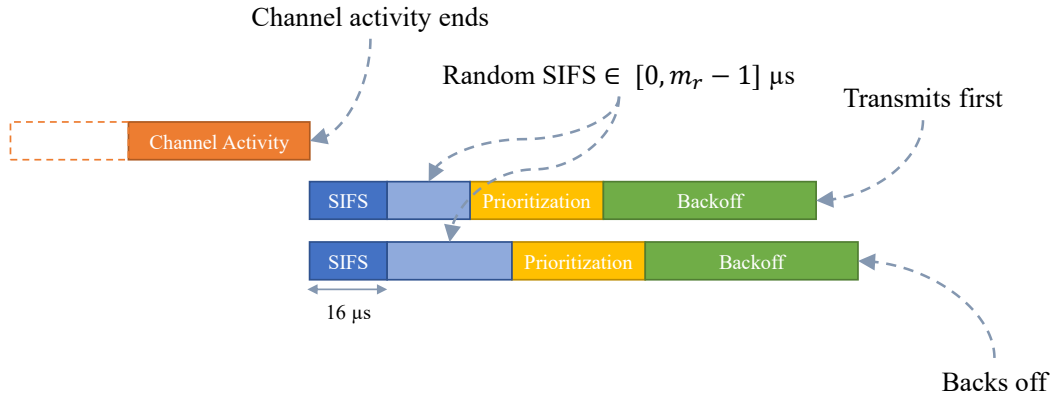


Figure 5.2: Timing relationship of the proposed LBT scheme illustrating the additional random SIFS period.

2. \mathcal{F} is the event space where $\mathcal{F} \in \Omega$, and
3. P is a probability function that assigns each event a number between 0 and 1.

Consider a random variable $X : \Omega \rightarrow \mathbb{R}^2$ that describes the backoff counter (X_1) and RSIFS (X_2) selection processes:

$$X = \begin{bmatrix} X_1 \\ X_2 \end{bmatrix}.$$

Let the Probability Mass Function (PMF) of X be $f(x) = f(x_1, x_2)$, and let the PMFs of its components X_1 and X_2 be $f_1(x_1)$ and $f_2(x_2)$, respectively. Since X_1 and X_2 are independent random variables,

$$f_1(x_1 | x_2) \equiv f_1(x_1)$$

and

$$f(x_1, x_2) = f_1(x_1)f_2(x_2).$$

For simplification, let us assume that the backoff counter is at the maximum stage of its class m_c and, as discussed in Section 4.1, it has a uniform distribution.

Let t_r be the value of RSIFS uniformly distributed over a fixed range for all priority classes, such that $t_r \in [0, m_r - 1]$, where m_r is the maximum value RSIFS can tolerate in microseconds. Therefore,

$$f_1(x_1) := \begin{cases} \frac{1}{W_{c,m_c}}, & x_1 \in [0, W_{c,m_c} - 1] \\ 0, & \text{otherwise} \end{cases}$$

$$f_2(x_2) := \begin{cases} \frac{1}{m_r}, & x_2 \in [0, m_r - 1] \\ 0, & \text{otherwise} \end{cases}$$

consequently, joint PMF would be

$$f(x_1, x_2) = f_1(x_1)f_2(x_2) = \begin{cases} \frac{1}{m_r W_{c,m_c}}, & x_1, x_2 \in [0, W_{c,m_c} - 1] \times [0, m_r - 1] \\ 0, & \text{otherwise} \end{cases}.$$

Evidently, probabilities of joint PMF are smaller than those of both individual PMFs. Figures 5.3 and 5.4 provide the following example: $W_{c,m_c} = 8$ corresponding to the maximum backoff stage for class 4 and $m_r = 9$.

5.2 Performance Evaluation

The proposed modification was implemented in the C++ simulator and evaluated in terms of ECU and mean access delay performance. Figure 5.5 compares ECU performance in dense deployments of the four priority classes. As the figure suggests, all priority classes demonstrate improved ECU with the proposed modifications incorporated in LBT. Especially for classes 3 and 4, approximately 60% and 70% improvements are observed, respectively, when 20 nodes share the channel. The increase in total channel efficiency is a result of the reduction in collisions among coexisting stations with similar traffic priority, as indicated in the previous section. The probability of selecting the same backoff value is now reduced with the additional random process of RSIFS.

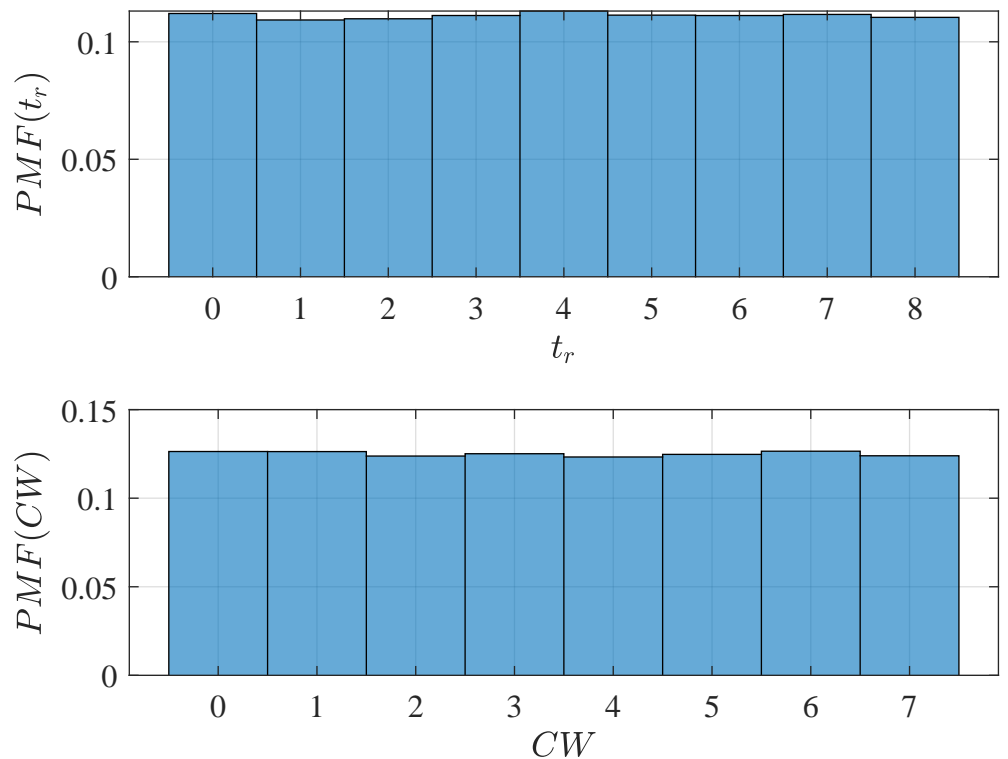


Figure 5.3: Individual PMFs of the RSIFS random process with $m_r = 9$ and the backoff random process with size $W_{c,m_c} = 8$.

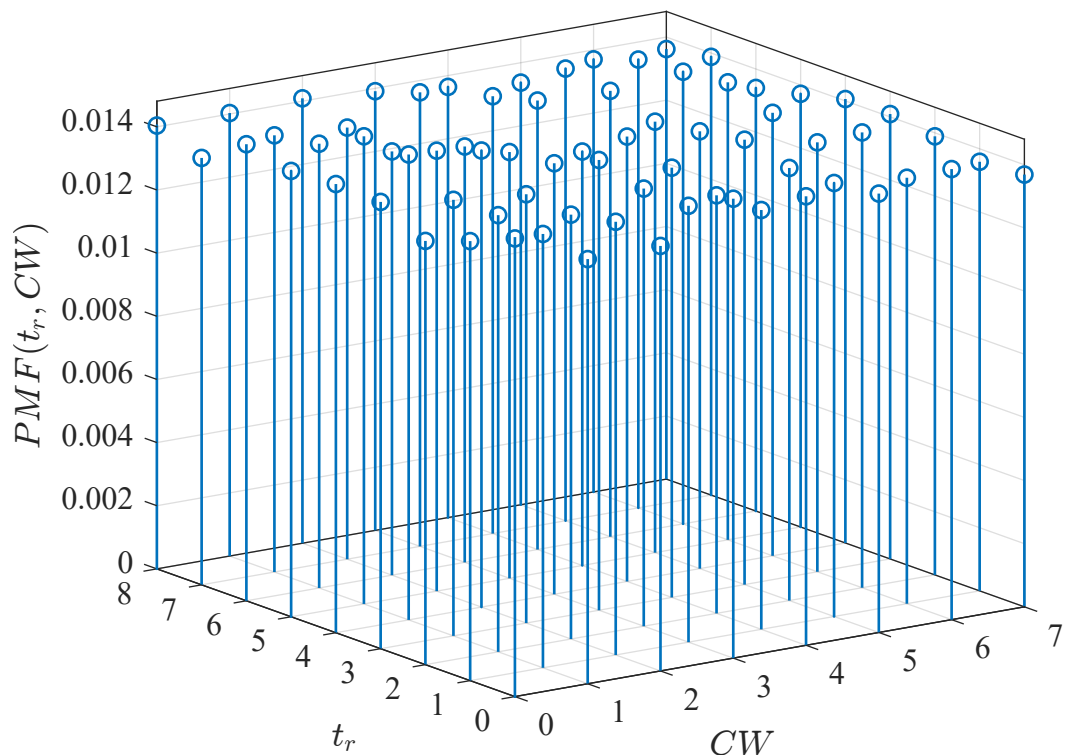


Figure 5.4: Joint PMF of the backoff and RSIFS processes.

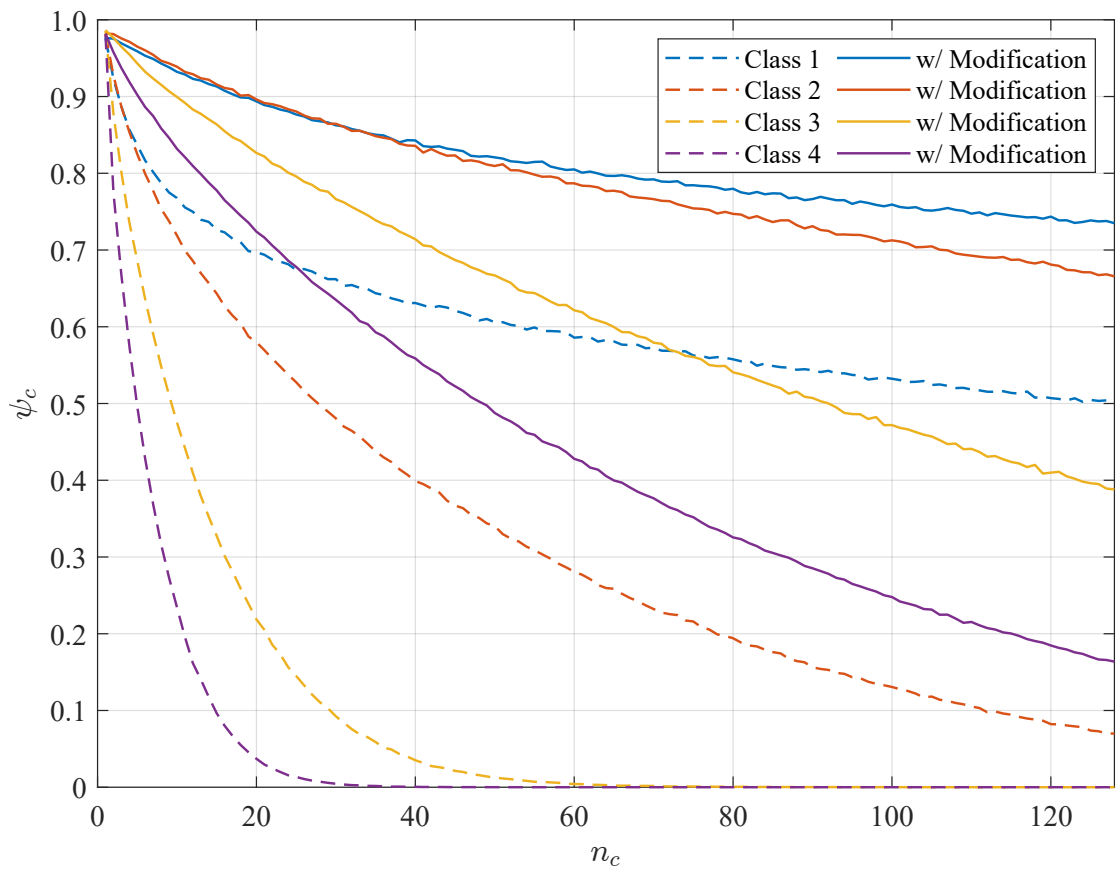


Figure 5.5: ECU performance of the proposed modification in dense deployments compared to regular LBT.

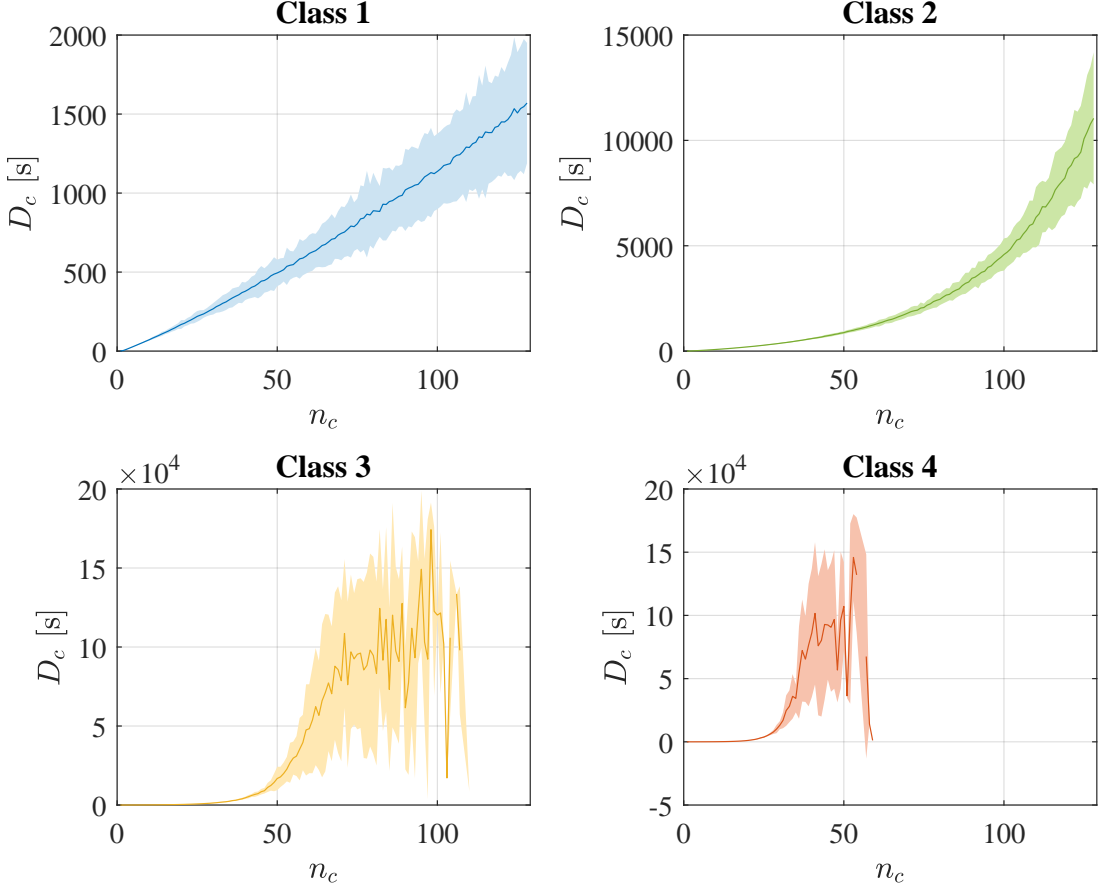


Figure 5.6: Mean access delay of regular LBT for the four priority classes in dense deployments.

Further analysis on the delay performance were completed to ensure that the proposed scheme incurs no additional latency. Per-station statistics were collected and analyzed by measuring the time between successful packet transmissions. Figures 5.6 and 5.7 compare the mean access delay for regular LBT and the proposed scheme, respectively. In addition to demonstrated improvement in mean delay performance, which is one order of magnitude, observed standard deviation in the modified LBT was lower than in the regular LBT. Given a scenario in which high priority classes 3 and 4 of regular LBT, Figure 5.6 depicts discontinuities in curves. This phenomenon is attributed to data loss at those points when simulating a high number of high priority class devices sharing the channel. Discontinuities represent the inability of stations to successfully transmit packets on the channel due to high collision rate. This observation is resolved in the modified LBT, which demonstrated better channel accessibility and latency.

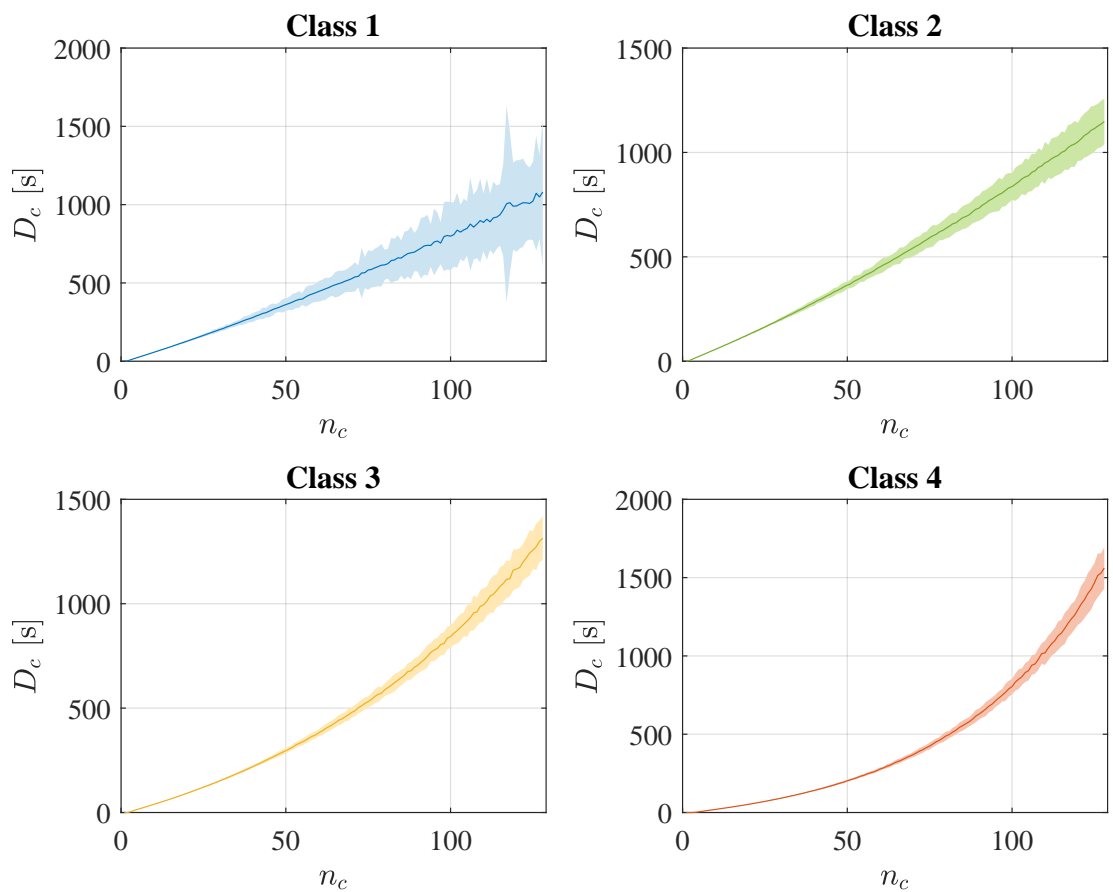


Figure 5.7: Mean access delay of the modified LBT for the four priority classes in dense deployments.

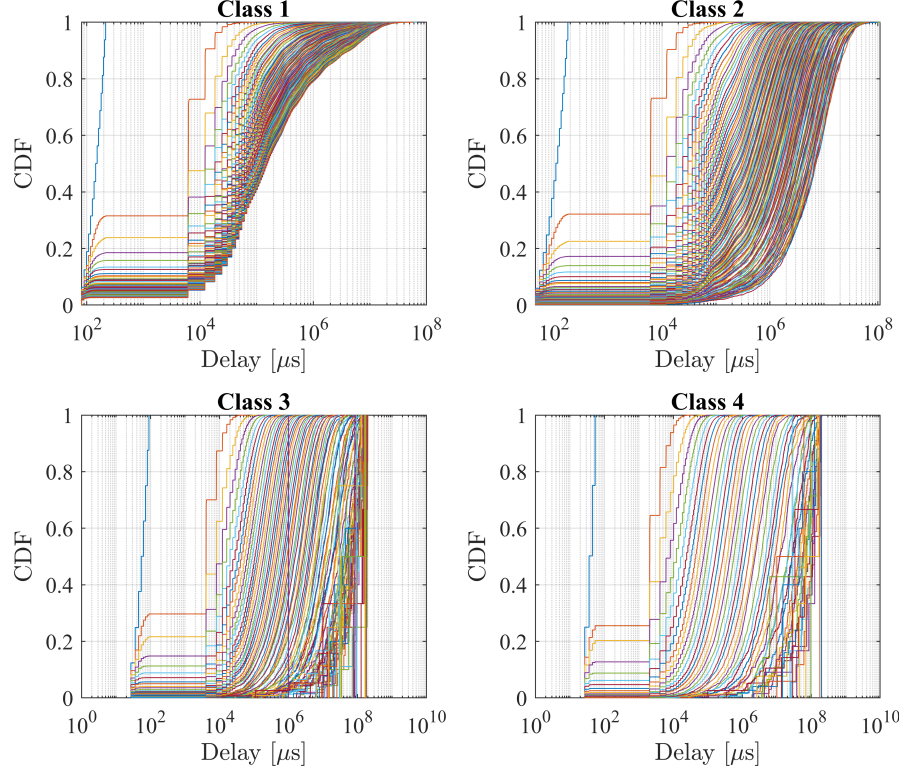


Figure 5.8: CDF of access delays for regular LBT simulations with 1 to 128 nodes sharing the channel.

In Figures 5.8 and 5.9, cumulative distribution function (CDF) of delays are plotted for regular and modified LBT, respectively. Curves from left to right represent the delay CDFs corresponding to simulations for 1 to 128 devices. The figures illustrate how most nodes experience less latency when using the proposed LBT compared to regular LBT. Results are more so for classes 3 and 4.

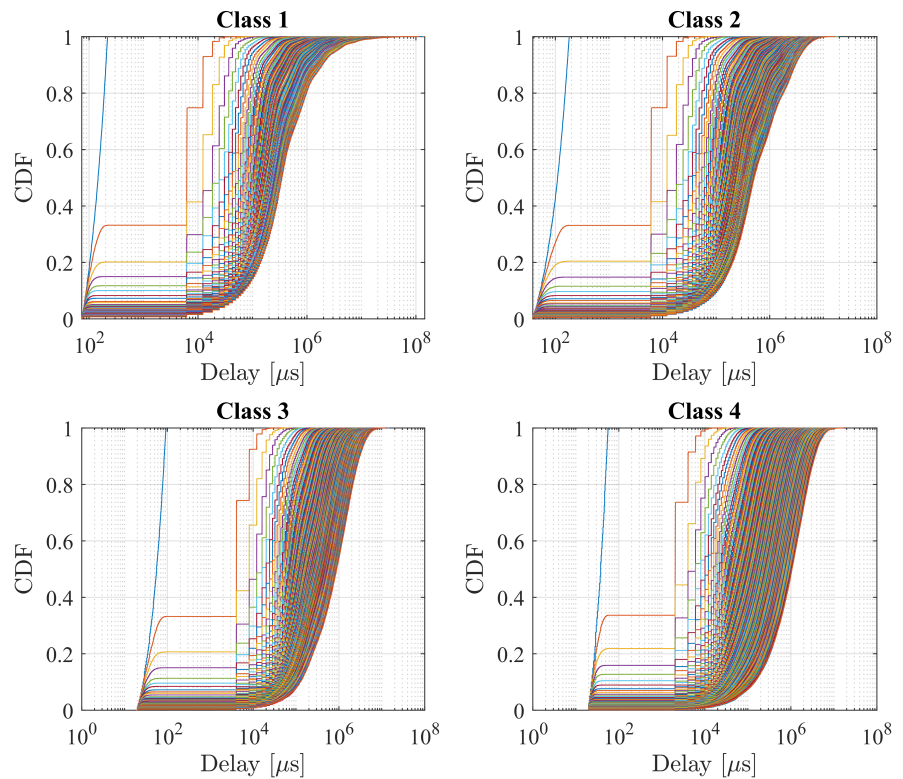


Figure 5.9: CDF of access delays for modified LBT simulations with 1 to 128 nodes sharing the channel.

Chapter 6

Empirical Coexistence Analysis of BLE 5 and Cellular LBT

The 2.4 GHz spectrum is home to several RATs, including ZigBee, BLE, and Wi-Fi. Accordingly, the technologies' spectrum-sharing qualities have been extensively studied in literature. LTE-LAA LBT has been identified in technical reports as the foundation of the channel access mechanism for 5G NR-U operating in the 2.4 GHz ISM band. The introduction of NR-U into this band raises new concerns regarding coexistence of the newcomer with traditional incumbents. This chapter reports an investigation of BLE 5 and cellular LBT coexisting systems by means of empirical evaluation. The importance of this study rests on the fact that the studied LBT mechanism is indicative of how 5G NR-U would perform in the 2.4 GHz band. Tests were performed in conformity with the American National Standards Institute (ANSI) C63.27 standard for evaluation of wireless coexistence; results were reported in terms of throughput and interframe delays. In accordance with the standard and under different BLE PHYs and LBT priority classes, three setups were investigated. These pertain to the three tiers of evaluation, which correspond to the criticality of the device under test.

6.1 Introduction

Equipped with novel advancements in wireless technologies, the IoT has ushered in an era of vast connectivity. Numerous devices will be seamlessly connected and exchange various amounts of information to enhance user experience. One pivotal enabler of such a paradigm shift in connectivity, namely BLE, has amassed favorable adoption from many market verticals. According to a Bluetooth Special Interest Group (SIG) market study based on ABI Research forecast, annual Bluetooth-enabled device shipments will exceed six billion by 2024 [70]. By virtue of its low power consumption and multiple features, BLE supports various applications in the wearables and smart infrastructure industries (home, buildings, cities, and others)—from smartwatches and fitness trackers to health sensors and medical innovations. Accordingly, the Bluetooth SIG has been regularly updating BLE specifications. For example, the fifth version [27] introduced new features to the PHY, such as high data rate and coding schemes to permit long-range communication links. Further enhancements were announced in revisions 5.1 and 5.2 (e.g., direction finding and audio streaming, respectively [71, 72]).

Nonetheless, mobile broadband networks have been challenged with accommodating the forthcoming colossal amount of data. According to an Ericsson report, by 2022 smartphones are forecast to generate more than 60 exabytes of data per month [5]. Consequently, unlicensed spectrum serves as a prospect for mobile network operators to accommodate increasing demand. In light of this, the 3GPP has facilitated the operation of 4G LTE in the 5 GHz unlicensed ISM band by means of LAA technology. This proposition has received much attention from the industry and academic institutions, primarily because it implies coexistence with incumbent technologies, especially widely used Wi-Fi devices [73]. LTE-LAA was established using LBT channel random-access scheme, which addressed compliance with spectrum etiquette set forth by regulators (e.g., ETSI [3]), as well as fairness with Wi-Fi [73, 74].

Recently, early-stage development of 5G cellular communication has been for-

mulated to consider unlicensed access (i.e., 5G NR-U). 3GPP's TR 38.889 [15] technical report identifies LBT used in LTE-LAA as a baseline for use in the 5 GHz unlicensed band, as well as a design start point for the newly regulated 6 GHz band [75]. Notably, unlike previous considerations for LTE-LAA, TR 38.889 includes the 2.4 GHz band within the scope of NR-U operations [4]. However, the 2.4 GHz ISM spectrum is already crowded with multiple incumbent technologies (e.g., Bluetooth, ZigBee, and IEEE 802.11b/g/n/ax). In addition, IEEE has formed a study group to discuss a potential amendment, namely IEEE 802.11be Extremely High Throughput (EHT), which will build on 802.11ax and target all sub-7 GHz unlicensed spectrum (i.e., 2.4, 5, and 6 GHz bands) [13, 14]. Furthermore, while Bluetooth systems are traditionally deployed in the 2.4 GHz, requests have been made to allow frequency-hopping systems to operate in the 5 and 6 GHz bands under the condition of a low-power transmission, i.e., Very Low Power (VLP). The European Communications Committee (ECC) has issued mandates to study the feasibility of narrowband VLP in the 6 GHz spectrum [16, 17]. Early proposals are projected to replicate the 2.4 GHz rules in the 5 and 6 GHz bands, making Bluetooth-like channel access schemes potential newcomers to those bands.

The work detailed in this dissertation was inspired by a need for greater understanding about the potential impact arising from the introduction of two technologies (i.e., cellular LBT and BLE) into unprecedented radio bands with respect to their conventional operating frequencies. The LBT-based LTE-LAA and Wi-Fi wireless coexistence in the 5 GHz band has been studied extensively in literature; observations could be extended to corresponding operations in the 2.4 GHz spectrum. However, the 2.4 GHz ISM band is used by diverse technologies other than Wi-Fi, such as BLE 5, that must be accounted for when the channel is accessed with LBT-based technologies. Of interest is that frequency hoppers have yet to be deployed in the Unlicensed National Information Infrastructure (UNII) bands; hence, the hoppers effect on incumbent RATs is clear. Since LBT has primarily been confined to the 5 GHz band, and likewise BLE to the 2.4 GHz band, there

are no reports in the literature investigating wireless coexistence of LBT and BLE 5 in the 2.4 GHz band. The work highlighted in this chapter contributes to the understanding of wireless coexistence of BLE devices operating with LBT cellular systems in the same environment, which, in turn, can inform wireless coexistence testing.

6.1.1 Contribution

To bridge the literature gap on LBT and BLE coexistence in the 2.4 GHz ISM band, this chapter presents an empirical evaluation of wireless coexistence among BLE 5 systems and others employing a cellular LBT channel access scheme in the 2.4 GHz band. This investigation offers an indication of how 5G NR-U would behave when deployed in realistic environments that use BLE devices (e.g., hospitals, homes, clinics). The interplay of different LBT channel access priorities and BLE physical layers was assessed, and the mutual impact is reported in terms of normalized throughput and interframe timings as a measure of delay. By doing so, this dissertation characterized and explored the boundaries of operation for BLE 5 when coexisting with LBT-based networks in the 2.4 GHz ISM band as the underlying wireless connectivity for wearable medical devices. The ANSI C63.27 [76] radiated anechoic chamber test method for evaluating wireless coexistence was adopted in the experimental setup. Findings can be used to augment the standardized ANSI C63.27 coexistence testing and inform the design, development, and deployment of co-located LBT-based and/or BLE 5-based wireless medical equipment.

6.2 Experimental Setup

The test setup was devised according to ANSI C63.27 standard [76] in which three-tier evaluations are specified to address different levels of criticality of the device under test. Consequences of failure in the Functional Wireless Performance

(FWP) regarding possible lack of coexistence determine the evaluation tier. In the example of wireless medical devices, the risk assessment and mapping to ANSI C63.27 evaluation tiers can be done using the Association for the Advancement of Medical Instrumentation (AAMI) Technical Information Report (TIR) 69 for risk management of radio-frequency wireless coexistence for medical devices and systems [69].

In the considered test setup, LBT network was treated as the unintended source of interference, while BLE network acted as the DUT (i.e., intended signal). The C63.27 standard provides band-specific test guidance for common RATs along with recommendations for selecting unintended signals for testing. Described guidance for BLE was followed, with the exception that the unintended IEEE 802.11n signals were replaced with signals representative of cellular LBT in all evaluation tiers. Because tier 1 is the most extensive level of evaluation, in which a rigorous set of unintended signals challenge the FWP of the DUT, three 20 MHz non-overlapping LBT channels were imposed on the DUT. Tier 2 is concerned with coexistence evaluation with lower level of rigor than tier 1. In this setup, unintended signals occupied 20 MHz channels that correspond to Wi-Fi channels 1 (2412 MHz) and 11 (2462 MHz). DUT was exposed to the minimum number of unintended signals in tier 3, and, therefore, one LBT channel was centered at 2437 MHz, which corresponded to Wi-Fi channel 6. Per ANSI C63.27 Annex A recommendations, LBT nodes were placed in a circular arrangement around the BLE source node with 1m radius to ensure equal power level at the DUT from all three channels of interference. Other test layouts can be used depending on DUT functionality and the intended environment (e.g., line-of-sight, non-line-of-sight). A BLE sink node was placed 2m from the source outside the circle, as depicted in Figure 6.1. According to BLE specifications, the receiving device must acknowledge each data packet by sending an empty packet. Furthermore, note that BLE does not perform CCA in typical fashion for Wi-Fi and LBT systems. Accordingly—and for the specific scenario in which both source and sink

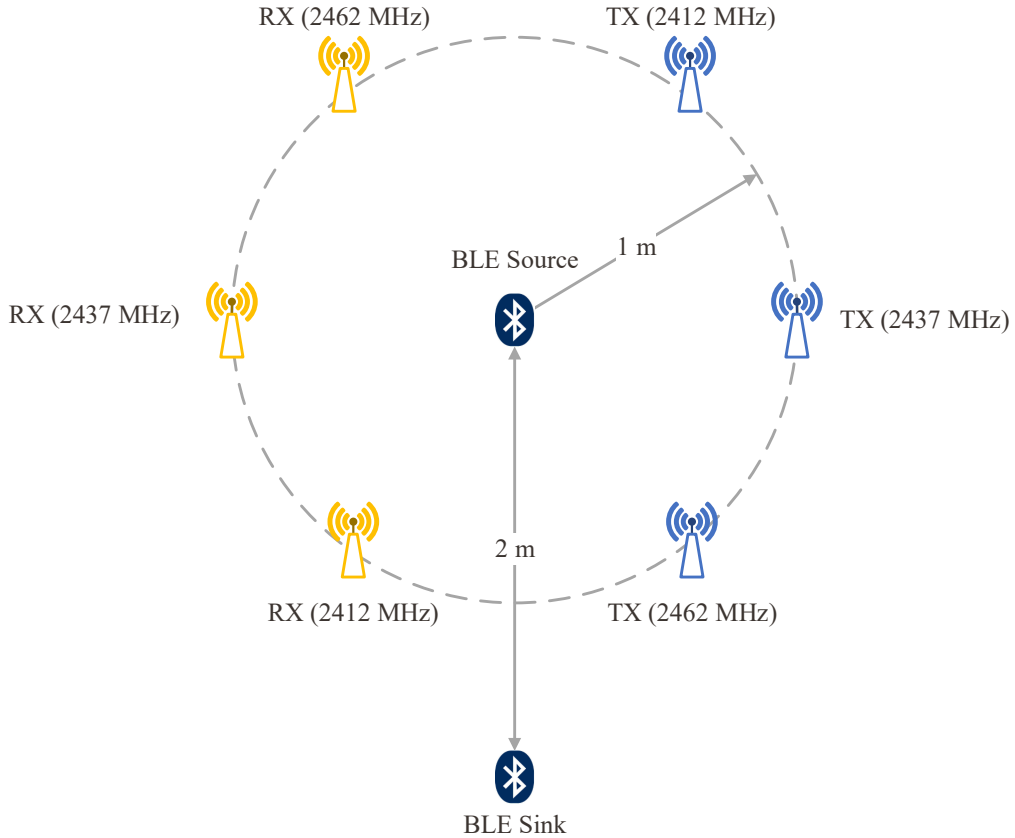


Figure 6.1: The experimental setup of the coexistence test illustrating the arrangement of BLE nodes and the three LBT pairs with center frequencies 2412 MHz, 2437 MHz, and 2462 MHz.

were configured with the same transmission power—swapping the roles of BLE devices is expected to have a similar outcome. Notably, the effect of a dropped acknowledgment packet is like that of a dropped data packet, as discussed below in Section 6.3. Tests were conducted in a semi-anechoic chamber to eliminate uncontrolled interference, and an NI PXIe-1071 [77] spectrum analyzer was used to measure power levels.

Three NI USRP 2943R [78] devices implementing the LBT mechanism using LabView were deployed as LBT networks. The setup utilized NI LAA implementation based on LTE Application Framework [79] and was also extended to support LBT channel access scheme. Details can be found in [80]. LBT and PHY were synthesized on the FPGA to account for critical timing requirements. Modifications to the LTE-LAA LBT code provided in [80] were made to resemble the

Table 6.1: BLE 5 Configuration Parameters

PHY	2M, 1M, LR (Coded)
Tx Power	-12, -8, -4, 0, 4, 8 dBm
ATT MTU Size	247 Bytes
Transfer Size	1024 KB
Connection Interval	7.5 ms

ETSI-compliant LBT detailed in Section 2.2. SIFS and P0 durations pertaining to the four-class priorities were incorporated. Parameters such as backoff window size and Transmission Opportunity (TXOP) duration (or COT) were made accessible in the user interface to change channel access priority in run-time, as per Table 2.2. Exponential backoff was not supported by the used devices. Accordingly, only maximum backoff window size was considered. [43] demonstrated that MCS has a negligible effect on channel utilization and that the highest MCS introduces the greatest impact on both coexisting systems. Consequently, to account for worst-case scenarios, the highest MCS was selected in all priority classes. Each node was set in an RF loop-back configuration. An internal loop-back allows the calculation of Cyclic Redundancy Check (CRC) of received data on the Physical Downlink Shared Channel (PDSCH) over the air. Achieved throughput was monitored and recorded for each test.

A Nordic Semiconductor nRF52480 dongle kit was used as the BLE network [81]. The throughput example provided in the software development kit was modified to support all three BLE PHYs (i.e., legacy 1M, high data rate 2M, coded LR) and different levels of transmission powers. The BLE source sent a configurable amount of random data (e.g., 1 MB) to the sink node and reported achieved throughput at the end of the test. During transmission, a BLE sniffer placed next to the sink collected and reported performance indicators (e.g., packet error rate and retransmission rate, as well as histogram of the utilized channels). Configuration parameters are listed in Table 6.1.

The use of 2.4 GHz ISM band for future LBT-based 5G NR-U networks might be targeted towards low traffic profiles, compared to the more accommodating

UNII bands at 5 GHz and the newly regulated 6 GHz unlicensed spectrum. Nevertheless, from an exploratory perspective, ANSI C63.27 recommends investigating the coexistence parameters (i.e., frequency, range, and time) to identify the characteristics of DUT failure modes. Hence, the unintended LBT nodes were operated in full buffer mode as a worst-case scenario, attempting to generate the highest channel utilization. To increase the chances of exposing weaknesses and further discover failure characteristics of coexisting RATs, a wider set of testing scenarios were examined by considering various Intended-to-Unintended Signal Ratios (I/Us) [76]. Using the spectrum analyzer, signal levels of the companion BLE device and the interferer LBT device were measured at the DUT (i.e., BLE source at the center of the circle). While DUT was off, the unintended signal was measured with a max hold detector over 2 MHz channel bandwidth, as observed by the BLE device. Subsequently, the intended signal was measured by reversing the BLE roles and transmitting from sink to source. When the unintended signal was measured at -48 dBm and the BLE transmission power changed between 8 dBm and -12 dBm for source and sink, a range of I/U ratios between 1 dB and -19 dB was noted.

For each evaluation tier, LBT nodes were configured to transmit packets pertaining to one of the four access priority classes. For each class, the BLE network was tested in a 2M, 1M, or LR PHY mode. BLE network transmission power was varied between 8 dBm and -12 dBm in 4-dB steps. Each test was repeated five times to ensure repeatability. A total of 1080 test vectors were collected.

6.3 Empirical Results

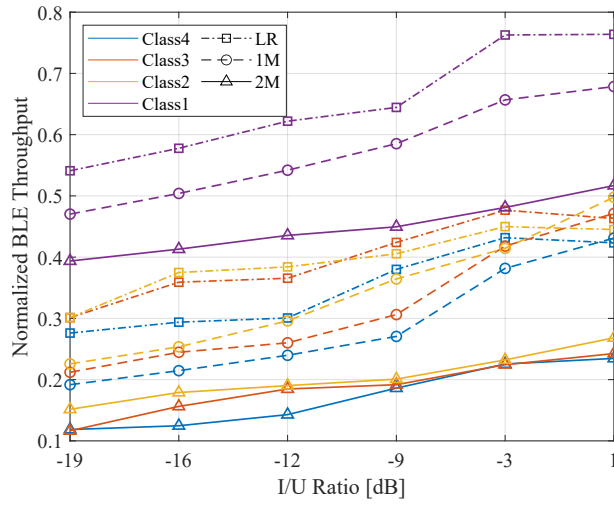
In this section results of the three tiers of evaluation are presented and followed by a discussion in a subsequent section. Notably, results indicate the expected coexistence behavior of cellular LBT and BLE 5. However, unique device implementations across the open system interconnection (OSI) layers warrant individual

evaluation when needed, as detailed in ANSI C63.27.

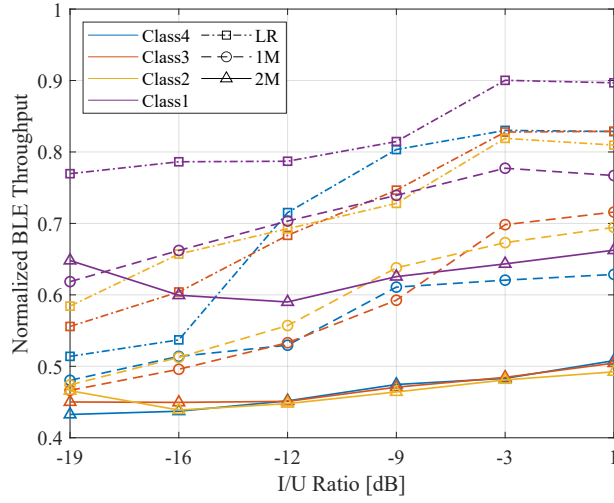
6.3.1 Impact of LBT on BLE 5 Performance

Tier 1—with three LBT interferers centered on frequencies 2412 MHz, 2437 MHz, and 2462 MHz—poses the biggest challenge to the BLE 5 network since LBT unintended signals utilize 60 MHz of the 2.4 GHz band. All three channels were used to transmit packets of the same priority class (e.g., 1, 2, 3, or 4). As the priority increases, the contention window size and channel occupancy time decreases. High priority nodes capture the channel faster than lower priority nodes, although the former utilize the channel for smaller durations. The effect of these signals on the normalized throughput of the 2M, 1M, and LR BLE PHYs acting as a function of the I/U ratio is shown in Figure 6.2a. Although all BLE PHYs experience reduction in their throughput to less than 50%, 2M sustains the highest impact under all priority classes of interferer. Though measurements indicate that LBT classes 4, 3, and 2 tend to have a decreasing effect on the achieved BLE throughput, their lines are clustered and their impact is relatively small under the same BLE PHY—except for class 1, which has the least impact on all physical layers. The figure accentuates the resilience of low data rate PHYs to interference, as noted in Section 2.3, which comes, however, at the expense of throughput; the maximum achieved by LR and 1M PHYs in baseline without interference is 26 Kbps and 226 kbps, respectively, compared to 340 kbps for 2M PHY. Curves in Figure 6.2 are normalized with respect to these maximum values.

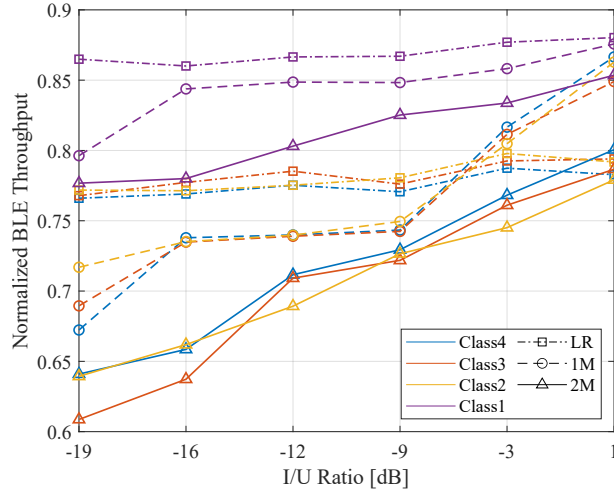
Since various applications depend on different key performance indicators, other metrics were evaluated. Interframe Spacing (IFS) durations between successful packet transmissions were analyzed using sniffer capture files as a measure of latency. Figure 6.3a compares calculated IFS for BLE 2M and LR physical layers under the four LBT priority classes and as a function of the I/U ratio. Interestingly, the figure suggests that average gap time between successfully received packets was higher for LR PHY than 2M PHY. Additionally, the figure demon-



(a) Tier 1



(b) Tier 2



(c) Tier 3

Figure 6.2: Normalized BLE throughput under LBT interferers of class 1, 2, 3, and 4.

strates that IFS for BLE 2M PHY increased as the I/U ratio decreased, whereas LR PHY did not exhibit a similar relationship, indicating that IFS is less sensitive to interference for that physical layer. BLE 1M PHY showed a similar trend to 2M PHY, with IFS values between 1 and 2 ms.

BLE throughput performance in tiers 2 and 3 was similar to tier 1: normalized throughput dropped as the I/U ratio decreased, and differences among LBT priority classes within the same BLE PHY were negligible. However, Figures 6.2b and 6.2c illustrate that 1M PHY performed better than LR in tier 3 when I/U was above -3 dB. Furthermore, LR-achieved throughput appeared to flatten as a function of I/U in tier 3, indicating less susceptibility to interference in relaxed conditions. Tiers 2 and 3 in Figures 6.3b and 6.3c, respectively, demonstrate similar behavior to tier 1 in terms of IFS durations with lower impact.

This observation of elevated implications on IFS in LR PHY and its resistance to I/U ratio can be explained in the context of connection interval and packet duration. Connection interval is defined as the time between two BLE connection events that involves data transfer between two BLE devices. The number of packets that can be sent during one connection event depends on the physical layer agreed upon at the beginning of a connection; therefore, the time spent transmitting a given amount of data using LR PHY is longer than 1M and 2M PHYs. Consequently, the number of packets sent in one connection event is less for LR compared to the other two PHYs, as illustrated in Figure 6.4.

If a packet—data or ACK—is not received or dropped (e.g., due to noisy channel or interference from other incumbents’ transmissions), the delay between two successive received packets increases, which also reduces achieved throughput. Notably, when interference causes the first frame of the connection event to be dropped, transmitter must wait for the next connection event to send its packets. The repercussions of such situations are higher on LR PHY than 2M and 1M since the number of packets that can be sent are fewer within the same connection interval. On the other hand, LR PHY implements FEC, which allows it to recover

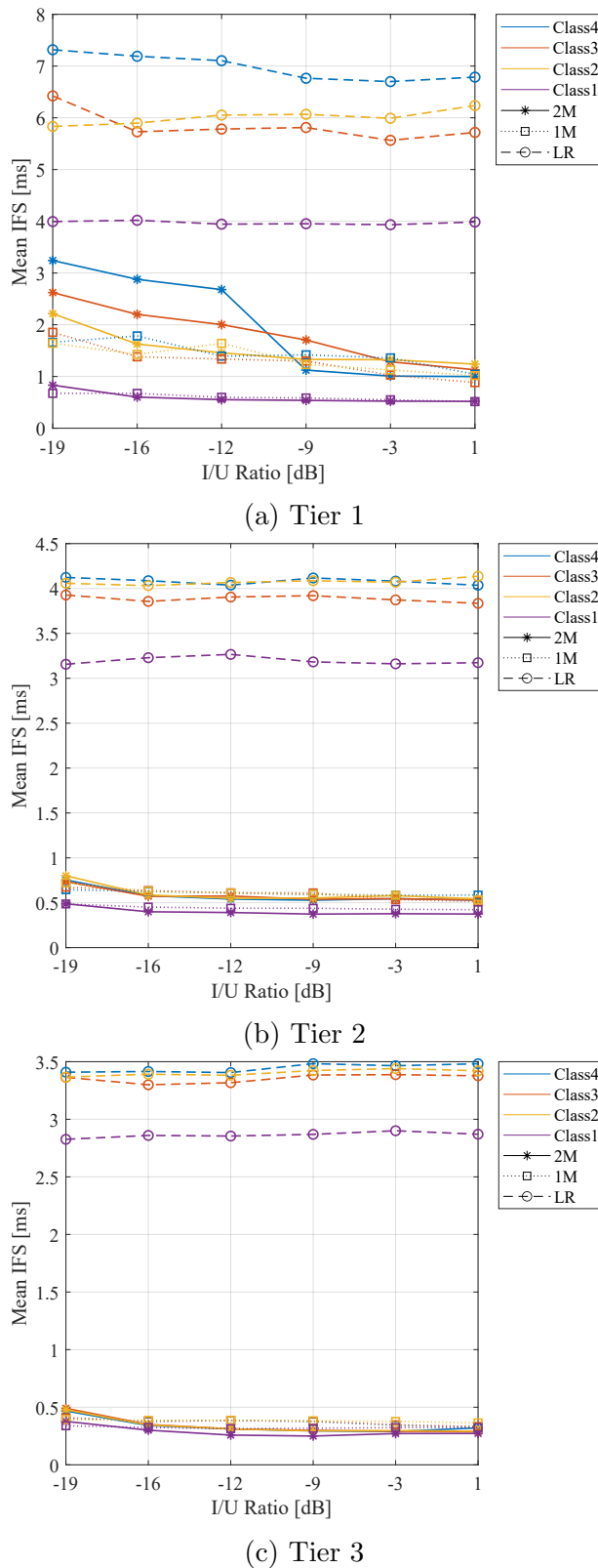


Figure 6.3: Mean IFS durations of BLE PHYs in three tiers as a function of the I/U ratio.

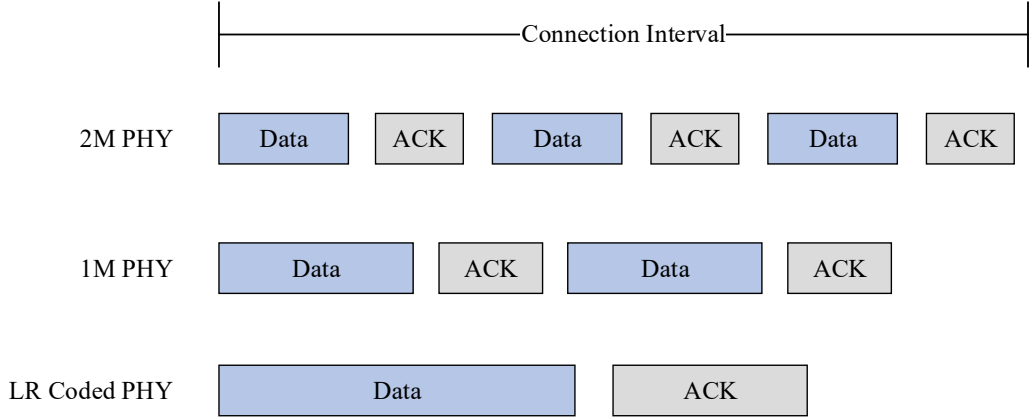


Figure 6.4: An example of the number of packets that can be sent during one connection event for 2M, 1M, and LR PHYs.

some erroneous bits on the receiver side without the need to retransmit the packet. Hence, the mean IFS is less susceptible to I/U ratio and more so to time activity of the interfering system; this is manifested by the effect of the access priority class of LBT, as shown in Figure 6.3. The figure also shows that class 2 has higher impact than class 3 across the three tiers, which is attributed to the fact that class 2 exhibits longer channel occupancy time (i.e., 6 ms) compared with 4 ms for class 3. Class 1 effect is comparatively less than the other three classes due to its exponentially large maximum contention window size.

Findings discussed in this subsection validate similar studies found in literature yet go beyond what has previously been presented by addressing all physical layers of BLE under single- and multi-channel interference. Ancans et al. [63] reported that BLE throughput using 2M and 1M PHYs was reduced by approximately 30% when subjected to single-channel interference from an unspecified variant of Wi-Fi protocol, configured on channel 1 (2412 MHz). Though the authors did not report BLE and Wi-Fi power configuration, their figures (6 and 7 in [63]) suggest that I/U was around -8 dB. Likewise, results of tier 3 scenario suggest that 2M and 1M PHYs sustain comparable reduction under class 4, 3, and 2 LBT interferers. Spörk et al. [64] also reported similar work with a single-node 802.11b interference centered on channel 6, which was configured to transmit a 1500-byte

long packet every 10 millisecond. BLE connection was configured to only use BLE data channels (12 to 19) overlapping with Wi-Fi’s channel 6. The presented results confirm that LR PHY provides better reliability under interference when compared to 2M and 1M PHYs.

6.3.2 Impact of BLE 5 on LBT Performance

LBT-based network performance was characterized in terms of normalized achieved throughput of the PDSCH traffic, which passed CRC check during wireless coexistence tests. Figure 6.5 depicts the mean normalized throughput of channels with center frequencies 2412 MHz, 2437 MHz, and 2462 MHz in the three evaluation tiers as a function of BLE PHY for each priority class. Measurements are normalized with respect to 43, 55, 55, and 33 Mbps, corresponding to LBT classes 4, 3, 2, and 1, respectively. In general, results reveal that the performance of LBT is hindered in the presence of BLE LR. In contrast, 2M and 1M PHY scenarios demonstrated better outcomes. Furthermore, the figure also denotes that under the same BLE PHY, LBT class performance decreased as the access priorities decreased—except for class 1 under LR PHY in tier 1 and 2 scenarios. Attained normalized throughput appears to surpass that of class 2. As indicated in the previous section, the lower the data rate of the physical layer in BLE, the longer it takes to transmit the same amount of data. Hence, 2M packets occupy the least airtime, followed by 1M and LR PHYs. Figure 6.6 corroborates this observation for the three physical layers of BLE with median durations of 76 μ s, 144 μ s, and 1.232 ms for 2M, 1M, and LR, respectively. The remarks on the behavior of BLE PHYs as observed on LBT performance are ascribed to the corresponding packet airtime durations. Effect of contention window size and COT pertaining to different LBT access priorities were also noted. Although low priority frames occupied the channel for longer times, they exhibited a wider contention window than higher priority classes. These two parameters, along with the duration of BLE packets sent, are cause for the dynamics behind the impact on the LBT network. Classes

1 and 2 have the same COT, per Table 2.2, although class 1 bears a maximum contention window size of 1024 compared to 64 for class 2. In a congested radio environment, as is the case in tier 1, class 1 avoids colliding with the coexisting RATs due to longer back-off periods, thus, improving achieved throughput.

Further analysis of BLE data revealed insights on its channel activity. Figure 6.7a and 6.7b illustrate BLE channel histograms as a function of I/U ratio for the three physical layers under tier 1 class 4 and tier 2 class 1 interferers, respectively. The figures indicate that BLE utilized channels within LBT's 20-MHz bandwidth (i.e., channels 1, 6, and 11) when temporal activity was low. This is demonstrated by the light blue squares in Figure 6.7b corresponding to class 1, compared to darker squares in Figure 6.7a corresponding to class 4. However, histogram data highlights that BLE used channels 4, 16, and 28 frequently within LBT transmissions, especially with physical layers 1M and 2M, as well as high transmission powers. Said channels coincided with the DC null subcarrier of OFDM waveform corresponding to LBT center frequencies 2412 MHz, 2437 MHz, and 2462 MHz. The result is related to the channel selection algorithm of BLE, which determined to use the specified channels since no transmission occurred at the subcarrier in the center of the channel. Nevertheless, this phenomenon caused interference with LBT, which translated into reduced throughput performance because corrupted packets did not pass the CRC check at the receiver side.

6.4 Discussion

Wireless coexistence evaluation is important for several applications, including medical devices. Because the healthcare industry is increasingly incorporating wireless connectivity in the end-user equipment, a number of use case scenarios are emerging in this domain (e.g., remote pervasive monitoring, healthcare for rural areas, and mobile health using wearables [68]). Such scenarios can employ various wireless technologies within proximity where coexistence issues might arise. Given

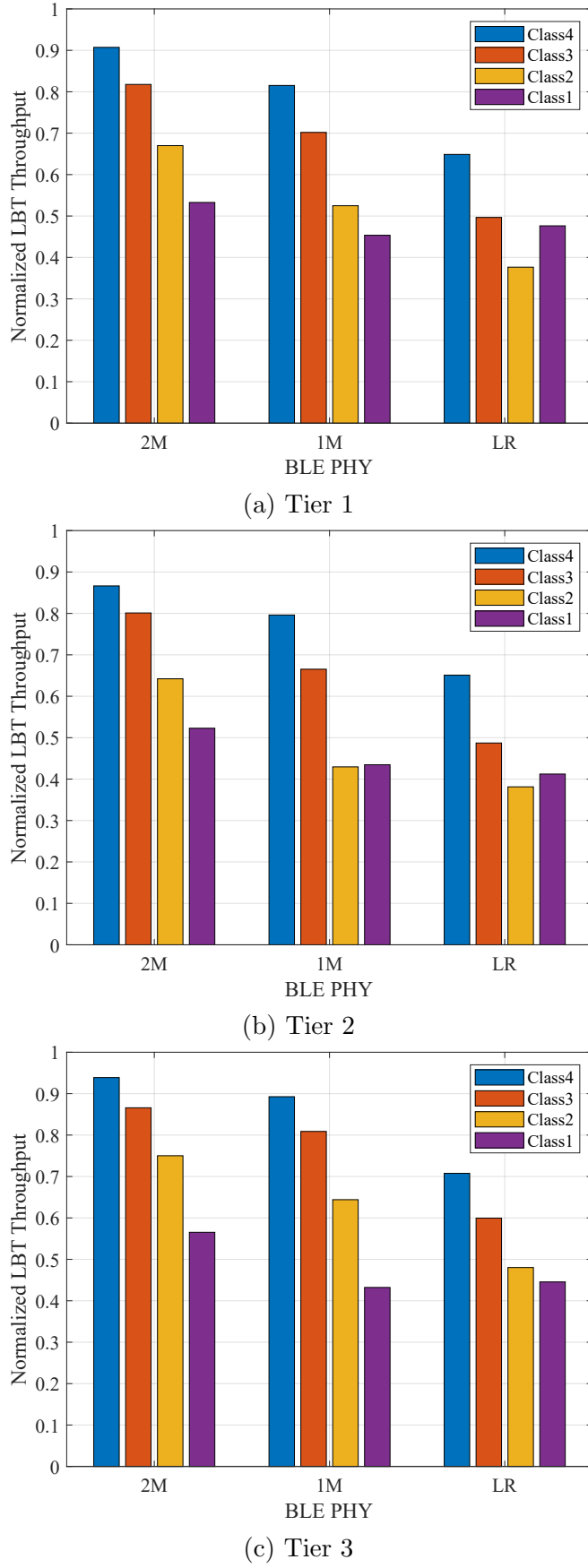


Figure 6.5: Normalized LBT throughput in the evaluation of three tiers.

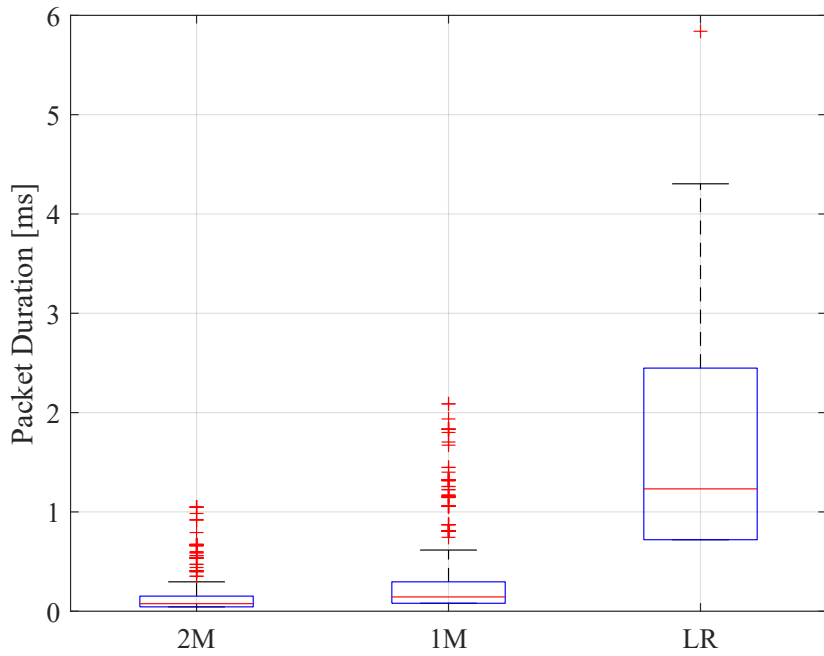


Figure 6.6: Box plot of packet durations for BLE physical layers from tier 1 scenario.

the risk to patients associated with the delay or disruption of a wireless communication link, evaluating the device for wireless coexistence was recommended in the U.S. Food and Drug Administration (FDA) guidance document on radio frequency wireless technology in medical devices [82]. The ANSI C63.27 standard [76] was developed to address this evaluation and provides manufacturers with detailed procedures to evaluate the coexistence of a given FWP against recommended test interferers. Tier of evaluation is determined based on the risk category associated with the FWP per AAMI TIR 69 [69]. TIR 69 specifies four risk categories for the wireless function of medical devices; these are listed in Table 4.1. Annex A of ANSI C63.27 details normative guidelines for some of the most common RATs and frequency bands. For example, it is recommended that a Bluetooth DUT operating in the 2.4 GHz ISM band be tested with IEEE 802.11n signals as an in-band interferer, as well as LTE signals on the lower and upper adjacent bands. A revised draft of C63.27 has been developed and currently in the balloting process of ANSI Accredited Standards Committee C63. A revision included addressing the coexistence of LTE-LAA and Wi-Fi systems in the 5 GHz band [83]. Since LBT-based

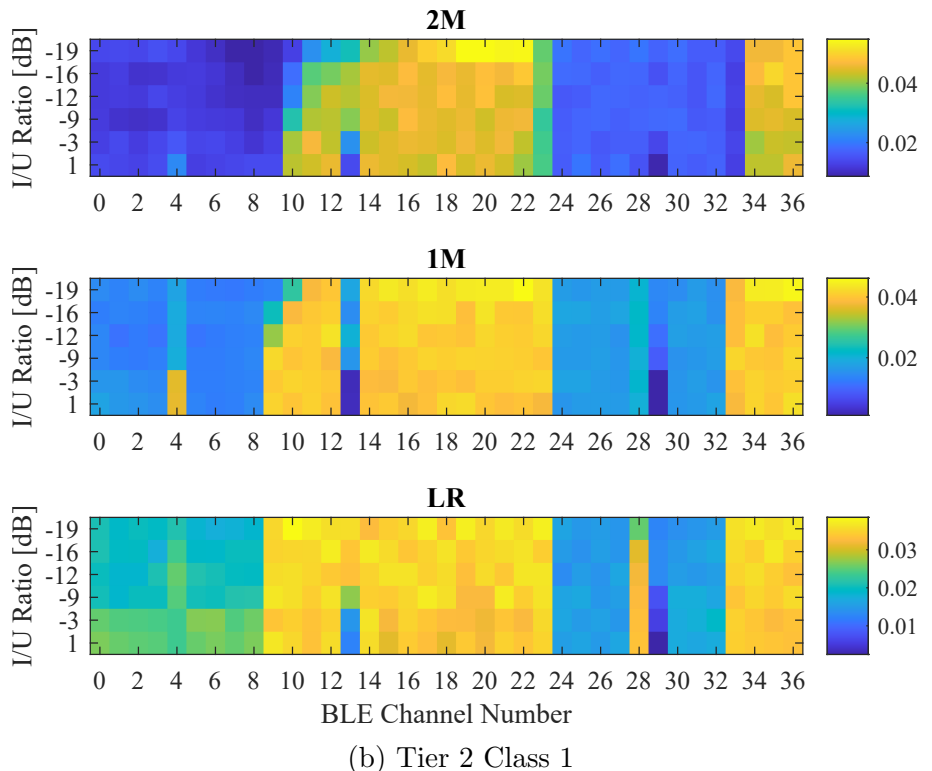
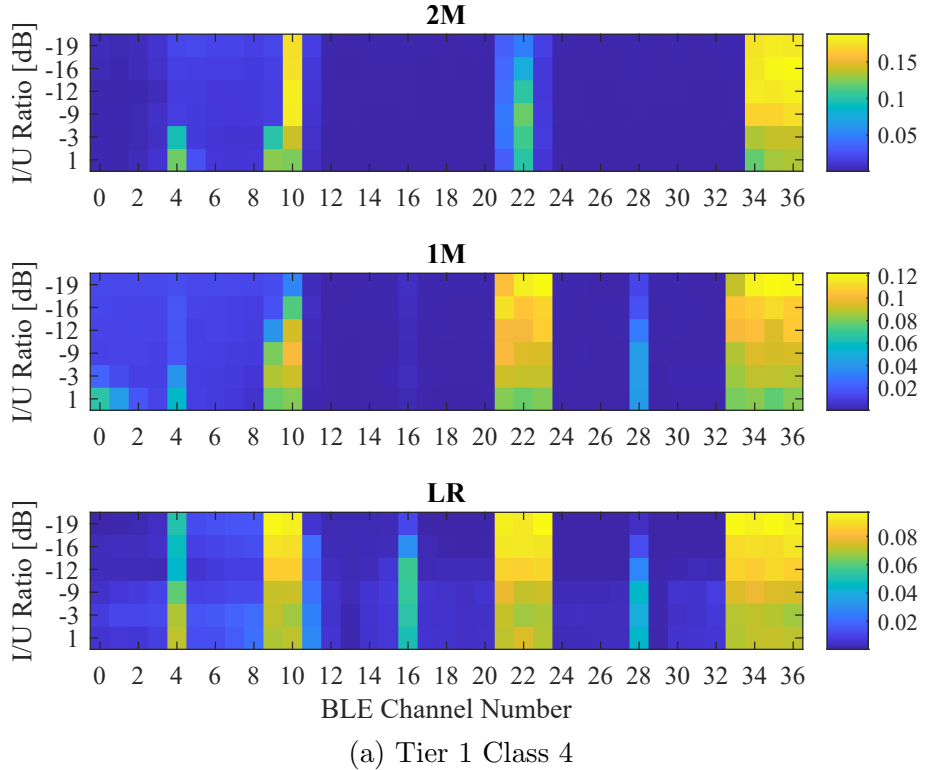


Figure 6.7: BLE channel histogram as a function of I/U ratio.

5G NR operation in the 2.4 GHz unlicensed spectrum (i.e., commonly known as 5G NR-U) has been recently identified in technical report TR 38.889 [15], it is reasonable to consider the coexistence characteristics of such systems and how to include them in the C63.27 test protocol. Accordingly, the presented experiment in this chapter, along with the results discussed in Section 6.3, can be used to devise comparable test plans for a BLE 5 DUT and LBT-based interferer in the 2.4 GHz ISM band—agreeably the choice of LBT class and BLE PHY.

Equally important, findings of coexistence testing could inform the design, development, and deployment of LBT-based and/or BLE 5-based applications within the same vicinity. Depending on the DUT’s FWP, pass/fail criteria can be defined and tested under a given operational condition (e.g., a throughput threshold, delay tolerance, and others). For example, if an application requires an achieved throughput no higher than 100 kbps, BLE PHYs 2M and 1M may be used if the intended environment is less likely to exhibit a busy spectrum band, like tier 1 scenarios where three interferers occupy the 2.4 GHz band. On the other hand, applications where long-distance links and resilience against interference are desired, LR PHY accommodates such needs by virtue of its error correction method at the expense of lower nominal throughput and higher interframe delays compared to the other two BLE physical layers. It is worth mentioning that in more relaxed conditions, where LBT might be serving low traffic applications, the time-domain channel utilization of the unintended signal—LBT in this case—is lower than the case of the assumed full buffer mode in the work presented in this dissertation. Hence, the mutual impact on both coexisting networks is alleviated, since such low LBT traffic would increase the chance for BLE to access the shared medium without colliding with LBT’s traffic. Similarly, LBT-based DUTs might employ results discussed herein to draw on the impact of BLE interference on system performance under different channel access priorities. Such assessments could be coupled with analytical techniques similar to the one reported in [18] to take into consideration the effect of same-technology devices with different

combinations of priority classes.

Chapter 7

Conclusion

The ever-increasing need for connectivity and ability to accommodate various numbers of wireless-enabled devices is driving changes in the evolution of information and communication technology. The IoT phenomenon is promising to forge densely connected societies where all ‘things’ have a digital identity and information to exchange. Centered around the big data paradigm, products and applications will require wireless infrastructure to acclimate to their technical necessities.

To this end, major enablers in the communications industry have begun to adapt and prepare for next-generation wireless systems. The IEEE has rolled out their new 802.11ax standard (also known as Wi-Fi 6) and already commenced studies for the next amendment 802.11be. 3GPP has also put effort into keeping up with the demand by introducing LTE-LAA in the 5 GHz UNII frequency band to supplement traffic on a primary link. Additionally, the development of 5G specifications comprises a license-free operation mode called NR-U. Unlike its predecessor, NR-U is expected to operate as a standalone (i.e., without an anchor link), which makes it a significant milestone on the roadmap. In addition to industry-wide endeavors, spectrum regulatory agencies have begun investigating the possibility of opening a prospective new frequency band to address the demand for high bandwidths. The FCC and the ETSI have approved 1200-megahertz of

spectrum in the 6 GHz band for unlicensed commercial use.

Given the changes in regulations and, subsequently, the user experience, the status quo channel access mechanism in the unlicensed spectrum must be reevaluated to ensure efficiency, fairness, and adaptability under anticipated deployment scenarios. This dissertation revisits the LBT scheme and assesses its performance in a homogeneous setting without interference from other possible coexisting technologies. A Markov chain model was developed for the LBT mechanism and its frame priority classes. ECU, collisions, mean access delay, and fairness were investigated for single-class and multi-class deployments. A case study on 5G NR-U-enabled ICU hospital environment was presented to highlight how the selection of channel access parameters can impact wireless coexistence of 5G-enabled medical devices with diverse risk profiles when operating in the unlicensed spectrum.

Analysis revealed that high priority classes do not perform well in a dense, single-class scenario in terms of channel utilization due to high collision rate. Furthermore, the high priority classes incur longer delays compared to lower priority classes. In a two-class deployment, high priority levels seem to hinder overall ECU due to intra-network interference among nodes. Moreover, collision analysis suggests that in a multi-class case internetwork collisions between high and low priority nodes has a significant impact on performance, especially with adjacent classes. In addition, high priority levels incur more negative effect on mean access delay of lower-class networks than they do among their own networks. Finally, although all four levels of traffic priority demonstrated fair share of the medium in a single-class case, the two-class analysis indicated that as priority levels increase, high priority classes utilize more airtime at the expense of coexisting lower counterparts.

In light of these results from the analytical investigation of LBT mechanism, a modified scheme was proposed to address the inefficiency in total channel utilization of homogeneous LBT deployments. A RSIFS period was introduced, in addition to SIFS, prioritization, and backoff periods of the original LBT. RSIFS

values are in absolute microseconds, unlike the prioritization and backoff counters with measured values in $9 \mu s$ time slots. All priority classes demonstrated improvements in ECU performance, especially for classes 3 and 4, which showed around 60% and 70 % improvements, respectively, when 20 devices shared the medium.

The possibility of LBT operation in the 2.4 GHz that has been indicated in recent technical reports raises new wireless coexistence concerns with incumbent RATs that have yet to be addressed. The LBT-based LTE-LAA and Wi-Fi wireless coexistence in the 5 GHz band has been studied extensively in literature, and observations could be extended to the 2.4 GHz spectrum. Notably, BLE is another prominent wireless standard that faces coexistence issues with cellular LBT systems. At the same time, the ECC intends to allow narrowband, low-power frequency hoppers in the 5 and 6 GHz bands, termed VLP systems. With early proposals aiming to replicate 2.4 GHz rules, Bluetooth systems are expected to be allowed in the new frequency bands. Such proposals are foreseen to trigger feasibility disputes over coexistence issues with incumbent RATs—like the ones made previously in the case of Bluetooth and 802.11b.

This dissertation reports on the mutual impact of BLE 5 and cellular LBT coexisting systems by means of empirical evaluation. Effects of various parameters of both RATs (e.g., LBT’s channel access priorities and BLE’s physical layers) were investigated. Results were presented in terms of achieved throughput and IFS delay under various parameter combinations and ANSI C63.27 evaluation tiers. Normalized BLE throughput was shown to decline as the intended-to-unintended signal ratio decreases; LBT classes exhibit a diminishing effect as the class priority descends. Furthermore, coded (LR) BLE PHY demonstrated less susceptibility to interference in relaxed conditions (e.g., single-channel interferer) compared to 2M and 1M BLE PHYs. Delay analysis indicated that LR sustains longer average gap times than the other two physical layers even though LR showed less sensitivity to interference in that regard. Alternatively, results demonstrated that low data rate

PHYs hinder LBT performance as they correspond to longer airtime durations. Outcomes of coexistence testing could help characterize and enhance BLE 5 device operations when sharing channel resources with a future LBT-based system in the 2.4 GHz ISM frequency band.

7.1 Future Work

This dissertation accentuates the significance of improving the channel access scheme of radio access technologies as they are introduced into new frequency bands. The 6 GHz band is a green field for almost all technologies aiming to extend their scope of operation therein. It presents an opportunity to pay closer attention to legacy mechanisms and try to improve facets, such as efficiency and fairness. Although the work detailed in this dissertation is aimed at increasing channel efficiency of LBT, further improvements in channel access fairness among priority classes must be addressed; intrinsic changes to the standard and/or its parameters might be required.

This work opens the door for further studies to address concerns about coexistence of cellular LBT systems with BLE 5 and other 2.4 GHz ISM band RATs, such as ZigBee. Additionally, the empirical analysis presented herein could be readily re-referenced in the context of 6 GHz to address concerns related to the operation and coexistence of VLP therein. Measurements and findings reported in this work could be expanded in the future by investigating more realistic settings (e.g., the effect of multipath). Influence of other connection parameters (e.g., BLE connection interval and packet size) are also important for a complete understanding of the performance and impact on coexisting RATs. The effect of heterogeneous LBT channel access priorities in the same channel and across different channels on the neighboring BLE network is an interesting direction for research.

Bibliography

- [1] Qualcomm, “How does unlicensed spectrum with NR-U transform what 5G can do for you?” no. June, 2020.
- [2] Rohde & Schwarz, “Be ahead in 5G. Demystifying 5G NR,” no. 6, pp. 5–6, 2020.
- [3] ETSI, “Harmonised European Standard EN 301 893,” Tech. Rep., 2017. [Online]. Available: http://www.etsi.org/deliver/etsi{_{}}en/301800{_{}}301899/301893/02.01.01{_{}}60/en{_{}}301893v020101p.pdf
- [4] 3GPP, “Study on Licensed-Assisted Access to Unlicensed Spectrum, document TR 36.889 V13.0.0,” The 3rd Generation Partnership Project (3GPP), Tech. Rep., 2015.
- [5] Ericsson, “Future mobile data usage and traffic growth,” 2019. [Online]. Available: <https://www.ericsson.com/en/mobility-report/future-mobile-data-usage-and-traffic-growth>
- [6] Qualcomm Incorporated, “LTE in Unlicensed Spectrum : Harmonious Coexistence with Wi-Fi,” *White Paper*, no. June, pp. 1–19, 2014.
- [7] FCC, “NPRM: Unlicensed Use of the 6 GHz Band,” Tech. Rep., oct 2018. [Online]. Available: <https://docs.fcc.gov/public/attachments/FCC-18-147A1.pdf>

- [8] Qualcomm Incorporated, “COMMENTS OF QUALCOMM INCORPORATED,” Tech. Rep., 2019. [Online]. Available: <https://ecfsapi.fcc.gov/file/1021644462961/QualcommCommentson6GHzNPRM.pdf>
- [9] Broadcom, “COMMENTS OF BROADCOM INC.” Tech. Rep., 2019. [Online]. Available: [https://ecfsapi.fcc.gov/file/10216284551574/Broadcom6GHzComments15Feb19\(final\).pdf](https://ecfsapi.fcc.gov/file/10216284551574/Broadcom6GHzComments15Feb19(final).pdf)
- [10] Intel, “NOTICE OF PROPOSED RULEMAKING COMMENTS OF INTEL CORPORATION,” Tech. Rep., 2020. [Online]. Available: https://ecfsapi.fcc.gov/file/10309001614572/IntelCorporation-FCCNPRMCOMMENT{_-}5{_-}9GHz.pdf
- [11] Apple, “REPLY COMMENTS OF APPLE INC.” Tech. Rep., 2019. [Online]. Available: <https://ecfsapi.fcc.gov/file/10319161806839/Apple6GHzNPRMReplyComments.pdf>
- [12] ETSI, “TR 103 524 - V1.1.1 - System Reference document (SRdoc); Wireless access systems including radio local area networks (WAS/RLANs) in the band 5 925 MHz to 6 725 MHz,” Tech. Rep., 2018.
- [13] “IEEE P802.11 Extremely High Throughput Study Group.” [Online]. Available: http://www.ieee802.org/11/Reports/ehtsg{_-}update.htm
- [14] D. Lopez-Perez, A. Garcia-Rodriguez, L. Galati-Giordano, M. Kasslin, and K. Doppler, “IEEE 802.11be Extremely High Throughput: The Next Generation of Wi-Fi Technology beyond 802.11ax,” *IEEE Communications Magazine*, vol. 57, no. 9, pp. 113–119, sep 2019.
- [15] 3GPP, “Study on NR-based access to unlicensed spectrum, document TR 38.889 V16.0.0,” Tech. Rep., 2018.
- [16] CEPT, “CEPT Report 75,” Tech. Rep. March, 2020.

- [17] ECC, “On the harmonised use of the frequency band 5945-6425 MHz for Wireless Access Systems including Radio Local Area Networks (WAS/RLAN),” Tech. Rep. November, 2020.
- [18] S. Muhammad, H. H. Refai, and M. O. Al Kalaa, “5G NR-U: Homogeneous Coexistence Analysis,” in *GLOBECOM 2020 - 2020 IEEE Global Communications Conference*. IEEE, dec 2020, pp. 1–6.
- [19] S. Muhammad, M. O. Al Kalaa, and H. H. Refai, “Wireless Coexistence of Cellular LBT Systems and BLE 5,” *IEEE Access*, vol. 9, pp. 24 604–24 615, 2021. [Online]. Available: <https://ieeexplore.ieee.org/document/9345670/>
- [20] 3GPP, “NR Physical Channels and Modulation, document TS 38.211,” Tech. Rep., 2019.
- [21] J. Wszołek, S. Ludyga, W. Anzel, and S. Szott, “Revisiting LTE LAA: Channel access, QoS, and Coexistence with Wi-Fi,” oct 2019. [Online]. Available: <http://arxiv.org/abs/1910.11002>
- [22] 3GPP, “Evolved Universal Terrestrial Radio Access (E-UTRA) Physical Layer Procedures, document TS 36.213 V13.6.0,” 3GPP, Tech. Rep., 2017.
- [23] IEEE, “Part 11: Wireless LAN Medium Access Control (MAC) and Physical Layer (PHY) Specifications,” *IEEE Std 802.11-2012 (Revision of IEEE Std 802.11-2007)*, vol. 2016, p. 2793, 2012.
- [24] B. Yu, L. Xu, and Y. Li, “Bluetooth Low Energy (BLE) based mobile electrocardiogram monitoring system,” in *2012 IEEE International Conference on Information and Automation, ICIA 2012*, 2012, pp. 763–767.
- [25] L.-H. Wang, W. Zhang, M.-H. Guan, S.-Y. Jiang, M.-H. Fan, P. A. R. Abu, C.-A. Chen, and S.-L. Chen, “A Low-Power High-Data-Transmission Multi-Lead ECG Acquisition Sensor System,” *Sensors*, vol. 19, no. 22, p. 4996, nov 2019.

- [26] “Tested by Nordic: Bluetooth Long Range.” [Online]. Available: [https://blog.nordicsemi.com/getconnected/tested-by-nordic-bluetooth-long-range](https://blog.nordicssemi.com/getconnected/tested-by-nordic-bluetooth-long-range)
- [27] Bluetooth SIG, *Bluetooth Core Specification*, 2019. [Online]. Available: <https://www.bluetooth.com/specifications/adopted-specifications>
- [28] “Bluetooth Core Specification Version 5.0 Feature Overview — Bluetooth® Technology Website.” [Online]. Available: <https://www.bluetooth.com/bluetooth-resources/bluetooth-5-go-faster-go-further/>
- [29] MathWorks, “The Communications Toolbox™ Library for the Bluetooth Protocol.” [Online]. Available: <https://www.mathworks.com/help/comm/bluetooth.html>
- [30] G. Bianchi, “Performance analysis of the IEEE 802.11 distributed coordination function,” *IEEE Journal on Selected Areas in Communications*, vol. 18, no. 3, pp. 535–547, mar 2000.
- [31] Y. Xiao, “Backoff-based priority schemes for IEEE 802.11,” in *IEEE International Conference on Communications*, vol. 3, 2003, pp. 1568–1572.
- [32] ——, “Performance analysis of priority schemes for IEEE 802.11 and IEEE 802.11e wireless LANs,” *IEEE Transactions on Wireless Communications*, vol. 4, no. 4, pp. 1506–1515, jul 2005.
- [33] J. Y. Lee and H. S. Lee, “A performance analysis model for IEEE 802.11e EDCA under saturation condition,” *IEEE Transactions on Communications*, vol. 57, no. 1, pp. 56–63, 2009.
- [34] Z. Kong, D.-K. Tsang, B. Bensaou, and D. Gao, “Performance Analysis of IEEE 802.11e Contention-Based Channel Access,” *IEEE Journal on Selected Areas in Communications*, vol. 22, no. 10, pp. 2095–2106, dec 2004.

- [35] Y. Zheng, K. Lu, D. Wu, and Y. Fang, “Performance analysis of IEEE 802.11 DCF in imperfect channels,” *IEEE Transactions on Vehicular Technology*, vol. 55, no. 5, pp. 1648–1656, sep 2006.
- [36] P. Chatzimisios, A. C. Boucouvalas, and V. Vitsas, “Performance analysis of IEEE 802.11 DCF in presence of transmission errors,” in *IEEE International Conference on Communications*, vol. 7, 2004, pp. 3854–3858.
- [37] I. N. Vukovic and N. Smavatkul, “Delay analysis of different backoff algorithms in IEEE 802.11,” in *IEEE Vehicular Technology Conference*, vol. 60, no. 6, 2004, pp. 4553–4557.
- [38] S. Asadallah and H. H. Refai, “Distributed adaptive backoff reservation (DABR) for IEEE 802.11 wireless networks,” in *2012 IEEE International Conference on Communications (ICC)*. IEEE, jun 2012, pp. 6890–6894.
- [39] M. Mehrnoush, V. Sathya, S. Roy, and M. Ghosh, “Analytical Modeling of Wi-Fi and LTE-LAA Coexistence: Throughput and Impact of Energy Detection Threshold,” *IEEE/ACM Transactions on Networking*, vol. 26, no. 4, pp. 1990–2003, aug 2018.
- [40] N. Bitar, M. O. Al Kalaa, S. J. Seidman, and H. H. Refai, “On the Coexistence of LTE-LAA in the Unlicensed Band: Modeling and Performance Analysis,” *IEEE Access*, vol. 6, pp. 52 668–52 681, 2018.
- [41] M. Hirzallah, Y. Xiao, and M. Krunz, “On Modeling and Optimizing LTE/Wi-Fi Coexistence with Prioritized Traffic Classes,” in *2018 IEEE International Symposium on Dynamic Spectrum Access Networks (DySPAN)*. IEEE, oct 2018, pp. 1–10.
- [42] Y. Ma, “Analysis of Channel Access Priority Classes in LTE-LAA Spectrum Sharing System,” in *2018 27th International Conference on Computer Communication and Networks (ICCCN)*, vol. 2018-July. IEEE, jul 2018, pp. 1–7.

- [43] M. O. A. Kalaa and S. J. Seidman, “Wireless Coexistence Testing in the 5 GHz Band with LTE-LAA Signals,” in *2019 IEEE International Symposium on Electromagnetic Compatibility, Signal & Power Integrity (EMC+SIPI)*. IEEE, jul 2019, pp. 437–442.
- [44] J. Xiao, J. Zheng, L. Chu, and Q. Ren, “Performance Modeling and Analysis of the LAA Category-4 LBT Procedure,” *IEEE Transactions on Vehicular Technology*, vol. 68, no. 10, pp. 10 045–10 055, oct 2019.
- [45] Z. Tang, X. Zhou, Q. Hu, and G. Yu, “Throughput Analysis of LAA and Wi-Fi Coexistence Network With Asynchronous Channel Access,” *IEEE Access*, vol. 6, pp. 9218–9226, feb 2018.
- [46] Y. Ma, D. G. Kuester, J. Coder, and W. Young, “Coexistence analysis of LTE and WLAN systems with heterogenous backoff slot durations,” in *2017 IEEE International Conference on Communications (ICC)*. IEEE, may 2017, pp. 1–7.
- [47] Y. Ma, D. G. Kuester, J. Coder, and W. F. Young, “Slot-Jamming Effect and Mitigation Between LTE-LAA and WLAN Systems With Heterogeneous Slot Durations,” *IEEE Transactions on Communications*, vol. 67, no. 6, pp. 4407–4422, jun 2019.
- [48] B. Mafakheri, L. Goratti, R. Abbas, S. Reisenfeld, and R. Riggio, “LTE/Wi-Fi Coordination in Unlicensed Bands: An SD-RAN Approach,” in *2019 IEEE Conference on Network Softwarization (NetSoft)*. IEEE, jun 2019, pp. 311–315.
- [49] M. Hirzallah, Y. Xiao, and M. Krunz, “MatchMaker: An Inter-operator Network Sharing Framework in Unlicensed Bands,” in *2019 16th Annual IEEE International Conference on Sensing, Communication, and Networking (SECON)*. IEEE, jun 2019, pp. 1–9.

- [50] U. Challita, L. Dong, and W. Saad, “Proactive Resource Management for LTE in Unlicensed Spectrum: A Deep Learning Perspective,” *IEEE Transactions on Wireless Communications*, vol. 17, no. 7, pp. 4674–4689, jul 2018.
- [51] E. Pei, J. Jiang, L. Liu, Y. Li, and Z. Zhang, “A chaotic Q-learning based licensed assisted access scheme over the unlicensed spectrum,” *IEEE Transactions on Vehicular Technology*, vol. 68, no. 10, pp. 1–1, oct 2019.
- [52] O. Baiyekusi, S. Vahid, and K. Moessner, “A Time-Based Fairness Approach for Coexisting 5G Networks in Unlicensed Bands,” in *2017 IEEE 85th Vehicular Technology Conference (VTC Spring)*, vol. 2017-June. IEEE, jun 2017, pp. 1–5.
- [53] Q. Tse, W. Si, and J. Taheri, “Estimating contention of IEEE 802.11 broadcasts based on inter-frame idle slots,” in *Proceedings - Conference on Local Computer Networks, LCN*. IEEE Computer Society, 2013, pp. 120–127.
- [54] H. Song, Q. Cui, Y. Gu, G. L. Stuber, Y. Li, Z. Fei, and C. Guo, “Cooperative LBT Design and Effective Capacity Analysis for 5G NR Ultra Dense Networks in Unlicensed Spectrum,” *IEEE Access*, vol. 7, pp. 50 265–50 279, 2019.
- [55] Z. Tang, X. Zhou, Q. Chen, G. Yu, X. Shi, and Q. Hu, “Adaptive \$p\\$-Persistent LBT for Unlicensed LTE: Performance Analysis and Optimization,” *IEEE Transactions on Vehicular Technology*, vol. 68, no. 9, pp. 8744–8758, sep 2019.
- [56] I. Howitt, V. Mitter, and J. Gutierrez, “Empirical study for IEEE 802.11 and Bluetooth interoperability,” in *IEEE VTS 53rd Vehicular Technology Conference, Spring 2001. Proceedings (Cat. No.01CH37202)*, vol. 2, no. 53ND. IEEE, 2001, pp. 1109–1113.
- [57] L. Pei, J. Liu, R. Guinness, Y. Chen, T. Kroger, R. Chen, and L. Chen, “The evaluation of WiFi positioning in a Bluetooth and WiFi coexistence envi-

- ronment,” in *2012 Ubiquitous Positioning, Indoor Navigation, and Location Based Service (UPINLBS)*. IEEE, oct 2012, pp. 1–6.
- [58] R. Natarajan, P. Zand, and M. Nabi, “Analysis of coexistence between IEEE 802.15.4, BLE and IEEE 802.11 in the 2.4 GHz ISM band,” in *IECON 2016 - 42nd Annual Conference of the IEEE Industrial Electronics Society*. IEEE, oct 2016, pp. 6025–6032.
- [59] Jiun-Ren Lin, T. Talty, and O. K. Tonguz, “An empirical performance study of Intra-vehicular Wireless Sensor Networks under WiFi and Bluetooth interference,” in *2013 IEEE Global Communications Conference (GLOBECOM)*. IEEE, dec 2013, pp. 581–586.
- [60] A. Mourad, S. Muhammad, M. O. Al Kalaa, P. A. Hoeher, and H. Refai, “Bluetooth and IEEE 802.11n System Coexistence in the Automotive Domain,” in *2017 IEEE Wireless Communications and Networking Conference (WCNC)*. IEEE, mar 2017, pp. 1–6.
- [61] A. Mourad, S. Muhammad, M. O. Al Kalaa, H. H. Refai, and P. A. Hoeher, “On the performance of WLAN and Bluetooth for in-car infotainment systems,” *Vehicular Communications*, vol. 10, no. August, pp. 1–12, oct 2017.
- [62] W. Bronzi, R. Frank, G. Castignani, and T. Engel, “Bluetooth Low Energy performance and robustness analysis for Inter-Vehicular Communications,” *Ad Hoc Networks*, vol. 37, pp. 76–86, feb 2016.
- [63] A. Ancans, J. Ormanis, R. Cacurs, M. Greitans, E. Saoutieff, A. Faucorr, and S. Boisseau, “Bluetooth Low Energy Throughput in Densely Deployed Radio Environment,” in *Proceedings of the 23rd International Conference Electronics 2019, ELECTRONICS 2019*. Institute of Electrical and Electronics Engineers Inc., jun 2019.
- [64] M. Spörk, C. A. Boano, and K. Römer, “Performance and trade-offs of the new PHY modes of BLE 5,” in *Proceedings of the International Symposium*

on Mobile Ad Hoc Networking and Computing (MobiHoc). New York, New York, USA: Association for Computing Machinery, jul 2019, pp. 7–12.

- [65] H. Karvonen, C. Pomalaza-Ráez, K. Mikhaylov, M. Hämäläinen, and J. Iinatti, “Experimental Performance Evaluation of BLE 4 Versus BLE 5 in Indoors and Outdoors Scenarios,” in *Internet of Things*. Springer International Publishing, 2019, pp. 235–251. [Online]. Available: http://link.springer.com/10.1007/978-3-030-02819-0{_}18
- [66] G. Bolch, S. Greiner, H. de Meer, and K. S. Trivedi, *Queueing Networks and Markov Chains*, 2nd ed. New York, USA: John Wiley & Sons, Inc., aug 1998.
- [67] C. Thuemmler, A. Paulin, and A. K. Lim, “Determinants of next generation e-Health network and architecture specifications,” in *2016 IEEE 18th International Conference on e-Health Networking, Applications and Services, Healthcom 2016*. Institute of Electrical and Electronics Engineers Inc., nov 2016.
- [68] G. Cisotto, E. Casarin, and S. Tomasin, “Requirements and Enablers of Advanced Healthcare Services over Future Cellular Systems,” *IEEE Communications Magazine*, vol. 58, no. 3, pp. 76–81, mar 2020.
- [69] AAMI, “AAMI TIR69:2017; Risk management of radio-frequency wireless coexistence for medical devices and systems,” Tech. Rep., 2017. [Online]. Available: www.aami.org.
- [70] Bluetooth SIG, “Bluetooth Market Update 2020,” 2020. [Online]. Available: https://www.bluetooth.com/wp-content/uploads/2020/03/2020{_}Market{_}Update-EN.pdf
- [71] “Bluetooth Core Specification Version 5.1 Feature Overview — Bluetooth® Technology Website.” [Online]. Available: <https://www.bluetooth.com/bluetooth-resources/bluetooth-core-specification-v5-1-feature-overview/>

- [72] “Bluetooth Core Specification Version 5.2 Feature Overview — Bluetooth® Technology Website.” [Online]. Available: <https://www.bluetooth.com/bluetooth-resources/bluetooth-core-specification-version-5-2-feature-overview/>
- [73] S. Zinno, G. Di Stasi, S. Avallone, and G. Ventre, “On a fair coexistence of LTE and Wi-Fi in the unlicensed spectrum: A Survey,” *Computer Communications*, vol. 115, pp. 35–50, jan 2018.
- [74] M. Mehrnoush, S. Roy, V. Sathya, and M. Ghosh, “On the Fairness of Wi-Fi and LTE-LAA Coexistence,” *IEEE Transactions on Cognitive Communications and Networking*, vol. 4, no. 4, pp. 735–748, dec 2018.
- [75] FCC, “Unlicensed Use of the 6 GHz Band,” apr 2020. [Online]. Available: <https://docs.fcc.gov/public/attachments/FCC-20-51A1{ }Rcd.pdf>
- [76] ANSI, *American National Standard for Evaluation of Wireless Coexistence C63.27*, 2017.
- [77] National Instruments, “PXIe-1071.” [Online]. Available: <https://www.ni.com/en-us/support/model.pcie-1071.html>
- [78] “USRP-2943 - NI.” [Online]. Available: <https://www.ni.com/en-us/support/model.usrp-2943.html>
- [79] National Instruments, “LabVIEW Communications LTE Application Framework.” [Online]. Available: <http://sine.ni.com/nips/cds/view/p/lang/en/nid/213083>
- [80] ——, “Real-time LTE/Wi-Fi Coexistence Testbed.” [Online]. Available: <https://www.ni.com/en-us/innovations/white-papers/16/real-time-lte-wi-fi-coexistence-testbed.html>
- [81] “nRF52840 Dongle - nordicsemi.com.” [Online]. Available: <https://www.nordicsemi.com/Software-and-tools/Development-Kits/nRF52840-Dongle>

- [82] U.S. Food and Drug Administration, “Radio Frequency Wireless Technology in Medical Devices: Guidance for Industry and Food and Drug Administration Staff.” [Online]. Available: <https://www.fda.gov/media/71975/download>
- [83] M. O. Al Kalaa and S. J. Seidman, “5-GHz Band LTE-LAA Signal Selection for Use as the Unintended Signal in ANSI C63.27 Wireless Coexistence Testing,” *IEEE Transactions on Electromagnetic Compatibility*, vol. 62, no. 4, pp. 1468–1476, aug 2020.

Acronyms

3GPP 3rd Generation Partnership Project

AAMI Association for the Advancement of Medical Instrumentation

AFH Adaptive Frequency Hopping

AIFS Arbitrary Inter-Frame Spacing

ANSI American National Standards Institute

BLE Bluetooth Low Energy

BWP Bandwidth Part

CCA Clear Channel Assessment

COT Channel Occupancy Time

CRC Cyclic Redundancy Check

CSA Channel Selection Algorithm

CSMA/CA Carrier Sense Multiple Access with Collision Avoidance

DCF Distributed Coordination Function

DTMC Discrete-Time Markov Chain

DUT device under test

ECC European Communications Committee

ECU Effective Channel Utilization

ED Energy Detection

EDCA Enhanced Distributed Channel Access

ETSI European Telecommunications Standards Institute

FBE Frame-Based Equipment

FCC Federal Communications Commission

FEC Forward Error Correction

FWP Functional Wireless Performance

I/U Intended-to-Unintended Signal Ratio

ICU intensive care unit

IEEE Institute of Electrical and Electronics Engineers

IFS Interframe Spacing

IoT Internet of Things

ISM Industrial, Scientific, and Medical

LBE Load-Based Equipment

LBT Listen-Before-Talk

LTE Long-Term Evolution

LTE-LAA Long-Term Evolution License-Assisted Access

LTE-U LTE-Unlicensed

MAC Medium Access Control

MCS Modulation and Coding Scheme

NR-U New Radio-Unlicensed

PDSCH Physical Downlink Shared Channel

PDU Packet Data Unit

PHY physical layer

PMF Probability Mass Function

PRNG Pseudo Random Number Generator

RATs radio access technologies

RF radio frequency

RSIFS Random Short Interframe Spacing

SIFS Short Inter-Frame Spacing

TXOP Transmission Opportunity

UE User Equipment

UNII Unlicensed National Information Infrastructure

VLP Very Low Power